

# Bond operator theory of doped antiferromagnets: from Mott insulators with bond-centered charge order, to superconductors with nodal fermions

Kwon Park<sup>1</sup> and Subir Sachdev<sup>1,2</sup>

<sup>1</sup>*Department of Physics, Yale University, P.O. Box 208120, New Haven, CT 06520-8120*

<sup>2</sup>*Department of Physics, Harvard University, Cambridge MA 02138*

(December 2, 2024)

The ground states and excitations of two-dimensional insulating and doped Mott insulators are described by a bond operator formalism. While the method represents the degrees of freedom of an arbitrary antiferromagnet exactly, it is especially suited to systems in which there is a natural pairing of sites into bonds, as in states with spontaneous or explicit spin-Peierls order (or bond-centered charge order). In the undoped insulator, as discussed previously, we obtain both paramagnetic and magnetically-ordered states. We describe the evolution of superconducting order in the ground state with increasing doping—at low doping, the superconductivity is weak, can co-exist with magnetic order, and there are no gapless spin 1/2 fermionic excitations; at high doping, the magnetic order is absent and we obtain a BCS  $d$ -wave superconductor with gapless spin 1/2, nodal fermions. We present the critical theory describing the onset of these nodal fermionic excitations. We discuss the evolution of the spin spectrum, and obtain regimes where a spin 1 exciton contributes a sharp resonance in the dynamic spin susceptibility. We also discuss the experimental consequences of low-energy, dynamically fluctuating, spin-Peierls order in an isotropic CuO<sub>2</sub> plane—we compute consequences for the damping and dispersion of an optical phonon involving primarily the O ions, and compare the results with recent neutron scattering measurements of phonon spectra.

## I. INTRODUCTION

By now, it is reasonably well established that the doped antiferromagnets found in the cuprate compounds have a superconducting ground state with a  $d$ -wave pairing symmetry. Moreover, essentially all low temperature ( $T$ ) properties appear to be well described in the framework of the conventional BCS theory of  $d$ -wave superconductors. There are a number of fascinating properties at temperatures above  $T_c$  (the critical temperature for the onset of superconductivity) which are not well understood, but there are numerous plausible candidate theories for these, involving crossovers between different competing orders in doped antiferromagnets<sup>1</sup>.

In this context, recent low  $T$  NMR measurements<sup>2,3</sup> of spin correlations in the vicinity of isolated Li impurities are especially notable, as they indicate disagreement with the minimal BCS theory even as  $T \rightarrow 0$ . The Li ion is nominally non-magnetic, having no  $d$  orbitals. Within the framework of the BCS theory, it would be natural to describe this ion by a strong local potential scatterer of the Cu electrons which form the Cooper pairs<sup>4</sup>. However, the  $T \rightarrow 0$  NMR observations do not agree with the predictions of such a theory. In the underdoped samples, the experiments show that the electrons on the Cu sites near the Li impurity contribute an impurity paramagnetic spin susceptibility,  $\chi_{\text{imp}}$ , given by

$$\chi_{\text{imp}} = \frac{S(S+1)}{3k_B T} \quad (1)$$

with spin  $S = 1/2$ . This Curie-like behavior extends to the lowest measured temperatures, and indicates the

presence of a free  $S = 1/2$  moment in the vicinity of the Li ion. The behavior (1) is expected to hold down to  $T$  so low that the exchange interactions between different Li ions become pertinent. A  $T \rightarrow 0$  divergence in the impurity susceptibility like (1) is only possible within the minimal BCS theory if there is localized quasiparticle state exactly at zero energy: such zero energy states do not appear without unacceptable fine tuning<sup>5</sup> *e.g.* unitarity limit scattering with a perfectly particle-hole symmetric band structure in the bulk. Moreover, even if such a zero energy state is present, the  $T$  dependence of its divergent susceptibility does not agree with (1). Of course, if we imagine adding Coulomb repulsion to the BCS theory, a localized quasiparticle state may be singly-occupied, and would then contribute a susceptibility as in (1)—however, this begs the question of how such Coulomb interactions can be added consistently on every site, which is the issue we wish to address here.

In this paper, we shall explore more completely a circle of theoretical ideas in which results like (1) may be understood. Our scenario has a number of important consequences for neutron scattering measurements of the spin excitations, and of the phonon spectra: we shall describe these in some detail and compare the results to existing experiments. Suggestions for further experimental studies to sharpen our theoretical understanding will also be made. As we will describe shortly, fluctuating or static “bond-centered charge order” plays a crucial role in our approach: in Section VI we will describe conditions under which such order may be directly observed in STM experiments.

Our theoretical framework<sup>6–12</sup> for understanding (1)

is sketched in Fig 1. The central idea is that it is helpful to view the  $d$ -wave superconducting ground state as being smoothly connected to a paramagnetic Mott insulator with *confinement*. The connection of the physics of non-magnetic impurities to confinement was also noted in the early experimental work of Finkelstein *et al.*<sup>13</sup>. The argument builds upon the influential work of Anderson<sup>14</sup>. He argued that Mott insulator  $\text{La}_2\text{CuO}_4$  (which is now known to have long-range Néel order in its ground state) is in or close to a regime with a paramagnetic ground state, and that high temperature superconductivity is a natural consequence of doping such a state. He also proposed a “resonating valence bond” (RVB) picture of the paramagnetic insulator, above which the elementary excitations were neutral,  $S = 1/2$ , spinons. However, closer examination of this idea revealed that RVB paramagnet had a fundamental topological instability which was present in the vicinity of its transition to the Néel state<sup>6,8</sup>: this instability led to confinement of spinons into stable, neutral  $S = 1$  particle excitations (“excitons”), along with broken translational symmetry associated with the spontaneous development of a spatial modulation in the exchange energies. In the cuprates, there are O ions between each Cu-Cu link, and a modulation in the exchange energies would be manifested as a corresponding modulation of charge density on the O sites. So, alternatively stated, the work of Refs 6,8 argued that the RVB paramagnet was unstable to a state with bond-centered charge density wave (CDW) order, in the vicinity of its transition to a state with magnetic long-range order. A promising candidate for the bond-centered CDW is the columnar spin-Peierls state shown in Fig 2a: in modern terminology, this state is a bond-centered charge stripe at wavevector  $(\pi, 0)$ . The caption of Fig 2 also presents a simple, physical argument for the stability of such a state—the columnar state has a maximum number of plaquettes around which the valence bonds can resonate, and the resulting gain in “quantum entropy” leads to the selection of a state with broken translational symmetry. As indicated in the cartoon pictures of wavefunctions in Fig 3, the presence of this broken translational symmetry also implies the confinement of  $S = 1/2$  spinons at all energy scales. Finally, returning to our opening discussion of NMR experiments on Zn/Li impurities, the confinement property of the paramagnet also implies that each Zn/Li impurity will confine a  $S = 1/2$  moment in its vicinity<sup>12</sup>—a pictorial argument for this is presented in Fig 4. Note, however, that the formation of a  $S = 1/2$  moment near an impurity is a “short distance” effect (unlike the permanent confinement of  $S = 1/2$  spinons), and does not really require truly long-range spin-Peierls order; the moment can form provided the spin-Peierls correlation length is sufficient large (even in a paramagnet in which the spinons are ultimately deconfined) —the length scale is determined by a competition between the energy cost of breaking a valence bond and the energy per unit length of the “string” of non-resonating bonds in Fig 4a. (This caution may be

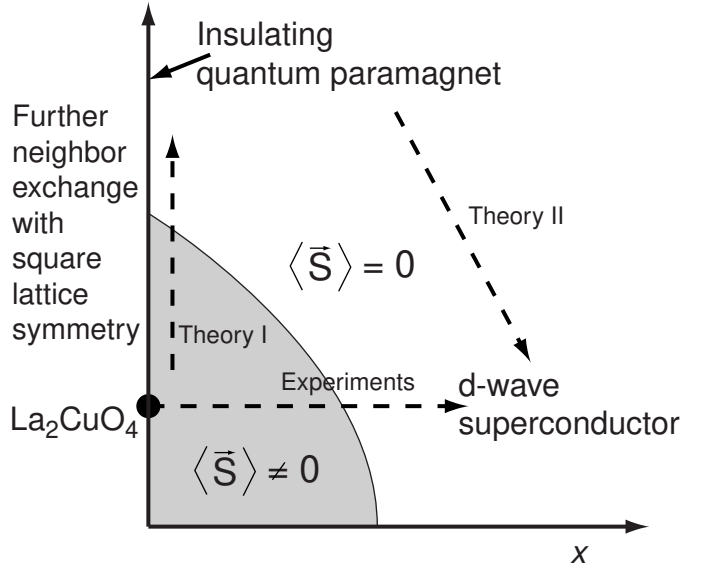


FIG. 1. Schematic phase diagram for the high temperature superconductors as a function of a ratio of the near neighbor exchange interactions and the hole concentration,  $x$ ; *e.g.* the vertical axis could be  $J_2/J_1$ , the ratio of the first to second neighbor exchange. The shaded region has broken spin-rotation symmetry, while the unshaded region does not. There are also numerous transitions in the charge ordering which are not shown. The path labeled “Theory I” represents studies of the insulating antiferromagnet in which the nearest neighbor square lattice Heisenberg antiferromagnet is modified to continuously destroy the Néel long-range order; such studies are reviewed in Section I and show that the non-magnetic region with  $\langle \vec{S} \rangle = 0$  has bond-centered charge order (possible the spin-Peierls order in Fig 2a). The path labeled “Theory II” represents studies of the doping of this spin-Peierls state (one such study is in Ref 9); one scenario, explored further in the present paper, is that the spin-Peierls order persists in a state with co-existing superconductivity, until there is eventually a phase transition to a  $d$ -wave superconductor at which translational symmetry is restored (with long-range Coulomb interactions, there must also be an insulating Wigner crystal state at very low doping). The nature of the magnetic ordering transition for  $\delta > 0$  (the line separating the shaded and unshaded regions) is expected to be in the same universality class<sup>9</sup> as that at  $\delta = 0$ ; for this reason, the combined theory along the paths I and II is expected to capture the essential physics of the experimental path (the horizontal dashed arrow).

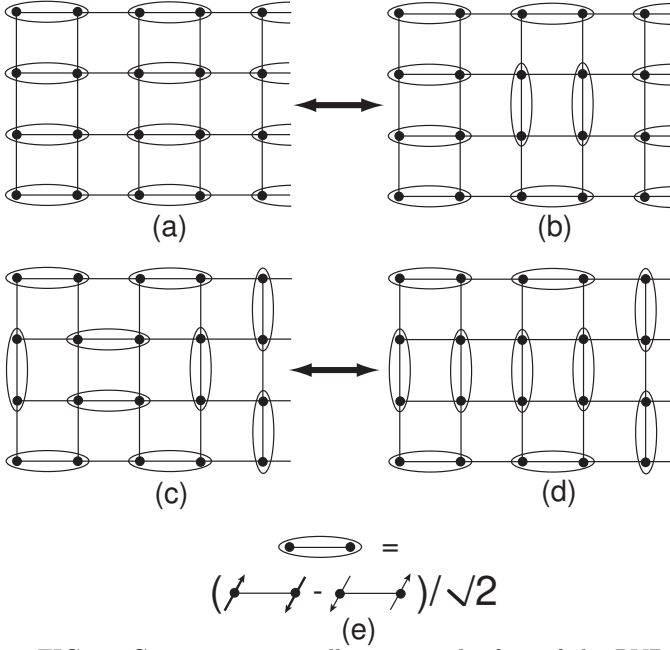


FIG. 2. Cartoon pictures illustrating the fate of the RVB state on the square lattice. The ellipses denote singlet valence bonds, as indicated in (e). There states (a) and (b) (and similarly, the states (c) and (d)) are connected by resonance around a plaquette. The state in (a) has the maximal number of plaquettes around which resonance can occur, and this was effect was shown<sup>6</sup> to lead to a broken lattice symmetry. A plausible candidate for the resulting quantum paramagnetic state is the one with spin-Peierls order—this state breaks the square lattice symmetry in the same pattern as the state in (a). Upon considering the O ions which lie on the centers of the bonds, we see that such a state may also be viewed as a bond-centered charge density wave of period 2.

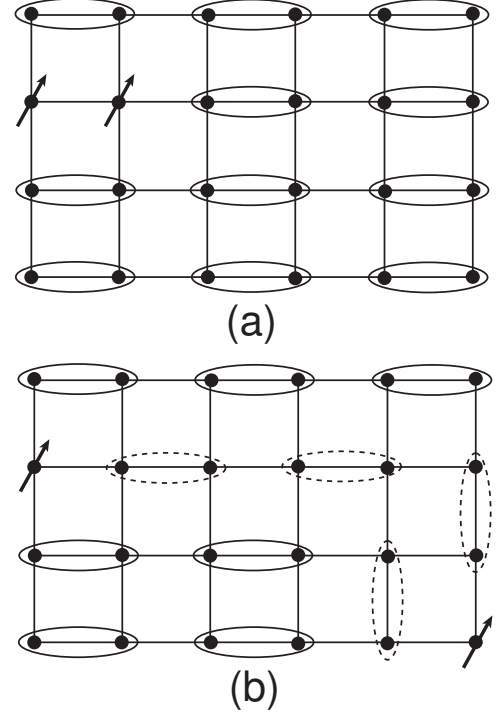


FIG. 3. (a) Cartoon picture of the bosonic  $S = 1$  particle excitation of the insulating paramagnet—a similar picture is also expected to apply in the superconductor. (b) Fission of the  $S = 1$  excitation into two  $S = 1/2$  spinons. Notice that the spinons are connected by a “string” of valence bonds (denoted by dashed lines) which are not able to resonate with their environment: this string costs a certain energy per unit length and leads to the confinement of spinons.

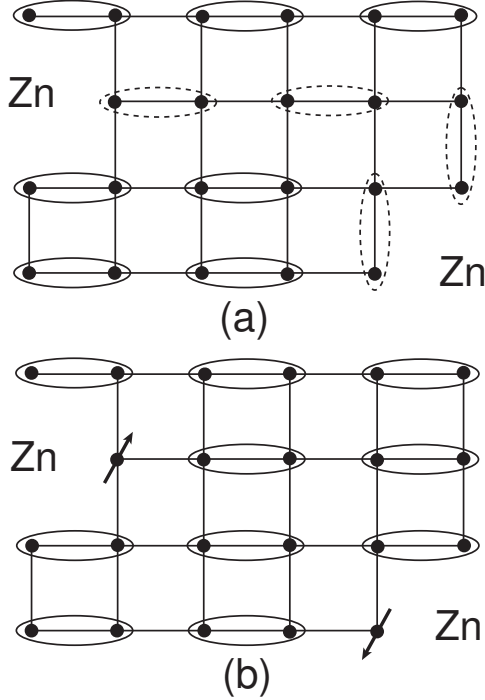


FIG. 4. Confinement of a  $S = 1/2$  moment near a non-magnetic Zn impurity<sup>12</sup>. We consider two Zn impurities and imagine moving them infinitely far apart. In the trial state in (a), all Cu spins are paired into singlet bonds; while this is preferable when the Zn impurities are not too far, there is a string of valence bonds connecting them which are not able to resonate, and this will eventually lead to the preference of the structure in (b). In this case there is no string defect in the spin-Peierls order, but each impurity has a free moment in its vicinity. For the case where the paramagnetic ground state was a deconfined “spin liquid”, we expect that a configuration like that in (a) would hold even when the impurities were infinitely far apart. We also emphasize an important distinction between Fig 3 and this figure: while true long-range charge order is required to guarantee the permanent confinement of  $S = 1/2$  spinons at all energy scales, the formation of a  $S = 1/2$  moment near a Zn impurity only requires that correlation length of the bond-centered charge order be “large enough” so that the energy cost of a broken bond in (b) is lower than that of the string in (a), and so may also happen in deconfined states.

relevant in the context of the ideas discussed recently by Senthil and Fisher<sup>15</sup>, who have argued that the proximity of deconfined paramagnetic states may be relevant to the understanding of broad photoemission spectra in the underdoped states—perhaps the cuprate superconductors are not too far from paramagnets near a confinement-deconfinement transition, and this could be way of satisfying apparently conflicting experimental requirements.)

It is also worth noting here that the above picture of confinement and bond-centered charge order in the paramagnet leads to a simple mechanism of binding of holes in pairs<sup>7,16</sup>. Just as the  $S = 1/2$  spinons in Fig 3 are confined are pairs, two holes injected into the paramagnet would also be confined to each other to minimize the disruption of the background charge order. Of course, it is also possible that each hole is confined separately with a  $S = 1/2$  spinon, and the two composites could then move infinitely far apart: however, this possibility involves the additional energy cost of the breaking a singlet bond into a pair of spinons.

It is important to keep in mind that all of the above discussion applies also to other confining, paramagnetic Mott insulators with bond-centered charge order, and not just to the spin-Peierls state in Fig 2a. The charge order could break the square lattice symmetry in other patterns, including possible states with plaquette order, or co-existing dimer and plaquette order<sup>17,18</sup>. We will study the spin-Peierls configuration in great detail here, but this is mainly because it serves as the simplest illustrative example of a confining, paramagnetic Mott insulator—the generalization to other patterns of bond-centered charge order should be straightforward.

Reviewing our discussion of two-dimensional Mott insulators so far: destroying the Néel order in the square lattice Heisenberg antiferromagnet by modifying the magnetic interactions leads to a quantum paramagnet with

- (i) a stable  $S = 1$  particle excitation (obtained by the confinement of  $S = 1/2$  spinons into a  $S = 1$  exciton),
- (ii) broken translational symmetry due to the appearance of a bond-centered CDW, and
- (iii) confinement of a  $S = 1/2$  moment in the vicinity of non-magnetic Zn/Li impurities.

We turn next to the second theoretical step outlined in Fig 1 (denoted Theory II): doping the confined Mott insulator with mobile charge carriers. Apart from a possible insulating Wigner crystal ground states at very low doping (such a Wigner crystal state must appear in the presence of long-range Coulomb interactions), the ground state is expected to be superconducting<sup>7,16,9</sup>, and this will also be the case in the calculations in the present paper. The pairing amplitude is found to be  $d$ -wave like<sup>7,9</sup> *i.e.* the pairing amplitude has opposite signs in the horizontal and vertical directions. By adjusting the strength of the Coulomb repulsion between the holes, we can modify the characteristic size of the hole pairs. Only for the larger hole pairs does the superconducting ground state possess gapless nodal fermionic excitations. The primary

purpose of our analysis here will be to assess the consequences of the contiguous confining Mott insulator on the properties of the superconductor. The central observation, as discussed in early work<sup>6,7</sup>, and more thoroughly investigated recently<sup>9</sup>, is that the properties (i)-(iii) of the Mott insulator survive for a finite range of non-zero hole concentration in the superconductor. Further, these results have received experimental support in recent years, which validates the strategy of Fig 1. We will discuss the fate of (i)-(iii) in the doped antiferromagnet, along with connections to the experiments in turn:

(i)  $S = 1$  collective spin exciton: In the confined insulator, the lowest energy excitation above the spin gap is a stable,  $S = 1$ , bosonic exciton with a minimum in its dispersion at  $(\pi, \pi)$ . Upon doping to the superconductor, additional gapped  $S = 1/2$  fermionic excitations are expected to appear<sup>19,20</sup> (these are the Bogoliubov quasiparticles). For sufficiently large doping, the fermionic spectral becomes gapless at four nodal points in the Brillouin zone, and so the global spin gap vanishes. In general, the  $S = 1$  boson will be unstable to decay into two of these fermionic excitations. However, constraints from momentum conservation can (and do) protect the integrity of the  $S = 1$  exciton in certain regions of the Brillouin zone. In particular, the  $S = 1$  exciton is likely to be stable near momenta  $(\pi, \pi)$ ; this can happen even if the fermionic excitations are gapless, provided the spacing between the nodal points does not equal  $(\pi, \pi)$ . Experimentally a  $S = 1$  neutron scattering resonance is indeed observed in the  $d$ -wave superconductors<sup>21–25</sup>, and it is our contention that this excitation is continuously connected to that in the spin-Peierls insulator. We will obtain explicit results for the evolution of the bosonic and fermionic spin excitations in this paper, from the spin-Peierls insulator, to the superconductor with gapless nodal excitations.

(ii) Broken translational symmetry: In the simplest scenario<sup>7,9</sup>, which can be realized for a range of couplings in models without long-range Coulomb interactions, the bond-centered CDW (or spin Peierls) order of the paramagnetic insulator survives in the doped superconductor all the way up to a critical doping at which full square lattice symmetry is restored in a transition to the  $d$ -wave superconductor; with Coulomb interactions, Wigner crystal states also appear for a range of very small hole doping, but otherwise the situation is similar. The critical theory of the vanishing of the bond-centered (or site-centered) CDW order in the  $d$ -wave superconductor has been discussed elsewhere<sup>9</sup>. For other parameters, more complex striped states are also possible, with a period larger than 2 sites and with modulation of the hole density on the sites. Experimentally, charge stripe states of period 4 have been clearly observed<sup>26,27</sup>, but it is not yet established whether the modulation of the spin density is site or bond centered. More recently, the observation of McQueeney *et al.*<sup>28</sup> in optimally doped and superconducting LSCO have been interpreted using a picture of bond-

centered charge stripes of period 2 (precisely those in Fig 2a). We will discuss these observations further in Section V.

(iii)  $S = 1/2$  moment near Zn/Li impurities: In principle, it is possible that the  $S = 1/2$  moment confined near a Zn/Li impurity in the paramagnetic Mott insulator disappears immediately at an infinitesimal hole doping concentration: one hole can be trapped near the Zn/Li impurity (at the position of the unpaired spin in Fig 4), and this configuration is compatible with the global preservation of the spin-Peierls (or other bond-centered charge-) order. However the kinetic energy cost, makes this unlikely. Barring this uninteresting possibility, the  $S = 1/2$  moment will survive in the superconductor, and this offers a natural explanation for the NMR experiments<sup>2</sup>. Eventually, the fermionic  $S = 1/2$  excitations of the superconductor will Kondo screen the moment<sup>29–31</sup>, but because of the linearly vanishing fermionic density of states at the Fermi level, this happens only above finite values of the impurity exchange coupling and particle-hole asymmetry (*i.e.* above a critical doping). Moreover, there is no fundamental reason for this Kondo screening transition to co-incide with the point at which translational symmetry is restored (this transition was discussed above in (i)). The two transitions could occur in either order as a function of increasing doping because, as discussed in (i), true long-range charge order is not required for the formation of the local  $S = 1/2$  moment. Indeed, the arguments of Fig 4 do not directly apply to the superconductor, which has deconfined, fermionic,  $S = 1/2$  excitations. However, they do guarantee the formation of local  $S = 1/2$  moment near an impurity in an insulator, and we are arguing here that this is a simple way of understanding the moment formation in the contiguous superconductor over a finite range of doping.

The purpose of this paper is to present a theory of doped antiferromagnets which displays the crossover from an insulator at zero doping (with or without long-range magnetic order) to a superconductor with gapless, nodal, fermionic  $S = 1/2$  excitations at some moderate doping. Further, we require the theory to obey properties (i)-(iii) directly at the mean-field level. While a large number of previous theories of doped antiferromagnets have been presented previously, none of them satisfy all of these requirements. The studies of Ref 9 were able to examine the intricate competition between different charge ordered states and superconductivity—however, the ground states were well away from a region of magnetic order, and there was no sharp, collective,  $S = 1$  excitation in the Gaussian fluctuations about the mean-field theory. Conversely, approaches which do yield confinement of spinons and collective  $S = 1$  excitations at zero or low doping<sup>6,32,33</sup> are not easily extended to reach a superconducting state with  $S = 1/2$  gapless nodal excitations at moderate doping.

Before embarking on the description of our method, we review some recent theoretical developments on related

questions.

Sushkov and collaborators have studied aspects of the phase diagram of Fig 1 both at zero and finite doping. At zero doping, they have examined the square lattice  $S = 1/2$  Heisenberg antiferromagnet with first ( $J_1$ ) and second ( $J_2$ ) neighbor exchange<sup>17</sup>: with increasing  $J_2/J_1$  they find a transition from the familiar Néel state to a paramagnetic state with bond-centered charge order as in Fig 2a, albeit with a small window of parameters at which the two orders co-exist; such a co-existence region is allowed in the framework of the earlier field-theoretic analysis<sup>8</sup>. At somewhat larger  $J_2/J_1$  they find further charge ordering which breaks an additional  $Z_2$  lattice symmetry: this pattern of charge ordering has also been seen in recent DMRG studies<sup>18</sup>. Sushkov<sup>34</sup> has also studied the evolution of the ground state as a function of doping along the experimental arrow in Fig 1: by a series expansion method he finds that after destruction of the Neel order, the ground state has the columnar spin-Peierls order of Fig 2a. Only at a significantly larger coupling is the full square lattice symmetry restored. All of these results are fully consistent with the approach outlined in our paper.

Mazumdar, Clay, and Campbell<sup>35–37</sup> have studied two-dimensional correlated electron models associated with the organic charge-transfer solids tetramethyl-tetrathiafulvalene (TMTTF), tetramethyl-tetraselenafulvalene (TMTSF), bisethylenedithio-tetrathiafulvalene (BEDT-TTF) and bisethylenedithio-tetraselenafulvalene (BETS). They have argued that these materials are characterized by quarter-filled band, and produced evidence for “bond order wave” in their models at quarter filling. These states are closely related to the period 4 bond-centered charge density wave state studied in Ref 9, and so also to the insulating and superconducting states with the symmetry of Fig 2a studied here.

Kivelson, Fradkin and Emery<sup>38</sup> have studied symmetry breaking in two-dimensional electronic systems using a rather general classification in terms of electronic liquid crystal phases. Their formulation (and their earlier theory<sup>39</sup> of the “spin gap proximity effect”) does not distinguish between the nature of bond- and site-centered charge order that we are paying particular attention to here. A significant portion of the superconducting state in their phase diagram overlaps with a region of nematic order. We believe that the orthorhombic anisotropy of this nematic order is ultimately driven by singlet bond correlations associated with the spin-Peierls order in Fig 2a; consequently this nematic region should show bond-centered smectic correlations with a period of 2 lattice spacings, as has been claimed in the experiments of Ref 28. We make this distinction more precise by discussing how the spin-Peierls and nematic orders are coupled. We can characterize the spin-Peierls order<sup>40</sup> in Fig 2a by a complex  $Z_4$  order parameter  $\Psi_{sp}$  which takes the values  $1, i, -1, -i$  on the four states obtained by rotating Fig 2a about any lattice site successively by  $90^\circ$ . Similarly, we can introduce a real Ising nematic order

parameter  $\Phi_n$  which is  $+1$  ( $-1$ ) for a nematic polarized along the  $x$  ( $y$ ) direction. Then the symmetry properties of the two order parameters show that<sup>40</sup>

$$\Phi_n \sim \Psi_{sp}^2. \quad (2)$$

A detailed Landau theory and fluctuation analysis of the interplay between these two order parameters is presented in Appendix A. It is our picture, based on the physical arguments above, that  $\Psi_{sp}$  is the primary order parameter, and that  $\Phi_n$  is tied to it via (2).

An important ingredient in the work of Carlson, Orgad, Kivelson, and Emery<sup>41,39</sup> is the crossover from the physics of a one-dimensional electron gas moving in the vertical direction in Fig 2a at short scales, to a coupled two-dimensional system at long scales. This should be contrasted from our approach, in which we do not find any quasi-one-dimensional regime. Although the lattice symmetry of our states is similar to those considered by these authors, the physics is always intrinsically two-dimensional, albeit with a spatial anisotropy. Indeed, the arguments for confinement and bond-centered charge order in Figs 2 and 3 rely crucially on the two-dimensionality of the system.

Zaanen and collaborators<sup>42</sup> have recently given a bold physical picture of the microstructure of stripes and their relationship to high temperature superconductivity. They take a solitonic, low-dimensional perspective, in which special attention is paid to excitations at various boundaries and dislocations in the stripe order. In contrast, our perspective here is a higher (two-) dimensional point of view, appropriate to systems not too far below their upper-critical dimension. So *e.g.* we view the spin-Peierls order parameter  $\Psi_{sp}$  as a “soft-spin” field with large and continuous variations in its local amplitude, rather than a field with 4 discrete possible values in different regions of space separated by identifiable domain walls. The advantage of our perspective is that it allows a complete (in principle) and systematic treatment of the coupling of fermionic degrees of freedom to the various order parameters in a Landau-theory like scattering framework<sup>9,43</sup>.

White and Scalapino<sup>44</sup> have presented results for charge order in DMRG studies of doped antiferromagnets. They find that site and bond centered stripes are almost degenerate in their energy. They do observe a period 4 bond-centered charge stripe state<sup>9</sup>, but have not so far seen a state with the period 2 symmetry of Fig 2a.

Castro Neto<sup>45</sup> has recently presented an interesting analysis of a striped superconductor, coupling transverse stripe fluctuations between regions of high and low hole density. Notably, he also finds pronounced tendency towards bond-centered charge order with the symmetry of Fig 2a.

Lannert, Fisher, and Senthil<sup>46</sup> have considered Berry phase effects in a  $Z_2$  gauge theory of correlated electron systems. Close to half-filling, they find that these Berry phases induce bond-centered charge order in both insulating and superconducting phases, in a manner closely

analogous to that found in Ref 6 in paramagnetic Mott insulators. They also discuss the critical properties of a transition between superconducting and insulating states at half filling, with both phases containing a background charge order with the symmetry of Fig 2a.

We now outline the remainder of the paper. In Section II we introduce the central formalism of bond operators, and its application to doped antiferromagnets. The main results of bond operator theory of the square lattice antiferromagnet are presented in Section III, with most details of the mean-field calculations being relegated to Appendices B, C and D: the important phase diagram is in Fig 6. The critical theory for the onset of nodal fermion excitations is in Section IV. Section V differs from the remainder of the paper in that it considers systems in which the bond-centered charge order is *not* present. Instead it considers the case when the spin-Peierls order is dynamically fluctuating and describes its influence on the optical phonon spectrum of the CuO<sub>2</sub> plane—we find that the calculated phonon spectrum is indeed strikingly similar to recent neutron scattering observations. The main conclusions are stated in Section VI. Finally, in Appendix A we describe the interplay between the spin-Peierls states considered in this paper, and states with electronic “nematic” order.

## II. BOND OPERATORS

Our approach is a generalization of the bond operator theory of Ref 47 (and the related work of Ref 48) to doped antiferromagnets. The earlier work<sup>47</sup> was designed for insulating systems, and has since been applied successfully in a number of studies of spin ladder and related compounds<sup>49–56</sup>, and also in bilayer quantum Hall systems<sup>57,58</sup>. Here we shall extend the formalism to doped antiferromagnets; a closely related extension was discussed by Lee *et al.*<sup>59</sup> but only applied to one-dimensional systems. Eder<sup>60</sup>, Sushkov<sup>34</sup>, and Vojta and Becker<sup>61</sup> have also considered doped systems by associated methods. Recently, Jurecka and Brenig<sup>62</sup> have used a bond operator method to analyze a Kondo lattice model using a formulation that bears some similarity to ours.

While our bond operator formalism can, in principle, be applied to an arbitrary doped antiferromagnet, it induces a bias by using a basis of states which explicitly refer to a preferred, disjoint pairing of all the sites. A full and exact solution of the bond operator Hamiltonian should restore the full symmetry of the underlying Hamiltonian in which this preferred pairing may be absent. However, in practice, this restoration of symmetry is difficult to achieve, and this is the principal shortcoming of the bond operator method. So the main utility of the approach lies in treating systems in which there is a natural pairing of sites in the ground state, either imposed by the Hamiltonian, or by a spontaneous symmetry break-

ing. In this paper, we will restrict consideration to the case where the ground state has spontaneously acquired the bond-centered charge density wave (spin-Peierls) order with the symmetry of Fig 2a: there is evidently a natural pairing of sites in this structure. In the presence of this background spin Peierls order, the method can then address the competition between magnetic Néel order and superconductivity, and follow the evolution of the fermionic  $S = 1/2$  and the bosonic  $S = 1$  excitations.

We will now introduce the formalism by showing the exact mappings between bond and site operators of a pair of sites. In hole-doped antiferromagnets, we can project out all states with 2 electrons on one site, and this leaves a total of 9 states in a pair of sites. Let  $c_{1a}^\dagger$  and  $c_{2a}^\dagger$  ( $a = \uparrow, \downarrow$ ) be the electron creation operators on the two sites. Then, as in the insulator<sup>47</sup>, we introduce four bond boson creation operators,  $s^\dagger$  and  $t_\alpha^\dagger$  ( $\alpha = x, y, z$ ) which are defined by ( $\sigma_{ab}^\alpha$  are the Pauli matrices, and  $\varepsilon_{ab}$  is the second-rank antisymmetric tensor with  $\varepsilon_{\uparrow\downarrow} = 1$ )

$$\begin{aligned} s^\dagger|v\rangle &= \frac{1}{\sqrt{2}}\varepsilon_{ab}c_{1a}^\dagger c_{2b}^\dagger|0\rangle \\ t_\alpha^\dagger|v\rangle &= \frac{1}{\sqrt{2}}\sigma_{bc}^\alpha\varepsilon_{ca}c_{1a}^\dagger c_{2b}^\dagger|0\rangle, \end{aligned} \quad (3)$$

where  $|0\rangle$  is the electron vacuum *i.e.* the state with no electrons on the two sites, while  $|v\rangle$  is an unphysical state in which none of the bond bosons or fermions are present. To describe the remaining 5 states of the doped antiferromagnet, we introduce the bond fermionic operators  $h_{1a}^\dagger$  and  $h_{2a}^\dagger$ , and the additional bond bosonic operator  $d^\dagger$  which are defined by

$$\begin{aligned} h_{1a}^\dagger|v\rangle &= c_{1a}^\dagger|0\rangle \\ h_{2a}^\dagger|v\rangle &= c_{2a}^\dagger|0\rangle \\ d^\dagger|v\rangle &= |0\rangle. \end{aligned} \quad (4)$$

The operators  $s, d, t_\alpha$  all obey the canonical boson commutation relations, while the  $h_{1a}, h_{2a}$  obey canonical fermion relations. Of course, the total space of states in Fock space of these 5 bosons and 4 fermions is much larger than the 9 states allowed in the doped antiferromagnet. To restrict to the physical subspace we must impose the single constraint

$$s^\dagger s + t_\alpha^\dagger t_\alpha + h_{1a}^\dagger h_{1a} + h_{2a}^\dagger h_{2a} + d^\dagger d = 1. \quad (5)$$

In the subspace constrained by (5), we can now write down exact expressions for arbitrary electron operators in terms of the bond operators. First, for the electron spin operators

$$\begin{aligned} S_{1\alpha} &= \frac{1}{2}c_{1a}^\dagger\sigma_{ab}^\alpha c_{1b} \\ S_{2\alpha} &= \frac{1}{2}c_{2a}^\dagger\sigma_{ab}^\alpha c_{2b}, \end{aligned} \quad (6)$$

we have the following expressions which generalize those in Ref 47

$$\begin{aligned}
S_{1\alpha} &= \frac{1}{2}(s^\dagger t_\alpha + t_\alpha^\dagger s - i\epsilon_{\alpha\beta\gamma} t_\beta^\dagger t_\gamma) + \frac{1}{2}\sigma_{ab}^\alpha h_{1a}^\dagger h_{1b} \\
&\equiv \tilde{S}_{1\alpha} + \frac{1}{2}\sigma_{ab}^\alpha h_{1a}^\dagger h_{1b} \\
S_{2\alpha} &= -\frac{1}{2}(s^\dagger t_\alpha + t_\alpha^\dagger s + i\epsilon_{\alpha\beta\gamma} t_\beta^\dagger t_\gamma) + \frac{1}{2}\sigma_{ab}^\alpha h_{2a}^\dagger h_{2b} \\
&\equiv \tilde{S}_{2\alpha} + \frac{1}{2}\sigma_{ab}^\alpha h_{2a}^\dagger h_{2b}, \tag{7}
\end{aligned}$$

where  $\epsilon_{\alpha\beta\gamma}$  is the third-rank antisymmetric tensor with  $\epsilon_{xyz} = 1$ . By considering various matrix elements of the electron creation operators, we can also obtain

$$\begin{aligned}
c_{1a}^\dagger &= h_{1a}^\dagger d + \frac{1}{\sqrt{2}}\epsilon_{ab}s^\dagger h_{2b} - \frac{1}{\sqrt{2}}\epsilon_{ac}\sigma_{cb}^\alpha t_\alpha^\dagger h_{2b} \\
c_{2a}^\dagger &= h_{2a}^\dagger d + \frac{1}{\sqrt{2}}\epsilon_{ab}s^\dagger h_{1b} + \frac{1}{\sqrt{2}}\epsilon_{ac}\sigma_{cb}^\alpha t_\alpha^\dagger h_{1b}. \tag{8}
\end{aligned}$$

Indeed, the expression (7) can be obtained (8) after repeated application of the constraint (5). In a similar manner, we can also obtain from (8) (or by direct consideration of matrix elements) the useful expressions

$$\begin{aligned}
S_{1\alpha}S_{2\alpha} &= \tilde{S}_{1\alpha}\tilde{S}_{2\alpha} = -\frac{3}{4}s^\dagger s + \frac{1}{4}t_\alpha^\dagger t_\alpha \\
c_{1a}^\dagger c_{2a} + c_{2a}^\dagger c_{1a} &= h_{1a}^\dagger h_{2a} + h_{2a}^\dagger h_{1a} \\
c_{1a}^\dagger c_{1a} &= 1 - h_{2a}^\dagger h_{2a} - d^\dagger d \\
c_{2a}^\dagger c_{2a} &= 1 - h_{1a}^\dagger h_{1a} - d^\dagger d. \tag{9}
\end{aligned}$$

We have now completed the definition of the bond operator formalism. By application of (7,8,9) an arbitrary Hamiltonian can be written down in terms of the bond operators. Notice that the right hand sides of all of these equations commute with constraint (5) and so will the resulting Hamiltonian. For most systems of interest, the Hamiltonian will only contain terms which are quartic in the bond operators—we will merely apply the simplest possible Hartree-Fock-BCS theory to solve such a model.

At this point, it is worth pointing an important distinction between the present approach and the familiar “slave” boson and fermion theories. A crucial advantage of our approach is that there are no long-range gauge forces associated with the fluctuations about our simple Hartree-Fock-BCS theory: the  $s$  boson is strongly condensed in all the phases, and so the  $U(1)$  gauge symmetry associated with (5) is always badly broken. Consequently, the quantum numbers of the bare excitations are also those of the renormalized quasiparticles; this is rarely the case in the slave particle approaches. In particular, in the insulating phases, the main elementary excitation will be the bosonic  $t_\alpha$  particle; in the paramagnet this is the  $S = 1$  exciton, while in the Néel state it reduces to the two spin waves. In the superconducting states, we will find that the  $t_\alpha$  excitations persist as the  $S = 1$  spin exciton, and the  $h_{1a}$ ,  $h_{2a}$  quanta turn into the fermionic,  $S = 1/2$  Bogoliubov quasiparticles. So there is a direct and transparent relationship between the quantum numbers of the bond operators and those of

the elementary excitations of all the ground states. This is main benefit of our approach, and we are not aware of any previous theory which has satisfied these criteria. Of course, some of the quantum numbers of our confining theory can also be obtained in a direct Hartree-Fock-BCS theory of an extended Hubbard model of the electrons. However, this has to be followed by an RPA analysis of collective modes to obtain the  $S = 1$  exciton; moreover, in such theories, the largest energy scale in the problem, the charge gap in the Mott insulator, is unphysically related to the strength of the magnetic or charge order, and is hence grossly underestimated.

We conclude this section by noting how the bond operator theory satisfies criteria (i)-(iii) of Section I. (i) As just noted, the  $t_\alpha$  quanta are gapped  $S = 1$  excitons in the insulating paramagnet, and persist as sharp excitations in the superconductor for a finite range of doping. (ii) Any mean-field theory using the bond operator formalism will prefer the bonds on which the operators reside over the others, and this naturally leads to a broken lattice symmetry for symmetric Hamiltonians. Indeed, the primary weakness of the bond operator formalism is that there is no simple way to restore this symmetry. (iii) Placing a Zn/Li impurity means that the partner of one site has been removed. The excitations of this site (and only this site) therefore cannot be described by the bond operators above: instead we need a fermionic spinor,  $h_a$ , to create the  $S = 1/2$  state with one electron, and a spinless boson,  $b$ , to represent the hole. At zero doping, the  $h_a$  particle constitutes the free  $S = 1/2$  moment near the impurity. This particle will be bound near the impurity site for a finite range of doping, and so the moment will persist for a while in the superconductor.

### III. RESULTS

We applied the bond-operator method to the  $t$ - $J$ - $V$  model defined by the Hamiltonian

$$\begin{aligned}
H = \sum_{\langle ij \rangle} &\left[ -t_{ij} \left( c_{ia}^\dagger c_{ja} + c_{ja}^\dagger c_{ia} \right) + J_{ij} S_{ia} S_{j\alpha} \right. \\
&\left. + V_{ij} c_{ia}^\dagger c_{ia} c_{jb}^\dagger c_{jb} \right] - \mu \sum_i c_{ia}^\dagger c_{ia}, \tag{10}
\end{aligned}$$

where the sum  $\langle ij \rangle$  extends over nearest neighbor pairs on a two-leg ladder or a square lattice, and it is implied that all states with two electrons on any site have been projected out. The  $t_{ij}$  are the electron hopping matrix elements, the  $J_{ij} > 0$  are the antiferromagnetic exchange interactions, the  $V_{ij} > 0$  are nearest neighbor repulsive Coulomb interactions, and  $\mu$  is the chemical potential. The values of the  $t_{ij}$ ,  $J_{ij}$  and  $V_{ij}$  are indicated in Fig 5 for both the two-leg ladder and the square lattice. For the two-leg ladder we have  $t_{ij} = t$ ,  $J_{ij} = J$ ,  $V_{ij} = V$  on the horizontal links, and  $t_{ij} = t$ ,  $J_{ij} = \lambda J$ , and  $V_{ij} = V$  on the vertical links. We view the square lattice as a



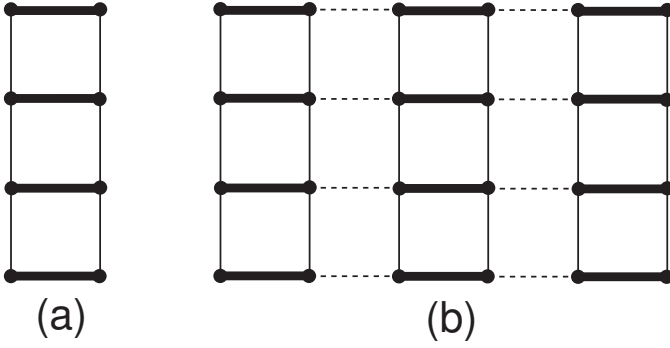


FIG. 5. Definition of the Hamiltonian  $H$  in (10). The two-leg ladder is in (a), while the square lattice is viewed as a set of coupled two-leg ladders in (b). Notice that the symmetry of (b) is the same as the state in Fig 2a. The thick links have  $t_{ij} = t$ ,  $J_{ij} = J$ ,  $V_{ij} = V$ , the thin vertical links have  $t_{ij} = t$ ,  $J_{ij} = \lambda J$ , and  $V_{ij} = V$ , while the dashed links have  $t_{ij} = t'$ ,  $J_{ij} = \lambda' J$ , and  $V_{ij} = V$ .

collection of adjacent two-leg ladders: then the couplings on each ladder are the same as before, while on the links between the ladders we have  $t_{ij} = t'$ ,  $J_{ij} = \lambda' J$ , and  $V_{ij} = V$ . This parameterization is chosen so that in both cases the exchange interaction decouples into disconnected pairs of sites (“dimers”) at  $\lambda = \lambda' = 0$ . Further, at  $\lambda = \lambda' = 1$ ,  $H$  has the full symmetry of the square lattice. However, as discussed earlier, our mean-field theory will continue to have a ground state with the symmetry of Fig 5b (or, equivalently, Fig 2a) even at these values of  $\lambda$ ,  $\lambda'$ : this implies the presence of spontaneous bond-centered charge order of period 2 in the ground state.

The calculation proceeds by the substitution of the operator representations in Section II into (10), followed by a Hartree-Fock-BCS treatment of all the quartic terms. The procedure is quite lengthy, but the computations are quite similar to those in earlier work. So details have been presented in Appendices: Appendix B deals with the two-leg ladder, while Appendix C considers the generalization to the coupled two-leg ladders making up the square lattice.

Here we will discuss the results of such a calculation. All of the phases can be characterized by a specification of the non-zero expectation values of various combinations of the bond operators in the ground state.

All states have the non-zero expectation values

$$\langle s \rangle \neq 0 \quad ; \quad \langle t_\alpha^\dagger t_\alpha \rangle \neq 0. \quad (11)$$

These non-zero values do not break any physical symmetries of the Hamiltonian, and merely serve to break the  $U(1)$  gauge symmetry associated with the constraint (5). As noted earlier, this is fortunate as no long-range gauge forces then appear in the fluctuations about our ground states. In addition, all phases will also have non-zero expectation values of the operators  $t_\alpha^\dagger t_\alpha$  and  $h_{1,2a}^\dagger h_{1,2a}$ , which do not break any symmetries of the Hamiltonian, and also commute with the constraints (5).

At zero and non-zero doping we have find also find magnetically ordered states. These are characterized by the non-zero expectation value

$$\langle t_\alpha \rangle \neq 0; \quad (12)$$

so condensation of single  $t_\alpha$  bosons (which are  $S = 1$  particles) leads to the appearance of magnetic order. This also implies that the magnetic ordering transition will be described by the field theory a 3-component spin-vector order parameter. Further, provided the ordering wavevector is not exactly equal to the spacing between the points of gapless fermionic excitations, the universality class of the transition is the same as that in the  $O(3)$  non-linear sigma model<sup>9,63</sup>. This is to be contrasted with magnetic ordering transitions in Schwinger boson theories, which are associated with the condensation of  $S = 1/2$  particles, possibly interacting with each other via gauge forces.

The singlet superconducting states have the anomalous expectation values

$$\langle d \rangle \neq 0 \quad ; \quad \varepsilon_{ab} \langle h_{1,2a} h_{1,2b} \rangle \neq 0. \quad (13)$$

The spatial pattern of these anomalous condensates determines the symmetry of the Cooper pair wavefunction, and whether there are any nodal fermionic quasiparticles.

Finally, we also found states with co-existing magnetic order and superconductivity, in which both (12) and (13) hold.

Our main results are summarized in Fig 6. First, let us review the results at  $x = 0$ , in the insulator. Here the calculations are very similar to those already considered in Ref 47. For small  $\lambda'$ , the ground state is an insulating paramagnet: the symmetry of the Hamiltonian and the ground state is that of Fig 5b, and the  $t_\alpha$  excitations have an energy gap: these excitations constitute a  $S = 1$  collective spin resonance (or a  $S = 1$  exciton). At a critical value of  $\lambda'$ , the excitation gap vanishes, and long-range Néel order sets in.

Now we turn to non-zero doping. In our Hartree-Fock-BCS mean-field theory, we find that superconductivity appears at any non-zero doping for small  $\lambda'$ . As one of us has discussed in Ref. 9 (along with references to the earlier literature), this is surely an artifact of our approximation at very small  $x$ : in the presence of long-range Coulomb interactions, Wigner crystal states will be present for very small hole concentration. Even in our theory without long-range Coulomb interactions, long-range charge inhomogeneities can also appear in our mean-field framework<sup>9</sup>; however, we will neglect these here for simplicity. As indicated in Fig 6, the superconductivity persists in a non-magnetic state even at  $\lambda' = 1$  for  $x > 0.082$ . In our present calculation, this small  $x$  superconducting state has bond-centered charge order of period 2, but more complex bond-centered charge-ordered states are also possible<sup>9,64</sup>. We also expect that the superconductivity will co-exist with antiferromagnetism, but we did not undertake a complete solution

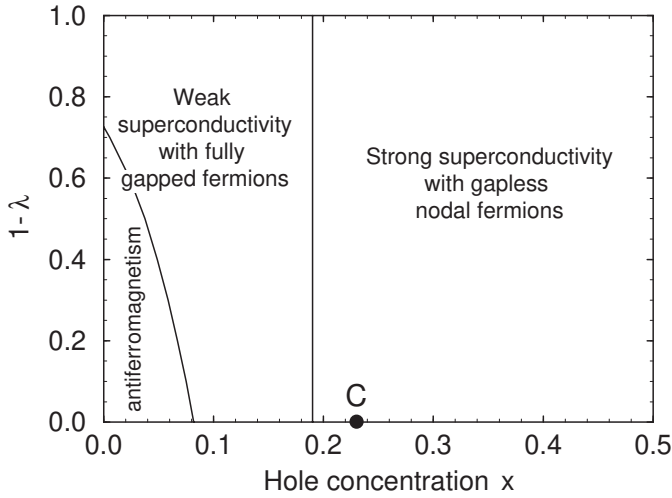


FIG. 6. Phase diagram of the square lattice Hamiltonian  $H$  in (10) for the configuration shown in Fig 5b. Notice the similarity of this phase diagram to the schematic phase diagram in Fig 1: the main difference is that the vertical axis here explicitly breaks the symmetry of the square lattice down to Fig 5b, while the translational symmetry breaking is spontaneous everywhere in Fig 1. Results are shown here for  $t' = t$ ,  $\lambda = 1$  and  $t/J = 3.0$  as a function of the hole concentration  $x$  and  $1 - \lambda'$ . The model has full square lattice symmetry at  $1 - \lambda' = 0$ , and the exchange interaction separates into that on decoupled two-leg ladders at  $1 - \lambda' = 1$ . The nearest-neighbor Coulomb repulsion,  $V$  is taken to have a very large positive value, and the results are indistinguishable from those at  $V = \infty$ . The phase boundary towards antiferromagnetism was determined by the point at the  $t_\alpha$  excitation spectrum had a vanishing spin gap, signaling the onset of a phase in which (12) was valid. The “weak” and “strong” superconductivity distinction is qualitative, and is indicated by the rapid change in the physical superconducting order parameter in Fig 7 around  $x = 0.2$ . The antiferromagnetic phase co-exists with weak superconductivity at non-zero  $x$ . The nearly vertical phase boundary indicates the quantum phase transition at which nodal fermions first appear: this transition is discussed in Section IV. C denotes the point where the spontaneous bond-centered charge order of the square lattice is expected to disappear with increasing  $x$ ; the bond-centered charge order is explicitly present in the Hamiltonian for  $1 - \lambda' > 0$ , and is spontaneous only for non-zero  $x$  before the point C and  $1 - \lambda' = 0$ . The present bond operator approach was not used to determine the position of C; nevertheless, following Ref 9 we are able to present a theory of the critical properties of C in Appendix A

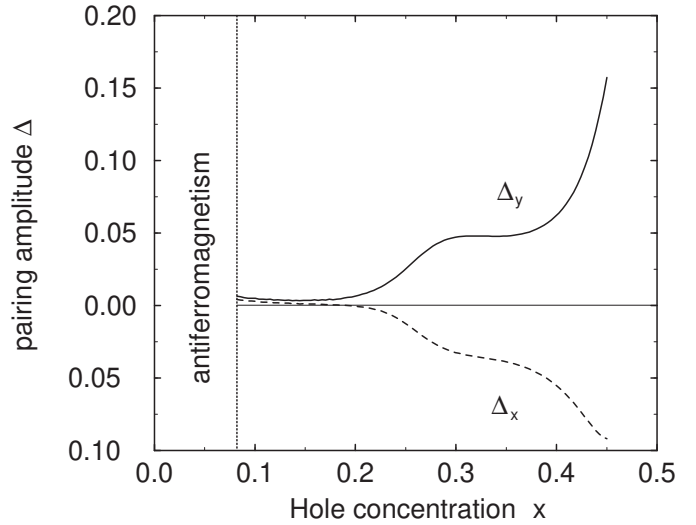


FIG. 7. Pairing amplitudes ( $\Delta$ ) as a function of hole concentration ( $x$ ) when  $t/J = 3.0$ , and  $\lambda = \lambda' = 1.0$ , i.e. the isotropic case. The pairing amplitude in the vertical direction of Fig 5b is  $\Delta_y$ , and that in the horizontal direction is  $\Delta_x$ . For  $x \leq 0.082$ , there is instability to long-range antiferromagnetism due to the collapse of the gap of  $S = 1$  particle excitation,  $t_\alpha$ . When  $0.082 < x \leq 0.192$ , non-magnetic superconducting state is stable, and the pairing amplitudes are of the same sign, but of very small value. For doping concentration larger than roughly 0.2, the pairing amplitudes have opposite signs, which, in turn, gives rise to nodal fermions.

of the mean-field equations within the antiferromagnetic phase because of the complexity of the calculation. As in the insulator, the onset of antiferromagnetism was determined by the point where the  $t_\alpha$  boson had a vanishing gap in its spectrum.

We characterized the superconducting state by determining pairing amplitudes,  $\Delta_{x,y}$ , which characterize the pairing of the holes,  $h_{1,2}$ , in the  $x$  and  $y$  directions. These quantities are described more precisely in Appendices B and C, and their connection to the physical electron pairing amplitudes is discussed in Appendix C1. Their values are plotted as a function of the hole concentration,  $x$ , in Fig 7. Note that  $\Delta_x$  and  $\Delta_y$  are roughly of the same magnitude: this means that the superconductivity is genuinely two-dimensional, and there is no regime in which a quasi-one-dimensional Luther-Emery liquid-like behavior holds. Indeed, it is even possible for  $\Delta_x$  to be larger than  $\Delta_y$ , which would make the superconductivity stronger in the  $x$  direction rather than in the vertical “stripe” direction. This latter phenomenon appears to be similar in spirit to the analyses of Refs 35–37.

For small  $x$ , the pairing amplitudes are non-zero but quite small; moreover, the pairing amplitudes in the horizontal and vertical directions have the same sign in our mean field theory. We will refer to this as the weak superconductivity regime. It is possible that, upon including quantum fluctuations, the ground state in this weak pairing regime is easily susceptible to a quantum transition

to an insulating state with some additional translational symmetry breaking. Also note that the pairing amplitude is nonzero at the boundary of the onset of antiferromagnetic order: we therefore expect the superconductivity to survive within the antiferromagnetic phase.

For larger  $x$ , the pairing amplitude in Fig 7 increases rapidly and we reach a “strong superconductivity” regime. The pairing amplitudes now have opposite signs in the horizontal and vertical directions, and this permits gapless nodal fermionic quasiparticle excitations, as shown explicitly in our results below. However, there is one important feature associated with the appearance of the nodal particles that is worth emphasizing. Originally, our calculations were carried out with the nearest-neighbor Coulomb repulsion  $V = 0$ . In this case we found that the pairing of the holes occurred primarily by the condensation of the  $d$  bosons. Because of the resulting very short-range pairing we found no nodal points, even though the pairing amplitude had opposite signs in the horizontal and vertical directions. It was only when we had turned on a  $V$  of the order of the bandwidth, which significantly reduced the amplitude of the  $d$  boson condensate and made the hole pairing more long-ranged, did we find the appearance of the nodal excitations.

We now describe our results for the elementary excitations of the superconducting states in our phase diagram. First, we discuss the fermionic  $S = 1/2$  excitations; in principle, these are observable in photoemission or tunneling experiments. Note that the unit cell of Fig 5b has two sites, and so the first Brillouin zone extends between  $-\pi/2$  and  $\pi/2$  in the  $x$  direction, and between  $-\pi$  and  $\pi$  (as usual) in the  $y$  direction. Consequently, half the fermionic excitations in the first Brillouin zone of the original square lattice will be folded back, by a Bragg reflection in the vertical planes at  $\pm\pi/2$ , into a second band in the first Brillouin zone of the lattice of Fig 5b. We will refer to these two bands as the ‘bonding’ and ‘anti-bonding’ bands, based upon their wavefunctions within the dimers, as discussed in Appendices B and C. We show the  $S = 1/2$  fermionic bands in the weak-pairing regime in Figs 8 and 9. There is a gap across the entire Brillouin zone. However, because of the very small pairing amplitude, the fermionic excitation energy becomes very small along an incipient “Fermi surface” in the Brillouin zone. This Fermi surface line is indicated by the solid line in the inset of Fig 9. The position of this Fermi surface is similar to that in the computation by Sushkov<sup>34</sup>, who also discussed its relationship to photoemission experiments.

Next, we turn to a discussion of the fermionic excitations at larger  $x$ , where the superconductivity is stronger. The  $S = 1/2$  excitation spectra are now shown in Figs 10 and 11. Overall, the results at higher energies, are quite similar to those in Figs 8 and 9, but there is now a dramatic difference at lower energies. There is a gapless nodal-point near  $(\pi/2, \pi/2)$ , and this is made possible by the  $d$ -wave-like pairing amplitudes. The spectra in Fig 9 and 11 cannot be continuously connected, and there must

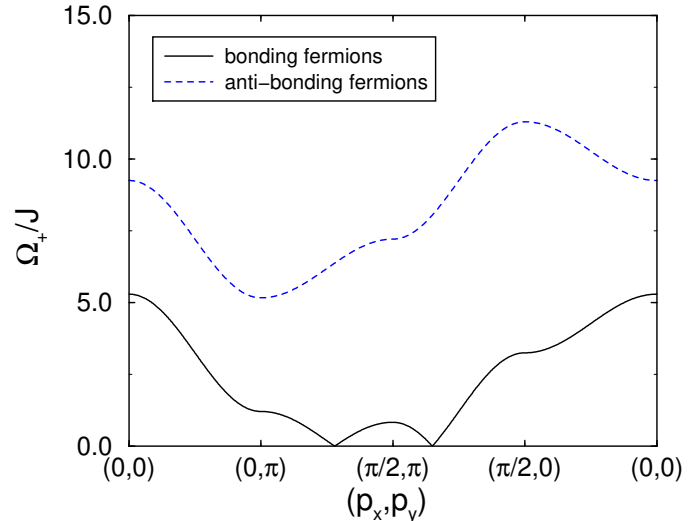


FIG. 8. Dispersion curves of the bonding and anti-bonding  $= 1/2$  fermionic excitations in the weak pairing regime with  $x = 0.1$ ,  $t/J = 3.0$ , and  $\lambda = \lambda' = t'/t = 1$ . There appear to be fermionic excitations at energies very close to 0, but the blow-up in Fig 9 shows that there is indeed a gap in the fermionic spectrum. The  $x$ -axis is chosen to take a representative straight path connecting points in the first Brillouin zone: from  $(p_x, p_y) = (0, 0)$  to  $(0, \pi)$  to  $(\pi/2, \pi)$  to  $(\pi/2, 0)$  to  $(0, 0)$ .

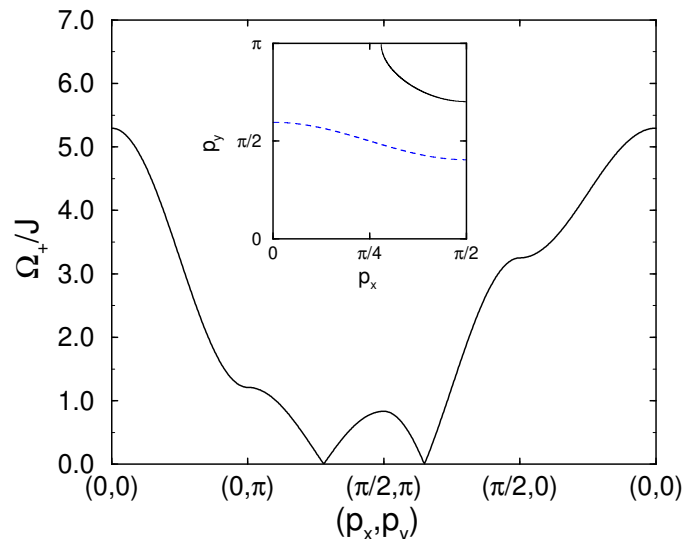


FIG. 9. Blow-up of the fermionic dispersion in Fig 8 at the lowest non-zero energies. Notice that there is indeed a finite gap in the fermionic spectrum. This is also made clear in the inset: the solid line shows the line at  $\tilde{\epsilon}_+(\mathbf{k}) = 0$  while the dashed line indicates where  $\tilde{D}_+(\mathbf{k}) = 0$  (notations described in Appendices B and C). For gapless excitations, both quantities have to vanish, and the absence of a crossing point between the lines indicates that a gap is always present. The solid line in the inset is also the location of the incipient Fermi surface which has been quenched by pairing—the position of this surface is similar to that in Ref 34.

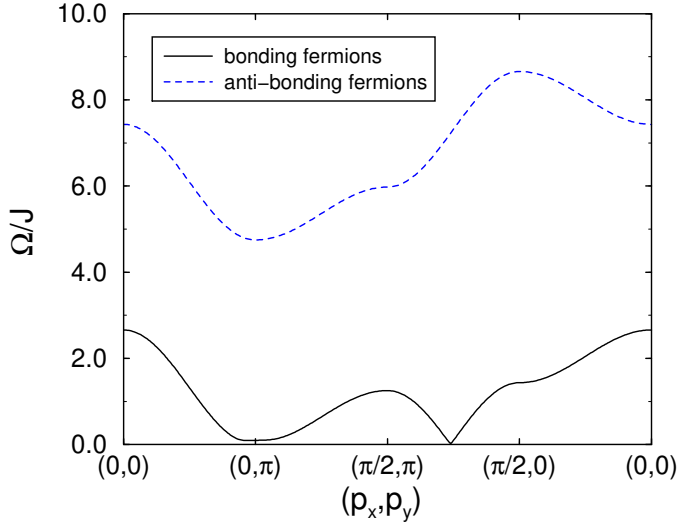


FIG. 10. Dispersion curves of the bonding and anti-bonding  $S = 1/2$  fermionic excitations with  $x = 0.3$ ,  $t/J = 3.0$ , and  $\lambda = \lambda' = t'/t = 1$  (as in Fig 8 but at a larger doping). At this value of  $x$ , there is a nodal quasiparticle excitation not too far from  $(\pi/2, \pi/2)$ .

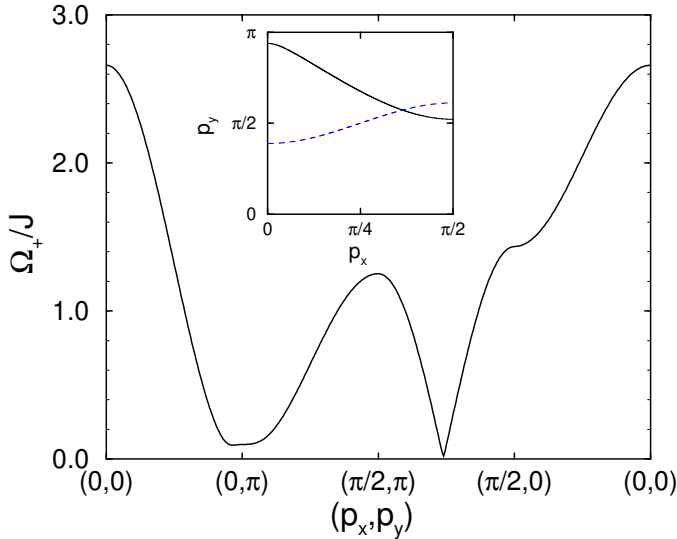


FIG. 11. Blow-up of the fermionic dispersion in Fig 10 at the lowest non-zero energies (as in Fig 9 but at a larger doping). Notice that there is clearly a gapless nodal point not too far from  $(\pi/2, \pi/2)$ , as is also clear from the inset, where the two curves now cross. The pairing gap near the “antinodal point”,  $(\pi, 0)$ , remains finite.

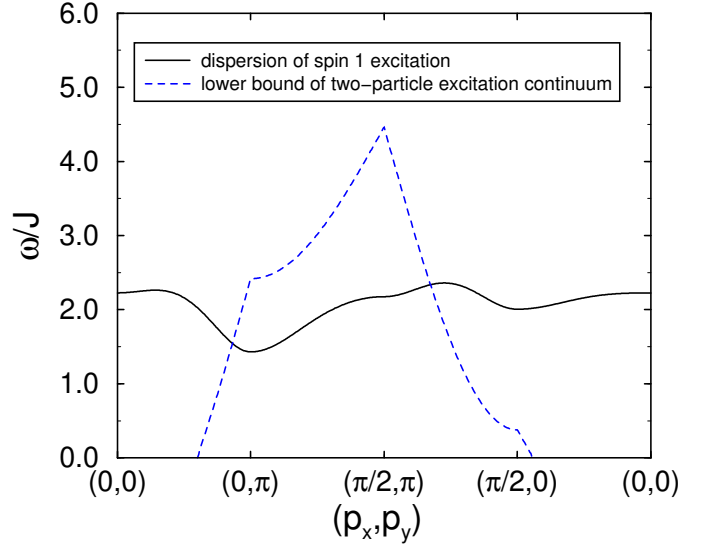


FIG. 12. Dispersion curve (full line) of  $S = 1$ ,  $t_\alpha$  particle excitation with  $x = 0.1$ ,  $t/J = 3.0$ , and  $\lambda = \lambda' = t'/t = 1$ . The pairing is weak for this value of doping. Also shown (dashed line) is the lower bound of the two-particle excitation continuum made up of a pair of  $S = 1/2$  excitations from Fig 8 and 9; in the notation of these figures and Appendices B and C, the position of this lower-bound is  $\text{Min}[\Omega_+(\mathbf{p} + \mathbf{q}) + \Omega_+(-\mathbf{q})]$ , where the minimum is taken over all possible values of  $\mathbf{q}$ . Note that the minimum of the  $t_\alpha$  excitation is at  $(0, \pi)$ , but because of the halving of the Brillouin zone this wavevector is crystallographically equivalent to  $(\pi, \pi)$ .

be a singular phase transition point at which the nodal fermion first appears. The position of this phase boundary is indicated in Fig 6, and the nature of the phase transition will be discussed below in Section IV.

Finally, we consider the  $S = 1$  excitations, which are visible in neutron scattering experiments. There are two categories of such excitations. First, we have the  $S = 1$ ,  $t_\alpha$  particles, with a definite energy-momentum relation: these may be viewed as a collective spin mode (or a triplet exciton) which goes soft at the antiferromagnetic ordering transition. These are the only  $S = 1$  excitations in the undoped antiferromagnet, but, connect smoothly to corresponding excitations in the doped antiferromagnet. The second class of  $S = 1$  excitations are scattering states of the fermionic  $S = 1/2$  excitations just discussed. These do not have a definite energy momentum relation, but exist over a continuum in a range of energies at any given momentum. We show a plot of the spectra of these two  $S = 1$  excitations in Figs 12 and 13.

At low doping, in Fig 12, not that the  $t_\alpha$  excitation has a well-formed minimum at  $(0, \pi)$ , and this minimum is *below* the lower-bound of the two-particle continuum. So the  $t_\alpha$  excitations are absolutely stable towards decay into 2 fermionic  $S = 1/2$  excitations over this range of energy and momenta. This stable  $S = 1$  excitonic excitation will lead to a resonance peak (in principle, infinitely sharp) in the neutron scattering cross-section at

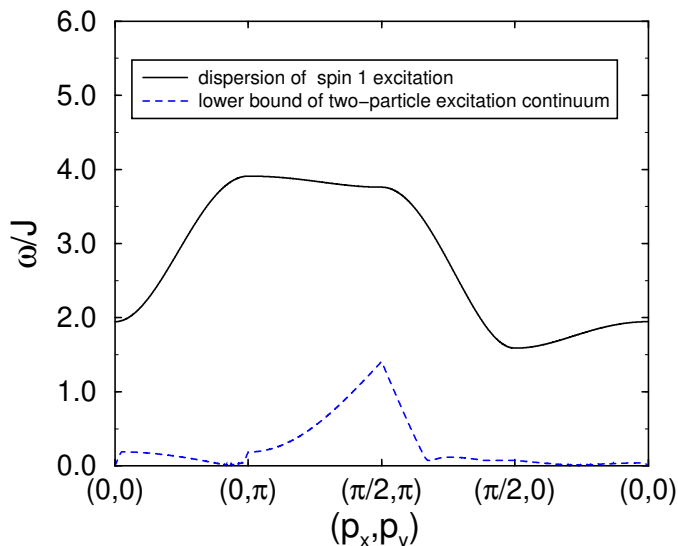


FIG. 13. As in Fig 12, but in the strong pairing region with nodal quasiparticles at  $x = 0.3$ .

the energy and momentum of the  $t_\alpha$  particle. Also, as the doping is lowered, the minimum of the  $t_\alpha$  dispersion gets lowered, until it hits zero also in a region which has no overlap with the fermionic two-particle continuum. This signals the transition to the antiferromagnetic phase: the absence of low energy fermionic excitations at near the minimum  $t_\alpha$  energy implies that the critical theory for the transition remains identical to that for the corresponding transition in the insulator, which has been discussed in much detail<sup>9,63</sup>. The condensation of the  $t_\alpha$  bosons occurs at momentum  $(0, \pi)$ , but note that because of the doubling of the unit cell this momentum is equivalent to  $(\pi, \pi)$ . Determination of the microscopic configuration of the spins using the operator representation in Section II shows that the mean moments indeed have the staggered arrangement associated with the conventional, two-sublattice Néel state.

The higher doping  $S = 1$  excitations are sketched in Fig 13. Now the  $t_\alpha$  excitations are well within the two-fermionic-particle continuum, and so will quickly decay and lose their identity. Note that the doping at which the  $t_\alpha$  excitations ceases to be stable at any momentum does not (in general) co-incide with the point at which nodal fermionic quasiparticles appear. As long as the nodal points are not exactly at  $(\pi/2, \pi/2)$ , the  $t_\alpha$  excitations can be stable at very low energies near  $(\pi, \pi)$ . In the present computation, the nodal points are quite close to  $(\pi/2, \pi/2)$  and to the  $t_\alpha$  excitation is quickly quenched. In a more general model, with second neighbor hopping, the  $t_\alpha$  excitations could be stable even in an isotropic  $d$ -wave superconductor, provided we moved the nodal points sufficiently far from  $(\pi/2, \pi/2)$ .

#### IV. ONSET OF GAPLESS NODAL FERMIONIC EXCITATIONS

The phase diagram of Fig 6 shows a phase boundary demarking superconductors with and without nodal quasiparticles. This is a quantum phase transition in the sense that there is a (weak) non-analyticity in the ground state energy as a function of doping at this point. A theory of this transition is implicit in the discussion of Appendix C, but here we will present a simplified treatment which captures its essential universal features. Such a transition was discussed earlier in Ref 9 and by Granath *et al.*<sup>65</sup>; the latter authors also reached conclusions on the universal properties which agree with our discussion here. A related, but distinct, theory for the annihilation of nodal particles in a  $d$ -wave superconductor was also discussed by Duncan and Sá de Melo<sup>66</sup>. They considered an isotropic superconductor as a function of electron density, and found that the nodal points vanished when all four of them collided at  $k = 0$ . This transition differs from that in the anisotropic superconductors of interest here, where the nodal points collide only in pairs, and the quantum critical points belong to distinct universality classes.

We approach this transition from the side of the  $d$ -wave superconductor with full square lattice symmetry. Here, the fermionic excitations are described by the BCS Hamiltonian

$$H_{BCS} = \sum_k \left[ \epsilon(k) c_{ka}^\dagger c_{ka} + \frac{\Delta(k)}{2} \left( \epsilon_{ab} c_{ka}^\dagger c_{-kb}^\dagger + \text{H. c.} \right) \right], \quad (14)$$

where, in the simplest nearest-neighbor model  $\epsilon_k = -2t(\cos k_x + \cos k_y) - \mu$ , and the pairing energy  $\Delta(k) = \Delta_0(\cos k_x - \cos k_y)$ . We now assume that there is an onset of bond-centered charge order at wavevector  $G = (\pi/a, 0)$  of amplitude  $\psi_{sp}$ —because this charge order wave is in the  $x$  direction,  $\psi_{sp}$  is the real part of the more general order parameter,  $\Psi_{sp}$  considered in Section I and Appendix A. This order will lead to a modulation in the fermion hopping matrix element and the pairing interaction at the wavevector  $G$ , and so induce the following additional terms in the Hamiltonian for the fermionic excitations

$$H_{sp} = i\psi_{sp} \sum_k \left[ a(k) c_{k,a}^\dagger c_{k+G,a} + \frac{b(k)}{2} \left( \epsilon_{ab} c_{ka}^\dagger c_{-k+G,b}^\dagger + \text{H. c.} \right) \right], \quad (15)$$

where  $a(k) = w_1 \sin k_x$  and  $b(k) = w_2 \sin k_x$ , with  $w_{1,2}$  some constants. These last factors of  $\sin k_x$  are a consequence of the bond-centered nature of the charge order<sup>67</sup>, but the results of this section are not crucially dependent upon this fact; similar results will apply also to site-centered charge orders.



It is possible to diagonalize the Hamiltonian  $H_{BCS} + H_{sp}$  and determine the fermionic excitation spectrum of the state with co-existing superconductivity and charge order. The energy eigenvalues are

$$\left[ \Lambda_1 \pm (\Lambda_1^2 - \Lambda_2^2 - \Lambda_3^2)^{1/2} \right]^{1/2} \quad (16)$$

where

$$\begin{aligned} \Lambda_1 &\equiv [\epsilon^2(k) + \epsilon^2(k+G) + \Delta^2(k) + \Delta^2(k+G)]/2 \\ &\quad + \psi_{sp}^2 [a^2(k) + b^2(k)] \\ \Lambda_2 &\equiv \Delta(k)\epsilon(k+G) + \Delta(k+G)\epsilon(k) - 2\psi_{sp}^2 a(k)b(k) \\ \Lambda_3 &\equiv \psi_{sp}^2 [a^2(k) - b^2(k)] \\ &\quad + \Delta(k)\Delta(k+G) - \epsilon(k)\epsilon(k+G). \end{aligned}$$

It is instructive to examine the evolution of the zeros of (16) as a function of  $\psi_{sp}$ . For  $\psi_{sp} = 0$ , there are four symmetric nodal points determined by the solutions of  $\epsilon(k) = 0$  and  $\Delta(k) = 0$ . It is assumed (as is the case at non-zero doping and in the absence of particle-hole symmetry), that the wavevector separating any two of these nodal points is not equal to  $G$ . If it was equal to  $G$ , then the nodal points would be gapped at an infinitesimal value of  $\psi_{sp}$ , and a non-trivial theory would describe the quantum critical fluctuations, as has already been discussed in Ref 9. Turning to the more general situation, where the separation between the nodal points is not equal to  $G$ , the quantum critical theory describing the onset of a non-zero  $\psi_{sp}$  is reviewed in Appendix A—the leading critical singularities do not involve the nodal fermions. As  $\psi_{sp}$  increases, examination of (16) shows that the four nodal points move towards the new Brillouin zone boundary at  $k_x = \pm\pi/2$ . Eventually, these points collide in pairs at

$$p_0 = (\pi/2, p_{0x}) \quad (17)$$

(and symmetry related points) and  $\psi_{sp} = \psi_{sp}^c$ , and there are no nodal points for  $\psi_{sp} > \psi_{sp}^c$ . We are interested here in describing the quantum critical theory of this nodal point collision. Clearly, the fluctuations of  $\psi_{sp}$  will not be critical at this point, as the transition occurs at a non-zero value of  $\psi_{sp}^c$ .

First, let us determine the values of  $\psi_{sp}^c$  and  $p_0$ . Using the facts that  $\epsilon(p_0) = \epsilon(p_0 + G)$  and  $\Delta(p_0) = \Delta(p_0 + G)$ , the condition for the presence of gapless nodal points in (16) becomes

$$\epsilon(p_0) = \psi_{sp}^c a(p_0) \quad ; \quad \Delta(p_0) = \psi_{sp}^c b(p_0). \quad (18)$$

The solution of these two equations determines the two unknowns  $\psi_{sp}^c$  and  $p_{0x}$ . At this same point, the second eigenvalue in (16) remains non-zero and finite. This fermionic mode will play no role in the critical theory, and so it pays to perform a canonical transformation at an early stage to project it out. To leading order in the distance from the critical point, this merely means that we

have to take only the linear combination of  $c_{ka}$  and  $c_{k+G,a}$  which appears in gapless eigenvalue associated with (18). So, we introduce a new fermionic degree of freedom,  $f_{qa}^+$ , where the small momentum  $q$  is measured as a deviation from  $p_0$  (and a corresponding fermionic mode  $f_{qa}^-$  which resides at momenta near  $-p_0$ ); using the structure of the gapless eigenvalue at  $\psi_{sp} = \psi_{sp}^c$  and  $k = p_0$ , we see that we should parameterize

$$\begin{aligned} c_{ka} &= f_{qa}^+/\sqrt{2} \\ c_{k+G,a} &= i\varepsilon_{ab}f_{qb}^+/\sqrt{2}, \end{aligned} \quad (19)$$

where  $k = p_0 + q$ , and  $q$  is small; a similar parameterization is made near  $-p_0$  with  $f_a^-$ . Finally, we insert (19) into  $H_{BCS} + H_{sp}$ , and expand in  $\psi_{sp} - \psi_{sp}^c$  and in gradients of  $f_a^\pm$ . This leads to the following effective action for the critical theory

$$\begin{aligned} S_f &= \int d^2r d\tau \left[ f_a^{\pm\dagger} \left( \frac{\partial}{\partial\tau} \pm iv_1 \frac{\partial}{\partial y} - \frac{1}{2m_1} \frac{\partial^2}{\partial x^2} + \delta_1 \right) f_a^\pm \right. \\ &\quad \left. + \varepsilon_{ab} f_a^- \left( v_2 \frac{\partial}{\partial y} - \frac{1}{2m_2} \frac{\partial^2}{\partial x^2} + \delta_2 \right) f_b^+ + \text{H.c.} \right] \quad (20) \end{aligned}$$

where  $\tau$  is imaginary time,  $r = (x, y)$  is the spatial coordinate,  $\delta_{1,2} = w'_{1,2}(\psi_{sp} - \psi_{sp}^c)$ , and  $v_{1,2}$ ,  $m_{1,2}$ ,  $w'_{1,2}$  are constants dependent upon the detailed momentum dependence of  $\epsilon(k)$  and  $\Delta(k)$ . The fermionic eigenenergy of (20) is easily determined; it is

$$\left[ \left( \delta_1 + v_1 q_y + \frac{q_x^2}{2m_1} \right)^2 + \left( \delta_2 + v_2 q_y + \frac{q_x^2}{2m_2} \right)^2 \right]^{1/2}. \quad (21)$$

The positions of the nodal points, if present, are easily determined from (21). Assuming  $v_{1,2}$ ,  $m_{1,2}$ ,  $w'_{1,2}$  are all positive, then for  $w'_1/v_1 > w'_2/v_2$  and  $m_1 v_1 < m_2 v_2$ , nodal points are present for  $\psi_{sp} < \psi_{sp}^c$ , but not for  $\psi_{sp} > \psi_{sp}^c$  (similar results hold for other signs and magnitudes of the various coupling constants). The trajectory of the nodal points is sketched schematically in Fig 14: they move on a parabolic trajectory with  $|q_y| \sim q_x^2$  before colliding along the Bragg reflection planes at  $k_x = \pm\pi/2$ .

The availability of the action  $S_f$  also allows one to determine the consequences of the interactions near the quantum critical point. Notice that at the critical point,  $\delta_1 = \delta_2 = 0$ ,  $S_f$  is invariant under the scale transformation  $\tau \rightarrow \tau/s$ ,  $y \rightarrow y/s$ ,  $x \rightarrow x/\sqrt{s}$ , and  $f \rightarrow s^{3/4}f$ . The simplest allowed four fermion coupling is  $\sim (f^\dagger f)^4$ , and power-counting shows that its co-efficient has a negative scaling dimension of  $-1/2$ . So this interaction is an irrelevant perturbation at the quantum critical point<sup>65</sup>. In a similar manner, it is not difficult to show that all other perturbations of  $S_f$  are irrelevant, and so  $S_f$  is the complete critical theory of the transition involving the onset of nodal fermionic excitations.

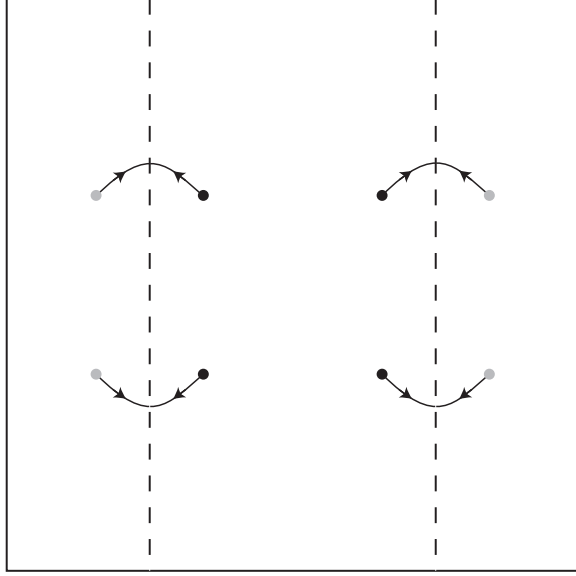


FIG. 14. Evolution of the gapless nodal points in the fermionic excitation spectrum as a function of  $\psi_{sp}$ . The square contains the first Brillouin zone of the original square lattice, extending between  $k_{x,y} = \pm\pi$ . The dark circles are the positions of the nodal points in this  $d$ -wave superconductor. Onset of a non-zero  $\psi_{sp}$  introduces Bragg reflection planes at  $k_x = \pm\pi/2$  and images of the nodal points indicated by the grey circles. As  $\psi_{sp}$  increases, the nodal points move towards the Bragg reflection planes and annihilate each other when they collide<sup>9</sup>. The critical theory of this transition is discussed in Section IV.

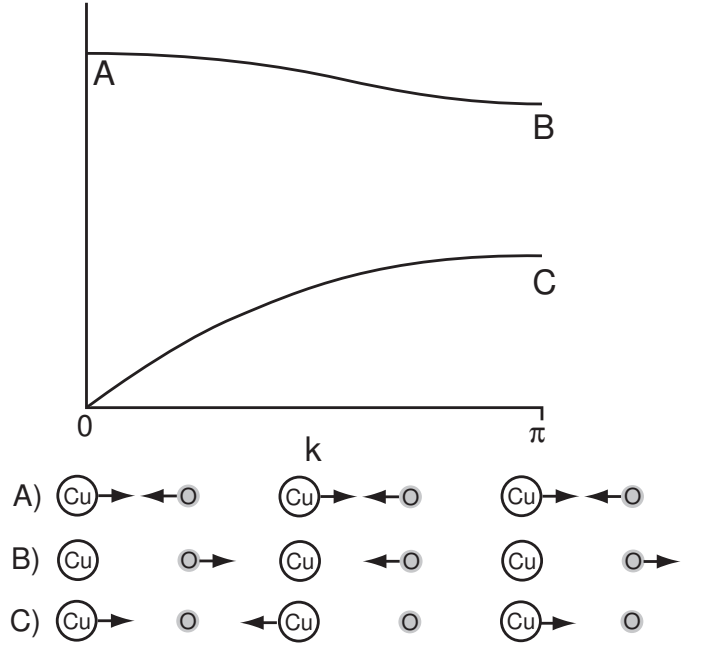


FIG. 15. Phonon frequencies (vertical axis) of the one-dimensional Cu-O chain. The frequency of the mode A is  $[2K(M_{Cu} + M_O)/(M_{Cu}M_O)]^{1/2}$ , that of B is  $[2K/M_O]^{1/2}$ , and that of C is  $[2K/M_{Cu}]^{1/2}$ . Only mode C is “Peierls active” *i.e.* couples linearly to the order parameter  $\Psi_{sp}$ , which measures the amplitude of a bond-centered charge order wave at wavevector  $(\pi/a, 0)$ .

## V. COUPLING OF SPIN PEIERLS ORDER TO PHONONS

A central actor in all the considerations so far has been the spin-Peierls order parameter,  $\Psi_{sp}$ . Experimental observations of the fluctuations of this order parameter would certainly be helpful in resolving the theoretical issues. However, this is a spin-singlet, charge zero mode and is only observable through its couplings to the ionic displacements. This section will therefore present a simplified discussion of the coupling between the dynamics of the spin Peierls order parameter and the phonon modes of the  $\text{CuO}_2$  plane. Indeed, it is probable that the phonons are more than merely spectators of the spin dynamics, and the spin-phonon coupling may play an important role in selecting between different charge orderings and in influencing the nature of the electronic ground state: the important phonon and spin excitation energies are roughly of the same order, and so a coupled dynamical model will be necessary for a complete microscopic understanding.

The spin-Peierls order parameter couples most directly to the “Peierls-active” phonon mode sketched as mode C in Fig 15: this is a staggered displacement of the Cu ions at the wavevector  $(\pi, 0)$ . Notice that the O ions are stationary in this phonon mode. As we will describe

below, the coupling between this Peierls-active phonon and the spin-Peierls order parameter is likely to lead to an additional low energy peak in the dynamic phonon structure factor at the energy scale of the characteristic spin-Peierls fluctuations. However, neutron scattering studies of the phonon spectra have so far<sup>28,68–70</sup> focused on optical phonons involving motion primarily of the O ions (the mode between A and B in Fig 15): the smaller O ion mass,  $M_O \approx M_{Cu}/4$ , increases the displacement of the O ions and makes these easier to observe. The O ion phonon at wavevector  $(\pi, 0)$  (mode B in Fig 15) is not Peierls-active in the sense just noted. However, following the suggestion of McQueeney *et al.*<sup>28</sup>, we will describe below a non-linear coupling in the spin-phonon Hamiltonian which leads to signatures of the spin-Peierls fluctuations in the A-B phonon mode at the wavevector  $(\pi/2, 0)$ .

It is also worth mentioning the recent work of Khalullin and Horsch<sup>71</sup>. In contrast to our focus on bond-centered charge fluctuations, they considered Cu site-centered charge density fluctuations at wavevectors near  $(\pi, 0)$  (in the notation of Nayak<sup>67</sup>, we are examining  $p_x$  density wave correlations at  $(\pi, 0)$ , while Ref 71 discusses  $s$  density wave correlations at  $(\pi, 0)$ ). These Cu site-centered fluctuations do indeed couple linearly to the phonon mode in the vicinity of the point B in Fig 15: this led to a broadening and softening of the phonon near B. As we will see below, our bond-centered spin-Peierls correlations instead modify the A-B phonon mode near  $(\pi/2, 0)$  in a manner which is consistent with experimental observations.

We will work here with a simplified one-dimensional model of the phonons in the  $\text{CuO}_2$  plane. All the phonons we are interested in are polarized both in wavevector and ionic displacement along the  $(1, 0)$  axis, and so neglecting the second dimension is not too serious. We will consider only a single chain of alternating Cu and O ions, and consider displacements of the ions along the chain direction (see Fig 15). A more complete treatment is certainly possible, but we will not attempt it here: we hope that with improved experimental resolution, a more precise and microscopic theoretical study of the two-dimensional phonon modes will be carried out, along the lines of the analyses of Refs 72,73 for  $\text{CuGeO}_3$ .

We begin by specifying our toy one-dimensional model of the phonons in an alternating chain of Cu and O ions. We place the Cu ions on the sites,  $i$  (integer), of a chain with spacing  $a$ , while the O ions are at the centers of the links of the chain. We denote the displacement of these ions by  $u_i$  and  $v_i$  respectively, where the  $i$ 'th O ion is taken to be immediately to the right of the  $i$ 'th Cu ion. The harmonic action for the phonon modes is (in imaginary time,  $\tau$ ):

$$S_{\text{ph}} = \int d\tau \sum_i \left[ \frac{M_{\text{Cu}}}{2} \left( \frac{du_i}{d\tau} \right)^2 + \frac{M_O}{2} \left( \frac{dv_i}{d\tau} \right)^2 \right.$$

$$\left. + \frac{K}{2} \{ (u_i - v_i)^2 + (u_i - v_{i-1})^2 \} \right], \quad (22)$$

where  $K$  is a “spring constant” which determines the phonon frequencies. It is a simple matter to diagonalize  $S_{\text{ph}}$  and obtain the phonon normal mode frequencies: they are

$$\omega_{\pm}^2 = \frac{K}{M_{\text{Cu}}M_O} \left[ M_{\text{Cu}} + M_O \pm ((M_{\text{Cu}} - M_O)^2 + 4M_{\text{Cu}}M_O \cos^2(k/2))^{1/2} \right], \quad (23)$$

and are sketched in Fig 15.

We also have to consider the dynamics of the spin Peierls order  $\Psi_{\text{sp}}$  introduced in Section I and considered in Section IV and Appendix A. In our present one-dimensional toy model, we need only consider  $\psi_{\text{sp}} = \text{Re}[\Psi_{\text{sp}}]$ . For this order parameter  $\psi_{\text{sp}}$ , the dynamics of an interacting effective action like  $S$  in (A1) is assumed to be captured by the following effective quadratic action<sup>9</sup>:

$$S_{\text{sp}} = \frac{T}{2} \sum_{k, \omega_n} |\psi_{\text{sp}}(k, \omega_n)|^2 \chi_{\text{sp}}^{-1}(k, i\omega_n) \quad (24)$$

$$\chi_{\text{sp}}^{-1}(k, i\omega_n) \equiv \omega_n^2 + 2a^2c_1^2(1 - \cos(k)) + \Delta_{\text{sp}}^2 + \Gamma_{\text{sp}}|\omega_n|.$$

Here  $\omega_n$  is a Matsubara frequency, and  $\Delta_{\text{sp}}$  and  $\Gamma_{\text{sp}}$  are effective energy scales determining the mean frequency and damping of the  $\psi_{\text{sp}}$  fluctuations; the values of  $\Delta_{\text{sp}}$  and  $\Gamma_{\text{sp}}$  are determined by the non-linear interactions in (A1). Also we have replaced the spatial gradient in (A1) by a nearest-neighbor lattice derivative in (24). As one approaches the onset of spin-Peierls order (approaching point C in Fig 6 from the right), the value of  $\Delta_{\text{sp}}$  will decrease to zero, while  $\Gamma_{\text{sp}}$  becomes of order  $T$ , representing the damping of the order parameter mode in the quantum-critical region. We will work here in the  $\Delta_{\text{sp}} > 0$  regime, staying to the right of C in Fig 6. The velocity  $c_1$  should be order the spin-wave velocity, and this is about 10 times larger than the velocity of the acoustic phonon mode, C, in Fig 15.

Finally, we have to couple  $\psi_{\text{sp}}$  to the phonon modes. This coupling<sup>72–75</sup> arises from the dependence of the exchange constant  $J$  between neighbor Cu spins on the displacements of the Cu and O ions. We assume that  $J \sim t_{pd}^4$ , where  $t_{pd}$ , the overlap between neighboring O and Cu orbitals is a function of  $(u_i - v_i)$  and  $(u_i - v_{i-1})$ . Expanding  $J$  in derivatives of these variables, we obtain first the simple linear coupling

$$S_{1c} = \int d\tau \sum_i [\lambda(-1)^i \psi_{\text{sp},i} (u_{i+1} - u_i)], \quad (25)$$

where  $\lambda$  is the linear coupling constant, and  $\psi_{\text{sp},i}$  is the spin-Peierls order parameter in real space; this naturally resides on the centers of the bonds, and we locate  $\psi_{\text{sp},i}$  on the same O site as  $v_i$ . As we noted earlier,  $S_{1c}$  couples the spin-Peierls order most strongly to the phonons in



the vicinity of the point C in Fig 15, and will lead to its broadening and softening. We are interested here primarily in the modifications of the optical phonon mode A-B, and so we will neglect  $S_{1c}$  in our computations below.

As indicated at the beginning of this section, the important effect on the A-B optical phonon arises from a non-linear spin-phonon coupling. Expanding to one higher order in the phonon displacements, the coupling between  $\psi_{sp}$  and the phonon displacements can be written in the form

$$S_{2c} = \int d\tau \sum_i \left[ (-1)^i \psi_{sp,i} \left\{ \gamma_1 (u_{i+1} - u_i)^2 + \gamma_2 (u_{i+1} + u_i - 2v_i)^2 \right\} \right], \quad (26)$$

where  $\gamma_{1,2}$  are the non-linear spin phonon coupling constants.

We examined the properties of  $S_{ph} + S_{sp} + S_{2c}$  in a simple one-loop approximation: we neglect the  $\omega_-$  phonon in (23), computed the self-energy of the  $\omega_+$  optical phonon at order  $\gamma_{1,2}^2$ . Finally, to compare to neutron scattering experiments, we computed

$$D(k, \omega) = \left\langle \left| b_{Cu} u(k, \omega) + b_O v(k, \omega) e^{ik/2} \right|^2 \right\rangle, \quad (27)$$

where  $b_{Cu} = 7.718$  and  $b_O = 5.803$  are the neutron scattering lengths of Cu and O respectively<sup>82</sup>. The results are shown in Figs 16 and 17 for a representative set of parameters. As  $\Delta_{sp}$  decreases, there is initially a broadening and a sharpening of the phonon mode near  $k = \pi/2$ . For even smaller  $\Delta_{sp}$  we see the incipient Brillouin zone boundary of the doubled unit cell developing near  $k = \pi/2$ : this is reflected in the apparent discontinuity of the dispersion and the appearance of “shadow” phonon bands reflected across the incipient Brillouin zone boundary. The first of these features is in excellent accord with all the available neutron scattering experiments<sup>28,68,70</sup>, and there has even been a claim of the observation of shadow bands<sup>28</sup>, although this has not been confirmed.

Another interesting feature of Figs 16 and 17 is that the intensity of the phonon is larger near the Brillouin zone boundary. This is a ‘form factor’ effect, and arises primarily from the interplay of the different scattering lengths in (27), and the distribution of the phonon normal mode between the O and Cu sites. Curiously, precisely such a dominance of intensity near  $k = \pi$  is observed in the experiments<sup>28,70</sup>.

## VI. CONCLUSIONS

This paper has introduced a bond operator formalism to represent the degrees of freedom of doped antiferromagnets. While the approach bears some similarities to the popular “slave” boson and fermion techniques, the

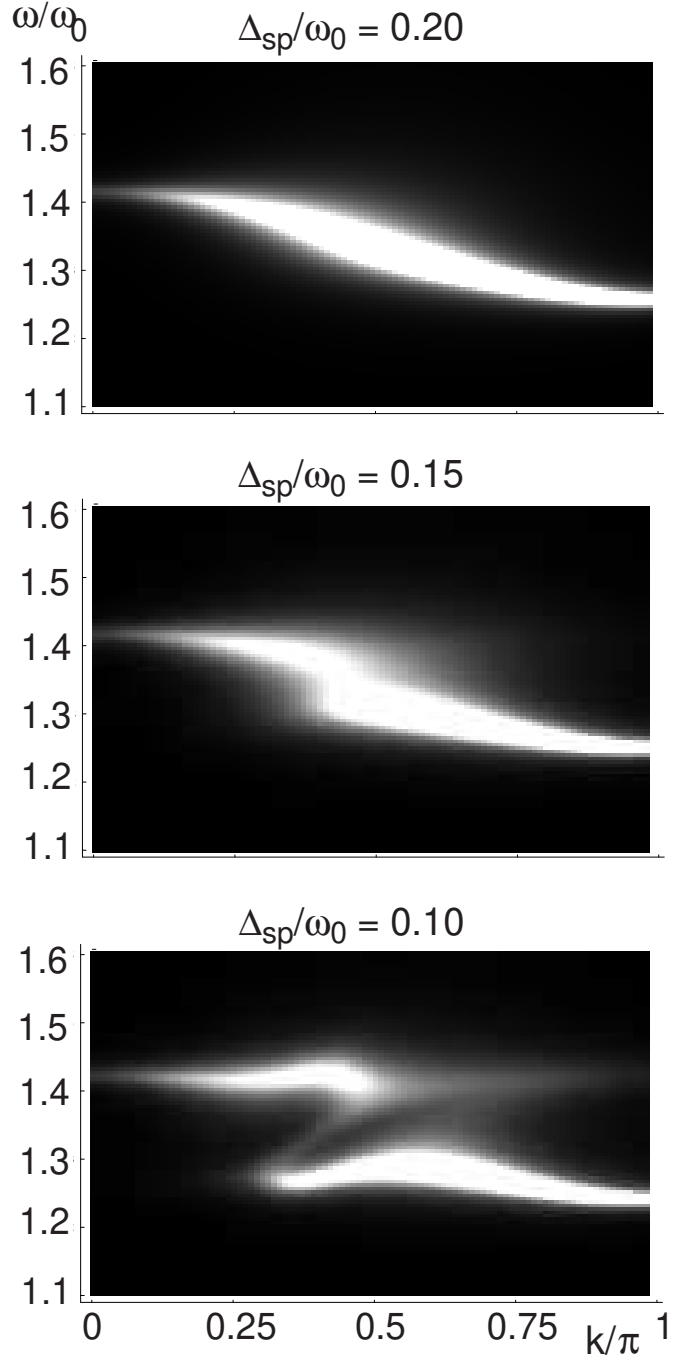


FIG. 16. Plot of the phonon spectral density  $\text{Im}D(k, \omega)$  defined in (27). The figure shows the influence of the spin-Peierls fluctuations described by (24) on the optical phonon mode A-B in Fig 15; the two degrees of freedom are coupled by the non-linear terms in (26). We used the parameters  $\omega_0 \equiv \sqrt{K/(1/M_{Cu} + 1/M_O)}$ ,  $\Gamma_{sp} = 0.5\omega_0$ ,  $T = 0.1\omega_0$ ,  $c = 10.0\omega_0$ , and  $\gamma_1 = \gamma_2 = 0.5K\omega_0$ . The figures show the evolution in the spectrum as a function of  $\Delta_{sp}/\omega_0$ .

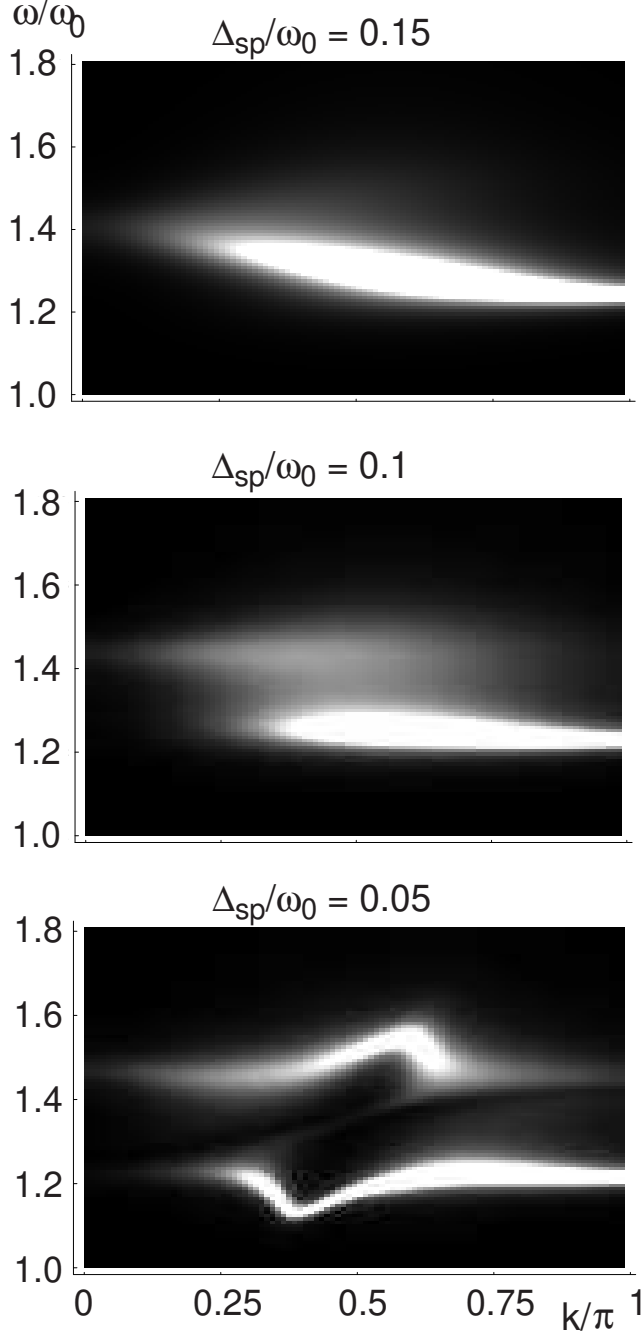


FIG. 17. As in Fig 16 but for  $\Gamma_{sp} = 0.2\omega_0$ ,  $T = 0.1\omega_0$ ,  $c = 5.0\omega_0$ , and  $\gamma_1 = \gamma_2 = 0.5K\omega_0$ .

implementation leads to theories with a rather different structure: there are no long-range gauge forces in the fluctuations about any reasonable saddle-point in the latter formalism, and the quantum numbers of the true elementary excitations are simply connected to those of the microscopic operators. This is a powerful advantage of the bond operator method, and allows much information to be gleaned from simple mean-field Hatree-Fock-BCS computations. The main disadvantage of the method is that it requires a pairing of the sites into bonds at the outset. Such a pairing is naturally present in systems with spontaneous or explicit bond-centered charge order (as in a spin-Peierls states), and it is for these systems that the approach is best suited.

The defining equations of the bond operator formalism were presented in Section II, and are contained in Eqns (3-8). Next, we applied this formalism to the two-dimensional doped antiferromagnet sketched in Fig 5b. The main phase diagram of the model is sketched in Fig 6, and the important properties of the phases are summarized in its caption. The remaining figures in Fig II and their captions summarizing the excitation spectra of the phases—the fermionic,  $S = 1/2$ , spectra are in Figs 8, 9, 10, and 11, while the  $S = 1$  excitations are in Figs 12 and 13; the latter consist of a bosonic,  $S = 1$  exciton, and the two-particle continua of the fermionic  $S = 1/2$  excitations.

The connection of these result to recent neutron scattering measurements of phonon spectra<sup>28,68–70</sup> was considered in Section V. This section did not use the bond operator formalism. Instead, it considered the consequences of incipient bond-centered charge order in an isotropic state, in a simple perturbative calculation using a spin-phonon model. We introduced an order parameter,  $\Psi_{sp}$ , characterizing the ordering pattern associated with Fig 5b, and wrote down a phenomenological free energy<sup>9,63</sup> describing its fluctuations in spacetime in the vicinity of the quantum critical point labeled by the point C in Fig 6. On the symmetric side of C (the region with  $\langle \Psi_{sp} \rangle = 0$ ), these fluctuations were controlled by an energy scale,  $\Delta_{sp}$ , which vanished as C was approached, and we considered the evolution of the optical phonon spectra as a function of decreasing  $\Delta_{sp}$ : these results are contained in Figs 16 and 17.

In the unifying language introduced by Nayak<sup>67</sup>, the bond-centered charge order parameter  $\Psi_{sp}$  may be considered as the amplitude of a  $p_x$  density wave at wavevector  $(\pi, 0)$ . The ordinary  $s$  density wave at wavevector  $(\pi, 0)$  is associated with Cu site-centered charge order, and these may also be strong in the lightly doped antiferromagnet, especially in the region with long-range magnetic order. Their influence on the optical phonon spectra was considered in Ref 71—the primary effect was a broadening of the O optical phonon near  $(\pi, 0)$ . This should be contrasted with the influence of the  $\Psi_{sp}$  fluctuations described above—the strongest effect was near  $(\pi/2, 0)$  where the phonon dispersion sharpened considerably, along with a significant amount of broadening. The

latter effects are clearly seen in recent neutron scattering experiments<sup>28,68</sup>, although some softening at  $(\pi, 0)$  is also apparent<sup>70</sup>. We hope that higher precision and more detailed neutron scattering experiments will be undertaken, and along with more microscopic theoretical computations, these should help sort out the relative roles of site- and bond-centered charge order as a function of increasing doping.

In addition to fluctuating charge-order modes detected in phonon scattering, it would also be useful to study systems in which the charge order is required to be static; in such situations, atomic resolution STM studies should yield much useful information on the microstructure of the charge order. Our physical picture implies that static charge order should be present in situations in which both magnetic and superconducting order have been suppressed (systems with one of these orders may only have fluctuating charge order). A convenient way to achieve this is by application of a strong magnetic field on underdoped samples<sup>76</sup>. A phenomenological theory of the phase diagram in a magnetic field has been provided recently in Ref 77: the “normal” state in this phase diagram is a very attractive candidate to bond-centered charge order very similar to that in Fig 2a. It would be especially interesting to conduct STM measurements on the strongly underdoped YBCO crystals that have become available recently<sup>78</sup>, after superconductivity has been suppressed by a static magnetic field. An alternative is to look for charge order in STM studies in which the superconductivity has only been locally suppressed, as is the case in the cores of vortices in the superconducting order<sup>79,80</sup>. However, the short-range nature of the suppression means that charge order is not required to appear, and may remain dynamic—this makes this approach less attractive. Recent indications<sup>81</sup> of mesoscale self-segregation of charge carriers in bulk samples also naturally raise the possibility of bond charge order in the lower density regions which (presumably) have suppressed superconductivity.

## ACKNOWLEDGMENTS

We thank G. Aeppli, D. Campbell, E. Carlson, T. Egami, S. Girvin, E. Fradkin, S. Kivelson, A. Polkovnikov, T. Senthil, M. Vojta and J. Zaanen for useful discussions. We are especially grateful to S. Kivelson for a critical reading of the manuscript. This research was supported by US NSF Grant DMR 0098226.

## APPENDIX A: INTERPLAY OF SPIN PEIERLS AND NEMATIC ORDERS

In Section I we discussed the relationship between states with spin-Peierls order, with the symmetry of Fig 2a, and the nematic electronic states discussed by

Kivelson, Fradkin and Emery<sup>38</sup>. We noted that the spin-Peierls state was characterized by a complex order parameter<sup>40</sup>  $\Psi_{\text{sp}}$  (which took the values 1,  $i$ ,  $-1$ ,  $-i$  on the four states obtained by rotating Fig 2a about any lattice site), the nematic was characterized by a real Ising order parameter  $\Phi_n$ , and the symmetry properties of these two order parameters implied the relationship (2) between them. More generally, we can write down the following simple effective action for them, keeping all low order terms consistent with the underlying symmetries:

$$S_{\text{sp-n}} = \int_0^{1/T} d\tau \int d^2x \left[ |\partial_\tau \Psi_{\text{sp}}|^2 + c_1^2 |\nabla_x \Psi_{\text{sp}}|^2 + r_1 |\Psi_{\text{sp}}|^2 + \frac{1}{2} (\partial_\tau \Phi_n)^2 + \frac{1}{2} c_2^2 (\nabla_x \Phi_n)^2 + \frac{r_2}{2} \Phi_n^2 - g \Phi_n (\Psi_{\text{sp}}^2 + \Psi_{\text{sp}}^{*2}) + \frac{u_1}{2} |\Psi_{\text{sp}}|^4 - \frac{v}{4} (\Psi_{\text{sp}}^4 + \Psi_{\text{sp}}^{*4}) - \frac{w}{2} \Phi_n^2 |\Psi_{\text{sp}}|^2 + \frac{u_2}{4} \Phi_n^4 \right], \quad (\text{A1})$$

where  $\tau$  is imaginary time, and  $u_1 > v > 0$ ,  $u_2 > 0$ , and  $u_2(u_1 - v) > w^2$  required for stability. We expect that the appearance of nematic order will enhance the probability of spin Peierls order, and so  $w > 0$ . We have, for now, neglected the couplings of these order to the fermionic excitations, and will consider the consequences of these later in this section.

First, let us analyze  $S_{\text{sp-n}}$  in mean-field theory. The results of such an analysis are shown in Fig 18. There are three phases: (i) the symmetric phase, where no lattice symmetry is broken, (ii) the spin Peierls phase, where both the spin Peierls and nematic order parameters are non-zero, and (iii), the nematic phase, where only the nematic order is non-zero. There can be a second-order phase transition between any two of these three phases, as indicated in Fig 18. The position of these second-order boundaries can be determined by a conventional Landau theory analysis in powers of the associated order parameter. In this manner, we find that the second-order line between the symmetric phase and the spin-Peierls phase is at  $r_1 = 0$ , while that between the symmetric phase and the nematic phase is at  $r_2 = 0$ . Finally, the second-order transition from the nematic to the spin-Peierls phase is at

$$r_1 = 2g\sqrt{-r_2/u_2} - wr_2/(2u_2). \quad (\text{A2})$$

Notice that these three second-order lines all appear to meet at the origin  $r_1 = 0$ ,  $r_2 = 0$ . However, as indicated in Fig 18, this is pre-empted by a line of *first order* transitions close to the origin. The reason for this may be seen by the following simple argument. Imagine integrating out the  $\Phi_n$  fluctuations to derive an effective action for the  $\Psi_{\text{sp}}$ : this always induces an effective quartic term  $\sim |\Psi_{\text{sp}}|^4$  with a coefficient  $\sim -g^2/|r_2|$ . So for small enough  $|r_2|$ , the net coefficient of  $|\Psi_{\text{sp}}|^4$  always becomes negative, and this drives the transitions involving

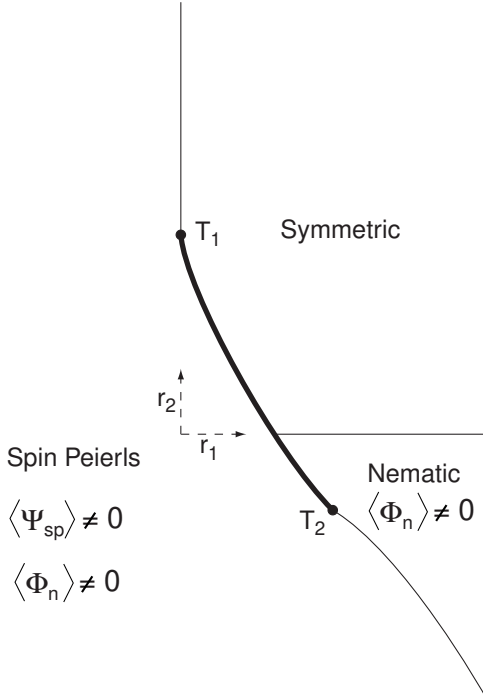


FIG. 18. Mean-field phase diagram of the action  $S_{sp-n}$  in (A1). The symmetric phase has no broken lattice symmetries. The thin (thick) lines represent second (first) order transitions. The positions of the second order transition lines is indicated in (A2) and above. The tricritical point  $T_1$  is at  $r_1 = 0$ ,  $r_2 = 4g^2/(u_1 - v)$ , while the tricritical point  $T_2$  is at the  $r_2 < 0$  which is a solution of  $2u_2g^2 + 4gw\sqrt{-r_2/u_2} + r_2(u_2(u_1 - v) - w^2/2) = 0$ , and  $r_1$  given by (A2) for this value of  $r_2$ . At  $T = 0$ , the coupling to the nodal fermions in a  $d$ -wave superconductor drives the transition from the symmetric to the nematic phase first order<sup>43</sup>.

onset of non-zero  $\langle \Psi_{sp} \rangle$  first order. A consequence of this line of first-order transitions is that there are two tricritical points  $T_1$ ,  $T_2$ , and their positions are indicated in the caption to Fig 18.

Let us now consider the nature of the fluctuations in the vicinity of the second-order phase transitions. We examine first the transition from the symmetric to the nematic phase, which has an Ising order parameter. For  $T > 0$ , these transitions will remain in the universality class of the two-dimensional Ising model. However, at  $T = 0$ , we have to also consider the influence of the fermionic excitations. A general analysis of such effects has been presented in Ref 43, and we recall the results relevant to our discussion here. The  $T = 0$  ground state is either an insulator or a superconductor, and only the gapless nodal fermionic excitations can influence the nature of the critical properties of a zero temperature quantum phase transition. In an anisotropic,  $d$ -wave superconductor, the four nodal points are described by a Dirac-like Hamiltonian for 2, four-component, fermionic Nambu spinors  $\Psi_1$ ,  $\Psi_2$  (we will follow the notation of Ref 43). The nematic order parameter has zero net momentum, and so has a simple linear coupling to these fermionic excitations<sup>43</sup>:

$$\Phi_n \left( \Psi_1^\dagger \tau^x \Psi_1 + \Psi_2 \tau^x \Psi_2 \right), \quad (A3)$$

where  $\tau^{x,y,z}$  are Pauli matrices in the Nambu space (again, in the notation of Ref 43). A renormalization group analysis of the consequences of (A3) has been carried out, and it is found that the couplings to the fermions drives the  $T = 0$  transition between the symmetric and nematic phases first order.

Now let us consider the remaining two second-order transitions in Fig 18, for which  $\Psi_{sp}$  is the order parameter. In contrast to  $\Phi_n$ , the spin-Peierls order has momentum  $(\pi, 0)$  or  $(0, \pi)$ , and so has no simple linear coupling to the nodal points, barring the exceptional case in which the nodal points are exactly at  $(\pi/2, \pi/2)$ . In general, the couplings between  $\Psi_{sp}$  and the fermions are of the form

$$\Psi_{sp}^2 \left( \Psi_1^\dagger \tau^x \Psi_1 + \Psi_2 \tau^x \Psi_2 \right), \quad (A4)$$

as can be expected from (2) and (A3), and also of the form

$$|\Psi_{sp}|^2 \left( \Psi_1^\dagger \tau^z \Psi_1 + \Psi_2 \tau^z \Psi_2 \right), \quad (A5)$$

Unlike (A3), the couplings in (A4,A5) are irrelevant, and so the fermions do not modify the leading critical properties of any transition in which  $\Psi_{sp}$  is the order parameter.

For the transition between the nematic and spin-Peierls phases, the order parameter is either the real or imaginary part of  $\Psi_{sp}$ : the presence of nematic order in both phases therefore makes the residual order parameter Ising-like. So this transition is in the universality class of three-dimensional (two-dimensional) Ising model at  $T = 0$  ( $T > 0$ ).

Finally, we consider the fluctuations near the second-order transition between the symmetric and the spin-Peierls phase. As we have just noted, the fermionic excitations can be neglected even at  $T = 0$ . Further, as  $\Psi_{\text{sp}}$  is the primary order parameter, we can integrate out the  $\Phi_n$  fluctuations at the cost of modifying the couplings in the effective action for the  $\Psi_{\text{sp}}$  alone. The resulting action has the same form as  $S$ , after dropping all the terms involving  $\Phi_n$ ; so near the critical point, we need only follow the flow of the nonlinear couplings  $u_1$  and  $v$ . For the  $T = 0$  transition, the standard Wilson-Fisher analysis of a phase transition in three spacetime dimension leads to the renormalization group flow equations

$$\begin{aligned}\frac{du_1}{d\ell} &= u_1 - 5u_1^2 - 9v^2 \\ \frac{dv}{d\ell} &= v - 6u_1v,\end{aligned}\quad (\text{A6})$$

where we have absorbed a phase-space factor by a rescaling of the couplings in a standard manner. The only stable fixed point of these equations is  $u_1 = 1/5$ ,  $v = 0$ . At the point  $v = 0$ , the effective action for  $\Psi_{\text{sp}}$  has the additional symmetry under the global  $U(1)$  change in the phase of  $\Psi_{\text{sp}}$ . So the  $T = 0$  critical point is in the universality class of three dimensional XY model. Related considerations can be applied to the  $T > 0$  transition between the symmetric and spin-Peierls phases: there, the anisotropy associated with  $v$  leads to phase transitions with continuously varying exponents, associated with physics of the Ashkin-Teller model<sup>83</sup>.

We conclude this section by summarizing the main physical implications of Fig 18. Starting from the symmetric phase, one may break a square lattice symmetry either by lowering temperature, or by reducing doping. One route to this is a direct second-order transition from the symmetric to the spin-Peierls phase; the latter phase also has nematic order. The implications of the physical arguments we have presented in Section I is that this is the preferred route. Alternatively, we can first undergo a transition to the nematic phase, and possibly have a further symmetry breaking into the spin-Peierls phase.

## APPENDIX B: COMPUTATIONS FOR THE TWO-LEG LADDER

We begin a bond operator theory of doped two-leg ladder by writing down the Hamiltonian for the pure t-J model. The effect of Coulomb repulsion will be considered in Appendix D.

$$\begin{aligned}H &= H_t + H_J \\ &= -t \sum_i \left\{ c_{1ia}^\dagger c_{2ia} + c_{2ia}^\dagger c_{1ia} \right\} \\ &\quad - t \sum_{\langle i,j \rangle} \left\{ c_{1ja}^\dagger c_{1ia} + c_{2ja}^\dagger c_{2ia} + (h.c.) \right\}\end{aligned}$$

$$\begin{aligned}&+ J \sum_i \mathbf{S}_{1i} \cdot \mathbf{S}_{2i} \\ &+ \lambda J \sum_{\langle i,j \rangle} \{ \mathbf{S}_{1i} \cdot \mathbf{S}_{1j} + \mathbf{S}_{2i} \cdot \mathbf{S}_{2j} \}\end{aligned}\quad (\text{B1})$$

where  $i$  indicates the position of the  $i$ -th dimer along the ladder direction and  $\langle i, j \rangle$  stands for the summation over the nearest neighbor, i.e.  $j = i + 1$ .

First, let us take a look at the hopping Hamiltonian  $H_t$ . Hopping between the sites inside a given dimer is given by:

$$c_{1ia}^\dagger c_{2ia} + c_{2ia}^\dagger c_{1ia} = h_{1ia}^\dagger h_{2ia} + h_{2ia}^\dagger h_{1ia} \quad (\text{B2})$$

Hopping between the sites of adjacent dimers is obtained as follows.

$$\begin{aligned}c_{1ia}^\dagger c_{1ja} &= \left\{ h_{1ia}^\dagger d_i + \frac{1}{\sqrt{2}} \varepsilon_{ab} s_i^\dagger h_{2ib} - \frac{1}{\sqrt{2}} \varepsilon_{ac} \sigma_{cb}^\alpha t_{i\alpha}^\dagger h_{2ib} \right\} \\ &\quad \times \left\{ d_j^\dagger h_{1ja} + \frac{1}{\sqrt{2}} \varepsilon_{ac} h_{2jc}^\dagger s_j - \frac{1}{\sqrt{2}} \varepsilon_{ae} \bar{\sigma}_{ed}^\beta h_{2jd}^\dagger t_{j\beta} \right\} \\ &\Rightarrow h_{1ia}^\dagger h_{1ja} d_i d_j^\dagger + \frac{1}{2} \varepsilon_{ab} \varepsilon_{ac} s_i^\dagger s_j h_{2ib} h_{2jc}^\dagger \\ &\quad + \frac{1}{\sqrt{2}} d_i s_j \varepsilon_{ac} h_{1ia}^\dagger h_{2jc}^\dagger + \frac{1}{\sqrt{2}} d_j^\dagger s_i^\dagger \varepsilon_{ab} h_{2ib} h_{1ja} \\ &\quad + \frac{1}{2} \varepsilon_{ac} \varepsilon_{ae} \sigma_{cb}^\alpha \bar{\sigma}_{ed}^\beta t_{i\alpha}^\dagger t_{j\beta} h_{2ib} h_{2jd}^\dagger\end{aligned}\quad (\text{B3})$$

where any term containing a single  $t$  boson operator is ignored assuming that there is no magnetic order. Similarly,

$$\begin{aligned}c_{2ia}^\dagger c_{2ja} &= \left\{ h_{2ia}^\dagger d_i + \frac{1}{\sqrt{2}} \varepsilon_{ab} s_i^\dagger h_{1ib} + \frac{1}{\sqrt{2}} \varepsilon_{ac} \sigma_{cb}^\alpha t_{i\alpha}^\dagger h_{1ib} \right\} \\ &\quad \times \left\{ d_j^\dagger h_{2ja} + \frac{1}{\sqrt{2}} \varepsilon_{ac} h_{1jc}^\dagger s_j + \frac{1}{\sqrt{2}} \varepsilon_{ae} \bar{\sigma}_{ed}^\beta h_{1jd}^\dagger t_{j\beta} \right\} \\ &\Rightarrow h_{2ia}^\dagger h_{2ja} d_i d_j^\dagger + \frac{1}{2} \varepsilon_{ab} \varepsilon_{ac} s_i^\dagger s_j h_{1ib} h_{1jc}^\dagger \\ &\quad + \frac{1}{\sqrt{2}} d_i s_j \varepsilon_{ac} h_{2ia}^\dagger h_{1jc}^\dagger + \frac{1}{\sqrt{2}} d_j^\dagger s_i^\dagger \varepsilon_{ab} h_{1ib} h_{2ja} \\ &\quad + \frac{1}{2} \varepsilon_{ac} \varepsilon_{ae} \sigma_{cb}^\alpha \bar{\sigma}_{ed}^\beta t_{i\alpha}^\dagger t_{j\beta} h_{1ib} h_{1jd}^\dagger\end{aligned}\quad (\text{B4})$$

By combining the above two equations, we get

$$\begin{aligned}&c_{1ia}^\dagger c_{1ja} + c_{2ia}^\dagger c_{2ja} + (h.c.) \\ &= d_i d_j^\dagger \{ h_{1ia}^\dagger h_{1ja} + h_{2ia}^\dagger h_{2ja} \} \\ &\quad + \frac{1}{2} s_i^\dagger s_j \varepsilon_{ab} \varepsilon_{ac} \{ h_{1ib} h_{1jc}^\dagger + h_{2ib} h_{2jc}^\dagger \} \\ &\quad + \frac{1}{\sqrt{2}} d_i s_j \varepsilon_{ac} \{ h_{2ia}^\dagger h_{1jc}^\dagger + h_{1ia}^\dagger h_{2jc}^\dagger \} \\ &\quad + \frac{1}{\sqrt{2}} d_j^\dagger s_i^\dagger \varepsilon_{ab} \{ h_{1ib} h_{2ja} + h_{2ib} h_{1ja} \} \\ &\quad + \frac{1}{2} \varepsilon_{ac} \varepsilon_{ae} \sigma_{cb}^\alpha \bar{\sigma}_{ed}^\beta t_{i\alpha}^\dagger t_{j\beta} \{ h_{1ib} h_{1jd}^\dagger + h_{2ib} h_{2jd}^\dagger \} + (h.c.)\end{aligned}\quad (\text{B5})$$

Assuming  $s$  and  $d$  bosons are condensed, i.e.  $s_i = \bar{s}$  and  $d_i = \bar{d}$ , one is able to express  $H_t$  as follows.

$$\begin{aligned}
H_t = & -t \sum_i \{h_{1ia}^\dagger h_{2ia} + h_{2ia}^\dagger h_{1ia}\} \\
& - t(\bar{d}^2 - \frac{1}{2}\bar{s}^2) \sum_{\langle i,j \rangle} \{h_{1ia}^\dagger h_{1ja} + h_{1ja}^\dagger h_{1ia} \\
& + h_{2ia}^\dagger h_{2ja} + h_{2ja}^\dagger h_{2ia}\} \\
& - \sqrt{2}t\bar{d}\bar{s} \sum_{\langle i,j \rangle} \varepsilon_{ab} \{h_{1ia}^\dagger h_{2jb}^\dagger \\
& + h_{2ia}^\dagger h_{1jb}^\dagger + h_{2jb} h_{1ia} + h_{1jb} h_{2ia}\} \\
& + H_{t^2 h^2}
\end{aligned} \tag{B6}$$

where

$$\begin{aligned}
H_{t^2 h^2} = & -\frac{t}{2} \varepsilon_{ac} \varepsilon_{ae} \sigma_{cb}^\alpha \sigma_{ed}^\beta \sum_{\langle i,j \rangle} \{t_{ia}^\dagger t_{j\beta} (h_{1ib} h_{1jd}^\dagger + h_{2ib} h_{2jd}^\dagger) \\
& + (h.c.)\}
\end{aligned} \tag{B7}$$

Now let us turn our attention to the Hamiltonian  $H_J$ . Contribution from the coupling inside the dimer has been shown previously. That is,

$$\mathbf{S}_{1i} \cdot \mathbf{S}_{2i} = -\frac{3}{4} s_i^\dagger s_i + \frac{1}{4} t_{i\alpha}^\dagger t_{i\alpha} \tag{B8}$$

Coupling term between the spins of different dimers is given by:

$$\begin{aligned}
S_{1i\alpha} S_{1j\alpha} = & \tilde{S}_{1i\alpha} \tilde{S}_{1j\alpha} + \frac{1}{4} \sigma_{ab}^\alpha \sigma_{cd}^\alpha h_{1ia}^\dagger h_{1ib} h_{1jc}^\dagger h_{1jd} \\
& + \frac{1}{2} h_{1ia}^\dagger \sigma_{ab}^\alpha h_{1ib} \tilde{S}_{1j\alpha} + \frac{1}{2} h_{1ja}^\dagger \sigma_{ab}^\alpha h_{1jb} \tilde{S}_{1i\alpha}.
\end{aligned} \tag{B9}$$

Remember that  $\tilde{S}_{1i\alpha} = \frac{1}{2}(s_i^\dagger t_{i\alpha} + t_{i\alpha}^\dagger s_i - i\varepsilon_{\alpha\beta\gamma} t_{i\beta}^\dagger t_{i\gamma})$  and  $\tilde{S}_{2i\alpha} = -\frac{1}{2}(s_i^\dagger t_{i\alpha} + t_{i\alpha}^\dagger s_i + i\varepsilon_{\alpha\beta\gamma} t_{i\beta}^\dagger t_{i\gamma})$ . The cross term can be ignored assuming that there is no contribution from the term containing a single  $t$  operator or  $t_\alpha^\dagger t_\beta$  with  $\alpha \neq \beta$ . In other words, it is assumed that there is no magnetic ordering. Therefore,

$$\begin{aligned}
S_{1i\alpha} S_{1j\alpha} + S_{2i\alpha} S_{2j\alpha} \\
= \tilde{S}_{1i\alpha} \tilde{S}_{1j\alpha} + \tilde{S}_{2i\alpha} \tilde{S}_{2j\alpha} + \frac{1}{\lambda J} H_{h^4}
\end{aligned} \tag{B10}$$

where

$$\begin{aligned}
H_{h^4} = & \frac{\lambda J}{4} \sum_{\langle i,j \rangle} \sigma_{ab}^\alpha \sigma_{cd}^\alpha \{h_{1ia}^\dagger h_{1ib} h_{1jc}^\dagger h_{1jd} \\
& + h_{2ia}^\dagger h_{2ib} h_{2jc}^\dagger h_{2jd}\}
\end{aligned} \tag{B11}$$

Coupling terms involving  $\tilde{S}$  are evaluated below.

$$\begin{aligned}
4(\tilde{S}_{1i\alpha} \tilde{S}_{1j\alpha} + \tilde{S}_{2i\alpha} \tilde{S}_{2j\alpha}) \\
= (s_i^\dagger t_{i\alpha} + t_{i\alpha}^\dagger s_i - i\varepsilon_{\alpha\beta\gamma} t_{i\beta}^\dagger t_{i\gamma})
\end{aligned}$$

$$\begin{aligned}
& \times (s_j^\dagger t_{j\alpha} + t_{j\alpha}^\dagger s_j - i\varepsilon_{\alpha\mu\nu} t_{j\mu}^\dagger t_{j\nu}) \\
& + (s_i^\dagger t_{i\alpha} + t_{i\alpha}^\dagger s_i + i\varepsilon_{\alpha\beta\gamma} t_{i\beta}^\dagger t_{i\gamma}) \\
& \times (s_j^\dagger t_{j\alpha} + t_{j\alpha}^\dagger s_j + i\varepsilon_{\alpha\mu\nu} t_{j\mu}^\dagger t_{j\nu}) \\
& = 2\{t_{i\alpha}^\dagger t_{j\alpha}^\dagger s_i s_j + t_{i\alpha} t_{j\alpha} s_i^\dagger s_j^\dagger \\
& + t_{i\alpha}^\dagger t_{j\alpha} s_j^\dagger s_i + t_{j\alpha}^\dagger t_{i\alpha} s_i^\dagger s_j\} \\
& - 2\varepsilon_{\alpha\beta\gamma} \varepsilon_{\alpha\mu\nu} t_{i\beta}^\dagger t_{i\gamma} t_{j\mu}^\dagger t_{j\nu}
\end{aligned} \tag{B12}$$

Therefore  $H_J$  is summarized as follows.

$$\begin{aligned}
H_J = & J \sum_i \{-\frac{3}{4} s_i^\dagger s_i + \frac{1}{4} t_{i\alpha}^\dagger t_{i\alpha}\} \\
& + \frac{\lambda J}{2} \sum_{\langle i,j \rangle} \{t_{i\alpha}^\dagger t_{j\alpha}^\dagger s_i s_j + t_{i\alpha} t_{j\alpha} s_i^\dagger s_j^\dagger \\
& + t_{i\alpha}^\dagger t_{j\alpha} s_j^\dagger s_i + t_{j\alpha}^\dagger t_{i\alpha} s_i^\dagger s_j\} \\
& - \underbrace{\frac{\lambda J}{2} \sum_{\langle i,j \rangle} \varepsilon_{\alpha\beta\gamma} \varepsilon_{\alpha\mu\nu} t_{i\beta}^\dagger t_{i\gamma} t_{j\mu}^\dagger t_{j\nu}}_{\equiv H_{t^4}} + H_{h^4} \\
\Rightarrow & -\frac{3}{4} J N \bar{s}^2 + \frac{J}{4} \sum_i t_{i\alpha}^\dagger t_{i\alpha} \\
& + \frac{\lambda J}{2} \bar{s}^2 \sum_{\langle i,j \rangle} \{t_{i\alpha}^\dagger t_{j\alpha}^\dagger + t_{i\alpha} t_{j\alpha} + t_{i\alpha}^\dagger t_{j\alpha} + t_{j\alpha}^\dagger t_{i\alpha}\} \\
& + H_{t^4} + H_{h^4}
\end{aligned} \tag{B13}$$

where  $N$  is the number of dimers and  $s$  boson is condensed so that  $s_i = \bar{s}$ . The total Hamiltonian (without constraints) is given by the sum of  $H_t$  and  $H_J$ .

$$\begin{aligned}
H = & H_t + H_J \\
= & -t \sum_i \{h_{1ia}^\dagger h_{2ia} + h_{2ia}^\dagger h_{1ia}\} \\
& - t(\bar{d}^2 - \frac{1}{2}\bar{s}^2) \sum_{\langle i,j \rangle} \{h_{1ia}^\dagger h_{1ja} + h_{1ja}^\dagger h_{1ia} \\
& + h_{2ia}^\dagger h_{2ja} + h_{2ja}^\dagger h_{2ia}\} \\
& - \sqrt{2}t\bar{d}\bar{s} \sum_{\langle i,j \rangle} \varepsilon_{ab} \{h_{1ia}^\dagger h_{2jb}^\dagger + h_{2ia}^\dagger h_{1jb}^\dagger \\
& + h_{2jb} h_{1ia} + h_{1jb} h_{2ia}\} \\
& - \frac{3}{4} J N \bar{s}^2 + \frac{J}{4} \sum_i t_{i\alpha}^\dagger t_{i\alpha} \\
& + \frac{\lambda J}{2} \bar{s}^2 \sum_{\langle i,j \rangle} \{t_{i\alpha}^\dagger t_{j\alpha}^\dagger + t_{i\alpha} t_{j\alpha} + t_{i\alpha}^\dagger t_{j\alpha} + t_{j\alpha}^\dagger t_{i\alpha}\} \\
& + H_{t^2 h^2} + H_{t^4} + H_{h^4}
\end{aligned} \tag{B14}$$

As one can see in the following sections, a convenient simplification is obtained by expressing the Hamiltonian in terms of the bonding and anti-bonding fermionic operators which are defined as follows:

$$\begin{aligned}
h_{i+a} &\equiv \frac{1}{\sqrt{2}}(h_{1ia} + h_{2ia}) \\
h_{i-a} &\equiv \frac{1}{\sqrt{2}}(h_{1ia} - h_{2ia})
\end{aligned} \tag{B15}$$

### 1. Mean-Field Hamiltonian without Quartic Terms

In this section we will ignore the terms from  $H_{t^4}$ ,  $H_{h^4}$  and  $H_{t^2h^2}$ . Then, the Hamiltonian is given in momentum space representation as follows.

$$\begin{aligned}
H = & -N\frac{3}{4}J\bar{s}^2 + \sum_{k_y} \left( \frac{J}{4} + \lambda J\bar{s}^2 \cos k_y \right) t_\alpha^\dagger(k_y) t_\alpha(k_y) \\
& + \sum_{k_y} \frac{\lambda J\bar{s}^2}{2} \cos k_y \{ t_\alpha^\dagger(k_y) t_\alpha^\dagger(-k_y) + t_\alpha(k_y) t_\alpha(-k_y) \} \\
& + \sum_{k_y} \{ t(\bar{s}^2 - 2\bar{d}^2) \cos k_y - t \} h_{+a}^\dagger(k_y) h_{+a}(k_y) \\
& + \sum_{k_y} \{ t(\bar{s}^2 - 2\bar{d}^2) \cos k_y + t \} h_{-a}^\dagger(k_y) h_{-a}(k_y) \\
& - 2\sqrt{2}t\bar{d}\bar{s} \sum_{k_y} \cos k_y \{ h_{+\uparrow}^\dagger(k_y) h_{+\downarrow}^\dagger(-k_y) \\
& - h_{-\uparrow}^\dagger(k_y) h_{-\downarrow}^\dagger(-k_y) + (h.c.) \}
\end{aligned} \tag{B16}$$

As mentioned previously, it is necessary to impose certain constraints. In this study, constraints are introduced in Lagrange multiplier method. In other words, “constraint Hamiltonian” ( $H_c$ ) is added to the original Hamiltonian. And then the unknown parameters are determined by the saddle point condition of the ground state energy.

$$\begin{aligned}
H_c = & -\mu \sum_i (s_i^\dagger s_i + t_{i\alpha}^\dagger t_{i\alpha} + h_{1ia}^\dagger h_{1ia} + h_{2ia}^\dagger h_{2ia} \\
& + d_i^\dagger d_i - 1) \\
& - \xi \sum_i (h_{1ia}^\dagger h_{1ia} + h_{2ia}^\dagger h_{2ia} + 2d_i^\dagger d_i - 2x) \\
\Rightarrow & -\mu \sum_{k_y} (t_\alpha^\dagger(k_y) t_\alpha(k_y) + \bar{s}^2 - \bar{d}^2 + 2x - 1) \\
& - \xi \sum_{k_y} (h_{+a}^\dagger(k_y) h_{+a}(k_y) + h_{-a}^\dagger(k_y) h_{-a}(k_y) \\
& + 2\bar{d}^2 - 2x)
\end{aligned} \tag{B17}$$

where  $x$  is the hole concentration.

Therefore the total Hamiltonian with constraints is given by:

$$\begin{aligned}
H = & N\epsilon_0 \\
& + \sum_{k_y} \{ A_{k_y} t_\alpha^\dagger(k_y) t_\alpha(k_y) \\
& + B_{k_y} (t_\alpha^\dagger(k_y) t_\alpha^\dagger(-k_y) + t_\alpha(k_y) t_\alpha(-k_y)) \}
\end{aligned}$$

$$\begin{aligned}
& + \sum_{k_y} \{ \epsilon_+(k_y) h_{+a}^\dagger(k_y) h_{+a}(k_y) \\
& - D(k_y) (h_{+\uparrow}^\dagger(k_y) h_{+\downarrow}^\dagger(-k_y) + h_{+\downarrow}(-k_y) h_{+\uparrow}(k_y)) \} \\
& + \sum_{k_y} \{ \epsilon_-(k_y) h_{-a}^\dagger(k_y) h_{-a}(k_y) \\
& + D(k_y) (h_{-\uparrow}^\dagger(k_y) h_{-\downarrow}^\dagger(-k_y) + h_{-\downarrow}(-k_y) h_{-\uparrow}(k_y)) \}
\end{aligned} \tag{B18}$$

where

$$\begin{aligned}
\epsilon_0 = & -\frac{3}{4}J\bar{s}^2 - \mu(\bar{s}^2 - \bar{d}^2 + 2x - 1) \\
& - \xi(2\bar{d}^2 - 2x)
\end{aligned} \tag{B19}$$

$$A_{k_y} = \frac{J}{4} - \mu + \lambda J\bar{s}^2 \cos k_y \tag{B20}$$

$$B_{k_y} = \frac{\lambda J}{2} \bar{s}^2 \cos k_y \tag{B21}$$

$$\epsilon_+(k_y) = t(\bar{s}^2 - 2\bar{d}^2) \cos k_y - t - \xi \tag{B22}$$

$$\epsilon_-(k_y) = t(\bar{s}^2 - 2\bar{d}^2) \cos k_y + t - \xi \tag{B23}$$

$$D(k_y) = 2\sqrt{2}t\bar{d}\bar{s} \cos k_y \tag{B24}$$

The above Hamiltonian can be diagonalized by using Bogoliubov transformation. That is,

$$\gamma_\alpha(k_y) = u_t(k_y) t_\alpha(k_y) + v_t(k_y) t_\alpha^\dagger(-k_y) \tag{B25}$$

$$\beta_{\pm a}(k_y) = u_\pm(k_y) h_{\pm a}(k_y) + v_\pm(k_y) \varepsilon_{ab} h_{\pm b}^\dagger(-k_y) \tag{B26}$$

where

$$u_t^2(k_y) = \frac{1}{2} \left( \frac{A_{k_y}}{\omega_{k_y}} + 1 \right) \tag{B27}$$

$$v_t^2(k_y) = \frac{1}{2} \left( \frac{A_{k_y}}{\omega_{k_y}} - 1 \right) \tag{B28}$$

$$u_t(k_y) v_t(k_y) = \frac{B_{k_y}}{\omega_{k_y}} \tag{B29}$$

$$\omega_{k_y} = \sqrt{A_{k_y}^2 - 4B_{k_y}^2} \tag{B30}$$

and

$$u_\pm^2(k_y) = \frac{1}{2} \left( 1 + \frac{\epsilon_\pm(k_y)}{\Omega_\pm(k_y)} \right) \tag{B31}$$

$$v_\pm^2(k_y) = \frac{1}{2} \left( 1 - \frac{\epsilon_\pm(k_y)}{\Omega_\pm(k_y)} \right) \tag{B32}$$

$$u_\pm(k_y) v_\pm(k_y) = \mp \frac{D(k_y)}{\Omega_\pm(k_y)} \tag{B33}$$

$$\Omega_\pm(k_y) = \sqrt{\epsilon_\pm^2(k_y) + D^2(k_y)} \tag{B34}$$

In terms of Bogoliubov variables, Hamiltonian is written as follows.

$$\begin{aligned}
H = & N\epsilon_0 + \sum_{k_y} \omega_{k_y} \gamma_\alpha^\dagger(k_y) \gamma_\alpha(k_y) + \frac{3}{2} \sum_{k_y} (\omega_{k_y} - A_{k_y}) \\
& + \sum_{k_y} \Omega_+(k_y) \beta_{+a}^\dagger(k_y) \beta_{+a}(k_y)
\end{aligned}$$

$$\begin{aligned}
& + \sum_{k_y} \left\{ \epsilon_+(k_y) - \sqrt{\epsilon_+^2(k_y) + D^2(k_y)} \right\} \\
& + \sum_{k_y} \Omega_-(k_y) \beta_{-a}^\dagger(k_y) \beta_{-a}(k_y) \\
& + \sum_{k_y} \left\{ \epsilon_-(k_y) - \sqrt{\epsilon_-^2(k_y) + D^2(k_y)} \right\} \quad (B35)
\end{aligned}$$

*a. Ground State Energy and Saddle-Point Equations*

Now the ground state energy per particle is given by:

$$\begin{aligned}
\epsilon_{gr} &= \frac{\langle H \rangle_{gr}}{N} \\
&= \epsilon_0 + \frac{3}{2} \int_0^\pi \frac{dk_y}{\pi} (\omega_{k_y} - A_{k_y}) \\
&\quad + \int_0^\pi \frac{dk_y}{\pi} \{ \epsilon_+(k_y) - \Omega_+(k_y) \} \\
&\quad + \int_0^\pi \frac{dk_y}{\pi} \{ \epsilon_-(k_y) - \Omega_-(k_y) \} \\
&= \epsilon'_0 + \frac{3}{2} \int_0^\pi \frac{dk_y}{\pi} \omega_{k_y} \\
&\quad - \int_0^\pi \frac{dk_y}{\pi} \Omega_+(k_y) - \int_0^\pi \frac{dk_y}{\pi} \Omega_-(k_y) \quad (B36)
\end{aligned}$$

where

$$\epsilon'_0 = -\frac{3}{4} J \bar{s}^2 - \mu (\bar{s}^2 - \bar{d}^2 + 2x - \frac{5}{2}) - \xi (2 + 2\bar{d}^2 - 2x). \quad (B37)$$

Note that constants obtained from integrating  $A_{k_y}$  and  $\epsilon_\pm(k_y)$  are ignored.

The term contributed from the triplet bosons ( $t_\alpha$ ) can be intergrated explicitly by using the elliptic function  $\mathbf{E}$ .

$$\begin{aligned}
\epsilon_{gr} &= \epsilon'_0 + \frac{3}{\pi} J \left( \frac{1}{4} - \frac{\mu}{J} \right) \sqrt{1+\eta} \mathbf{E} \left( \sqrt{\frac{2\eta}{1+\eta}} \right) \\
&\quad - \int_0^\pi \frac{dk_y}{\pi} \Omega_+(k_y) - \int_0^\pi \frac{dk_y}{\pi} \Omega_-(k_y) \quad (B38)
\end{aligned}$$

where

$$\eta = \frac{2\lambda \bar{s}^2}{\frac{1}{4} - \frac{\mu}{J}}. \quad (B39)$$

Parameters in the Hamiltonian are determined by the saddle point condition in the mean-field approximation. In other words,

$$\frac{\partial \epsilon_{gr}}{\partial \bar{s}} = \frac{\partial \epsilon_{gr}}{\partial \mu} = \frac{\partial \epsilon_{gr}}{\partial \bar{d}} = \frac{\partial \epsilon_{gr}}{\partial \xi} = 0. \quad (B40)$$

Explicit saddle-point equations are written as follows.

$$\begin{aligned}
\frac{\partial(\epsilon_{gr}/J)}{\partial \bar{s}^2} &= -\frac{3}{4} - \frac{\mu}{J} + \frac{3\lambda}{\pi\eta} \left\{ \sqrt{1+\eta} \mathbf{E} \left( \sqrt{\frac{2\eta}{1+\eta}} \right) \right. \\
&\quad \left. - \frac{1}{\sqrt{1+\eta}} \mathbf{K} \left( \sqrt{\frac{2\eta}{1+\eta}} \right) \right\} \\
&\quad - \frac{t/J}{\bar{s}} \int_0^\pi \frac{dk_y}{\pi} \cos k_y \left\{ \frac{\bar{s}\epsilon_+(k_y) + \sqrt{2}\bar{d}D(k_y)}{\Omega_+(k_y)} \right. \\
&\quad \left. + \frac{\bar{s}\epsilon_-(k_y) + \sqrt{2}\bar{d}D(k_y)}{\Omega_-(k_y)} \right\} = 0 \quad (B41)
\end{aligned}$$

$$\begin{aligned}
\frac{\partial(\epsilon_{gr}/J)}{\partial(\mu/J)} &= \bar{d}^2 - \bar{s}^2 + \frac{5}{2} - 2x \\
&\quad - \frac{3}{2\pi} \left\{ \sqrt{1+\eta} \mathbf{E} \left( \sqrt{\frac{2\eta}{1+\eta}} \right) \right. \\
&\quad \left. + \frac{1}{\sqrt{1+\eta}} \mathbf{K} \left( \sqrt{\frac{2\eta}{1+\eta}} \right) \right\} = 0 \quad (B42)
\end{aligned}$$

$$\begin{aligned}
\frac{\partial(\epsilon_{gr}/J)}{\partial \bar{d}^2} &= \frac{\mu}{J} - 2\frac{t}{J} \frac{\xi}{t} \\
&\quad + \frac{t/J}{\bar{d}} \int_0^\pi \frac{dk_y}{\pi} \cos k_y \left\{ \frac{2\bar{d}\epsilon_+(k_y) - \sqrt{2}\bar{s}D(k_y)}{\Omega_+(k_y)} \right. \\
&\quad \left. + \frac{2\bar{d}\epsilon_-(k_y) - \sqrt{2}\bar{s}D(k_y)}{\Omega_-(k_y)} \right\} = 0 \quad (B43)
\end{aligned}$$

$$\begin{aligned}
\frac{\partial(\epsilon_{gr}/J)}{\partial(\xi/J)} &= -2 - 2\bar{d}^2 + 2x \\
&\quad + \int_0^\pi \frac{dk_y}{\pi} \left\{ \frac{\epsilon_+(k_y)}{\Omega_+(k_y)} + \frac{\epsilon_-(k_y)}{\Omega_-(k_y)} \right\} = 0 \quad (B44)
\end{aligned}$$

*b. Limiting Case with  $\bar{d} = 0$*

The above saddle-point equations are highly non-linear as a function of parameters  $\bar{s}$ ,  $\mu$ ,  $\bar{d}$ , and  $\xi$ . Since analytic solution is not accessible in this case, it is natural to make use of a numerical method. In general, solving a set of non-linear equations numerically is quite sensitive to the initial guesses of parameters. Therefore, it is very desirable to have some limiting situation where an explicit, analytic solution is available. Such a situation is realized when we set  $\bar{d} = 0$ , i.e. turning off the pairing terms. Then, the ground state energy is given as follows.

$$\begin{aligned}
\epsilon_{gr} &= \epsilon_0 - \frac{3}{2} J \left( \frac{1}{4} - \frac{\mu}{J} \right) \left\{ 1 - \frac{2}{\pi} \sqrt{1+\eta} \mathbf{E} \left( \sqrt{\frac{2\eta}{1+\eta}} \right) \right\} \\
&\quad + \int_0^\pi \frac{dk_y}{\pi} \{ \epsilon_+(k_y) - \Omega_+(k_y) \} \quad (B45)
\end{aligned}$$

where the contribution from the anti-bonding fermion ( $h_-$ ) is ignored because, in the case of  $t/J \geq 1$ , the anti-bonding fermion will have a reasonably larger energy than the bonding one, separated by roughly  $2t$ . And



therefore its contribution to the ground state energy is very small.

The fermion contribution can be simplified further.

$$\begin{aligned}
& \int_0^\pi \frac{dk_y}{\pi} \left\{ \epsilon_+(k_y) - \Omega_+(k_y) \right\} \\
&= \frac{2}{\pi} \int_{k_F}^\pi dk_y [\epsilon_+(k_y)]_{\bar{d}=0} \\
&= \frac{2}{\pi} \int_{k_F}^\pi dk_y (t\bar{s}^2 \cos k_y - t - \xi) \\
&= -\frac{2}{\pi} \left\{ (t + \xi)(\pi - k_F) + t\bar{s}^2 \sin k_F \right\} \\
&= \frac{2}{\pi} t\bar{s}^2 \left\{ \pi x \cos(\pi x) - \sin(\pi x) \right\} \quad (\text{B46})
\end{aligned}$$

where the chemical potential  $\xi$  and the Fermi wavevector  $k_F$  are determined by:

$$\sum_{k_y} h_{+a}^\dagger(k_y) h_{+a}(k_y) = x \Leftrightarrow \frac{2}{\pi}(\pi - k_F) = 2x \quad (\text{B47})$$

$$\epsilon_+(k_F) = 0 \Leftrightarrow \xi = t\bar{s}^2 \cos k_F - t. \quad (\text{B48})$$

Now the saddle-point equations are reduced to the following equations.

$$\begin{aligned}
\frac{\partial(\epsilon_{gr}/J)}{\partial\bar{s}^2} &= -\left(\frac{3}{4} + \frac{\mu}{J}\right) + \frac{3\lambda}{\pi\eta} \left\{ \sqrt{1+\eta} \mathbf{E} \left( \sqrt{\frac{2\eta}{1+\eta}} \right) \right. \\
&\quad \left. - \frac{1}{\sqrt{1+\eta}} \mathbf{K} \left( \sqrt{\frac{2\eta}{1+\eta}} \right) \right\} \\
&\quad + \frac{2t}{\pi} (\pi x \cos(\pi x) - \sin(\pi x)) = 0 \quad (\text{B49})
\end{aligned}$$

$$\begin{aligned}
\frac{\partial(\epsilon_{gr}/J)}{\partial(\mu/J)} &= \frac{5}{2} - 2x - \bar{s}^2 - \frac{3}{2\pi} \left\{ \sqrt{1+\eta} \mathbf{E} \left( \sqrt{\frac{2\eta}{1+\eta}} \right) \right. \\
&\quad \left. + \frac{1}{\sqrt{1+\eta}} \mathbf{K} \left( \sqrt{\frac{2\eta}{1+\eta}} \right) \right\} = 0 \quad (\text{B50})
\end{aligned}$$

Note that the other saddle-point equations are explicitly solved. In other words,

$$\bar{d} = 0 \quad (\text{B51})$$

$$\xi = -t\bar{s}^2 \cos(\pi x) - t \quad (\text{B52})$$

Convenient simplification is realized from the fact that Eq.(B49) and (B50) can be combined to reduce to a equation containing only one parameter  $\eta$ . That is,

$$\begin{aligned}
& \frac{\eta}{2\lambda} \left\{ 1 - \frac{2}{\pi} \frac{t}{J} (\pi x \cos(\pi x) - \sin(\pi x)) \right\} \\
&= \frac{5}{2} - 2x - \frac{3}{\pi} \frac{1}{\sqrt{1+\eta}} \mathbf{K} \left( \sqrt{\frac{2\eta}{1+\eta}} \right) \quad (\text{B53})
\end{aligned}$$

where, once again,  $\eta = \frac{2\lambda\bar{s}^2}{1/4 - \mu/J}$ .

## 2. Mean-Field Hamiltonian with Quartic Terms

In this section, effects of quartic terms such as  $H_{t^4}$ ,  $H_{h^4}$ , and  $H_{t^2h^2}$  are included approximately by using quadratic decoupling. Let us start from  $H_{t^4}$ .

$$\begin{aligned}
H_{t^4} &= -\frac{\lambda J}{2} \sum_{\langle i,j \rangle} \epsilon_{\alpha\beta\gamma} \epsilon_{\alpha\mu\nu} t_{i\beta}^\dagger t_{i\gamma}^\dagger t_{j\mu}^\dagger t_{j\nu} \\
&= -\frac{\lambda J}{2} \sum_{\langle i,j \rangle} \{ t_{i\alpha}^\dagger t_{i\beta}^\dagger t_{j\alpha}^\dagger t_{j\beta} - t_{i\alpha}^\dagger t_{i\beta}^\dagger t_{j\beta}^\dagger t_{j\alpha} \} \quad (\text{B54})
\end{aligned}$$

Quadratic decoupling is carried out as follows.

$$\begin{aligned}
t_{i\alpha}^\dagger t_{j\alpha}^\dagger t_{i\beta} t_{j\beta} &\simeq \langle t_{i\alpha}^\dagger t_{j\alpha}^\dagger \rangle t_{i\beta} t_{j\beta} + t_{i\alpha}^\dagger t_{j\alpha}^\dagger \langle t_{i\beta} t_{j\beta} \rangle \\
&\quad - \langle t_{i\alpha}^\dagger t_{j\alpha}^\dagger \rangle \langle t_{i\beta} t_{j\beta} \rangle \quad (\text{B55})
\end{aligned}$$

$$\begin{aligned}
t_{i\alpha}^\dagger t_{j\beta}^\dagger t_{i\beta} t_{j\alpha} &\simeq \langle t_{i\alpha}^\dagger t_{j\alpha}^\dagger \rangle t_{j\beta}^\dagger t_{i\beta} + t_{i\alpha}^\dagger t_{j\alpha}^\dagger \langle t_{j\beta}^\dagger t_{i\beta} \rangle \\
&\quad - \langle t_{i\alpha}^\dagger t_{j\alpha}^\dagger \rangle \langle t_{j\beta}^\dagger t_{i\beta} \rangle \quad (\text{B56})
\end{aligned}$$

Therefore,  $H_{t^4}$  is given by:

$$\begin{aligned}
H_{t^4} &= \frac{\lambda J}{2} \sum_{\langle i,j \rangle} \{ P_y \left( t_{i\alpha}^\dagger t_{j\alpha} + t_{j\alpha}^\dagger t_{i\alpha} \right) \\
&\quad - Q_y \left( t_{i\alpha}^\dagger t_{j\alpha}^\dagger + t_{j\alpha} t_{i\alpha} \right) \} \\
&\quad - N \frac{\lambda J}{2} (P_y^2 - Q_y^2) \\
&= \frac{\lambda J}{2} \sum_{k_y} \cos k_y \{ 2P_y t_\alpha^\dagger(k_y) t_\alpha(k_y) \\
&\quad - Q_y (t_\alpha^\dagger(k_y) t_\alpha^\dagger(-k_y) + t_\alpha(-k_y) t_\alpha(k_y)) \} \\
&\quad - N \frac{\lambda J}{2} (P_y^2 - Q_y^2) \quad (\text{B57})
\end{aligned}$$

where

$$P_y \equiv \langle t_{i\alpha}^\dagger t_{j\alpha} \rangle = \sum_{k_y} \cos k_y \langle t_\alpha^\dagger(k_y) t_\alpha(k_y) \rangle \quad (\text{B58})$$

$$Q_y \equiv \langle t_{i\alpha}^\dagger t_{j\alpha}^\dagger \rangle = \sum_{k_y} \cos k_y \langle t_\alpha^\dagger(k_y) t_\alpha^\dagger(-k_y) \rangle. \quad (\text{B59})$$

Note that the translational symmetry is assumed. Now let us turn to the Hamiltonian  $H_{t^2h^2}$ .

$$\begin{aligned}
H_{t^2h^2} &= -\frac{t}{2} \epsilon_{ac} \epsilon_{ae} \sigma_{cb}^\alpha \sigma_{ed}^\beta \sum_{\langle i,j \rangle} \{ t_{i\alpha}^\dagger t_{j\beta} (h_{1ib} h_{1jd}^\dagger + h_{2ib} h_{2jd}^\dagger) \\
&\quad + (h.c.) \} \quad (\text{B60})
\end{aligned}$$

Remembering that, in the present approximation, non-zero quadratic contraction is obtained only when  $\alpha = \beta$  for  $\langle t_\alpha^\dagger t_\beta \rangle$ , and  $a = b$  for  $\langle h_a^\dagger h_b \rangle$ , the Hamiltonian  $H_{t^2h^2}$  is quadratically decoupled as follows.

$$+ \epsilon_{ac} \epsilon_{ae} \sigma_{cb}^\alpha \sigma_{ed}^\beta \sum_{\langle i,j \rangle} t_{i\alpha}^\dagger t_{j\beta} \{ h_{1ib} h_{1jd}^\dagger + (h.c.) \}$$

$$\begin{aligned}
&\simeq \varepsilon_{ac}\varepsilon_{ae}\sigma_{cb}^\alpha\bar{\sigma}_{eb}^\alpha \sum_{\langle i,j \rangle} t_{i\alpha}^\dagger t_{j\alpha} \{h_{1ib}h_{1jb}^\dagger + (h.c.)\} \\
&\simeq -\langle t_{i\alpha}^\dagger t_{j\alpha} \rangle h_{1ja}^\dagger h_{1ia} - t_{i\alpha}^\dagger t_{j\alpha} \langle h_{1ja}^\dagger h_{1ia} \rangle \\
&\quad + \langle t_{i\alpha}^\dagger t_{j\alpha} \rangle \langle h_{1ja}^\dagger h_{1ia} \rangle + (h.c.) \\
&= -P_y \left( h_{1ja}^\dagger h_{1ia} + h_{1ia}^\dagger h_{1ja} \right) - \Pi_y \left( t_{i\alpha}^\dagger t_{j\alpha} + t_{i\alpha}^\dagger t_{j\alpha} \right) \\
&\quad + 2P_y \Pi_y
\end{aligned} \tag{B61}$$

where

$$\Pi_y \equiv \langle h_{1ja}^\dagger h_{1ia} \rangle = \sum_{k_y} \cos k_y \langle h_{1a}^\dagger(k_y) h_{1a}(k_y) \rangle. \tag{B62}$$

Once again it is convenient to use the bonding and anti-bonding fermion representation. By using the reflection symmetry,  $\Pi_y$  is given by:

$$\begin{aligned}
\Pi_y &= \sum_{k_y} \cos k_y \langle h_{1a}^\dagger(k_y) h_{1a}(k_y) \rangle \\
&= \sum_{k_y} \cos k_y \langle h_{2a}^\dagger(k_y) h_{2a}(k_y) \rangle \\
&= \frac{1}{2} \sum_{k_y} \cos k_y \{ \langle h_{+a}^\dagger(k_y) h_{+a}(k_y) \rangle \\
&\quad + \langle h_{-a}^\dagger(k_y) h_{-a}(k_y) \rangle \}
\end{aligned} \tag{B63}$$

Finally, the Hamiltonian  $H_{t^2h^2}$  is given by:

$$\begin{aligned}
H_{t^2h^2} &= tP_y \sum_{k_y} \cos k_y \left( h_{+a}^\dagger(k) h_{+a}(k) + h_{-a}^\dagger(k) h_{-a}(k) \right) \\
&\quad + 2t\Pi_y \sum_{k_y} \cos k_y t_\alpha^\dagger(k_y) t_\alpha(k_y) \\
&\quad - 4tN P_y \Pi_y
\end{aligned} \tag{B64}$$

Now, quadratic decoupling of  $H_{h^4}$  is performed. First,  $H_{h^4}$  is given by:

$$\begin{aligned}
H_{h^4} &= \frac{\lambda J}{4} \sum_{\langle i,j \rangle} \sigma_{ab}^\alpha \sigma_{cd}^\alpha \{ h_{1ia}^\dagger h_{1ib} h_{1jc}^\dagger h_{1jd} \\
&\quad + h_{2ia}^\dagger h_{2ib} h_{2jc}^\dagger h_{2jd} \}
\end{aligned} \tag{B65}$$

Suppressing the site index within a dimer, i.e. 1 or 2, let us first consider the following term inside summation.

$$\begin{aligned}
&\sigma_{ab}^\alpha \sigma_{cd}^\alpha h_{ia}^\dagger h_{ib} h_{jc}^\dagger h_{jd} \\
&= 2 \{ h_{i\uparrow}^\dagger h_{i\downarrow} h_{j\downarrow}^\dagger h_{j\uparrow} + h_{i\downarrow}^\dagger h_{i\uparrow} h_{j\uparrow}^\dagger h_{j\downarrow} \} \\
&\quad + \{ h_{i\uparrow}^\dagger h_{i\uparrow} - h_{i\downarrow}^\dagger h_{i\downarrow} \} \{ h_{j\uparrow}^\dagger h_{j\uparrow} - h_{j\downarrow}^\dagger h_{j\downarrow} \} \\
&= -\frac{3}{2} \Pi_y (h_{ja}^\dagger h_{ia} + h_{ia}^\dagger h_{ja}) + \frac{3}{2} \Pi_y^2 \\
&\quad - 3\Delta_y (h_{i\uparrow}^\dagger h_{j\downarrow}^\dagger + h_{j\downarrow} h_{i\uparrow}) - 3\Delta_y (h_{j\uparrow}^\dagger h_{i\downarrow}^\dagger + h_{i\downarrow} h_{j\uparrow}) \\
&\quad + 6\Delta_y^2
\end{aligned} \tag{B66}$$

where, once again,  $\Pi_y$  is given by:

$$\begin{aligned}
\Pi_y &= \frac{1}{2} \sum_{k_y} \cos k_y \left\{ \langle h_{+a}^\dagger(k_y) h_{+a}(k_y) \rangle \right. \\
&\quad \left. + \langle h_{-a}^\dagger(k_y) h_{-a}(k_y) \rangle \right\},
\end{aligned} \tag{B67}$$

and also  $\Delta_y$  is defined as follows:

$$\begin{aligned}
\Delta_y &= \frac{1}{2} \sum_{k_y} \cos k_y \left\{ \langle h_{+\uparrow}^\dagger(k_y) h_{+\downarrow}^\dagger(-k_y) \rangle \right. \\
&\quad \left. + \langle h_{-\uparrow}^\dagger(k_y) h_{-\downarrow}^\dagger(-k_y) \rangle \right\}.
\end{aligned} \tag{B68}$$

Therefore  $H_{h^4}$  can be written as follows.

$$\begin{aligned}
H_{h^4} &= -\frac{3}{4} \lambda J \sum_{k_y} \cos k_y \left\{ \Pi_y h_{+a}^\dagger(k_y) h_{+a}(k_y) \right. \\
&\quad \left. + 2\Delta_y \left( h_{+\uparrow}^\dagger(k_y) h_{+\downarrow}^\dagger(-k_y) + h_{+\downarrow}(-k_y) h_{+\uparrow}(k_y) \right) \right\} \\
&\quad - \frac{3}{4} \lambda J \sum_{k_y} \cos k_y \left\{ \Pi_y h_{-a}^\dagger(k_y) h_{-a}(k_y) \right. \\
&\quad \left. + 2\Delta_y \left( h_{-\uparrow}^\dagger(k_y) h_{-\downarrow}^\dagger(-k_y) + h_{-\downarrow}(-k_y) h_{-\uparrow}(k_y) \right) \right\} \\
&\quad + \frac{3}{4} N \lambda J (\Pi_y^2 + 4\Delta_y^2)
\end{aligned} \tag{B69}$$

Including all the quartic terms, the full, mean-field Hamiltonian is finally given by:

$$\begin{aligned}
H &= N\epsilon_0 + \sum_{k_y} \left\{ A'_{k_y} t_\alpha^\dagger(k_y) t_\alpha(k_y) \right. \\
&\quad \left. + B'_{k_y} \left( t_\alpha^\dagger(k_y) t_\alpha^\dagger(-k_y) + t_\alpha(k_y) t_\alpha(-k_y) \right) \right\} \\
&\quad + \sum_{k_y} \left\{ \epsilon'_+(k_y) h_{+a}^\dagger(k_y) h_{+a}(k_y) \right. \\
&\quad \left. - D'_+(k_y) \left( h_{+\uparrow}^\dagger(k_y) h_{+\downarrow}^\dagger(-k_y) + h_{+\downarrow}(-k_y) h_{+\uparrow}(k_y) \right) \right\} \\
&\quad + \sum_{k_y} \left\{ \epsilon'_-(k_y) h_{-a}^\dagger(k_y) h_{-a}(k_y) \right. \\
&\quad \left. + D'_-(k_y) \left( h_{-\uparrow}^\dagger(k_y) h_{-\downarrow}^\dagger(-k_y) + h_{-\downarrow}(-k_y) h_{-\uparrow}(k_y) \right) \right\}
\end{aligned} \tag{B70}$$

where

$$\begin{aligned}
\epsilon_0 &= -\frac{3}{4} J \bar{s}^2 - \mu(\bar{s}^2 - \bar{d}^2 + 2x - 1) \\
&\quad - \xi(2\bar{d}^2 - 2x) \\
A'_{k_y} &= A_{k_y} + \lambda J P_y \cos k_y + 2t\Pi_y \cos k_y \\
&= \frac{J}{4} - \mu + \lambda J(\bar{s}^2 + P_y) \cos k_y + 2t\Pi_y \cos k
\end{aligned}$$

$$\begin{aligned}
B'_{k_y} &= B_{k_y} - \frac{\lambda J}{2} Q_y \cos k_y \\
&= \frac{\lambda J}{2} (\bar{s}^2 - Q_y) \cos k_y \\
\epsilon'_+(k_y) &= \epsilon_+(k_y) - \frac{3}{4} \lambda J \Pi_y \cos k_y + t P_y \cos k_y \\
&= t(\bar{s}^2 - 2\bar{d}^2 + P_y) \cos k_y - \frac{3}{4} \lambda J \Pi_y \cos k_y - t - \xi \\
\epsilon'_-(k_y) &= \epsilon_-(k_y) - \frac{3}{4} \lambda J \Pi_y \cos k_y + t P_y \cos k_y \\
&= t(\bar{s}^2 - 2\bar{d}^2 + P_y) \cos k_y - \frac{3}{4} \lambda J \Pi_y \cos k_y + t - \xi \\
D'_+(k_y) &= D(k_y) + \frac{3}{2} \lambda J \Delta_y \cos k_y \\
&= 2\sqrt{2}t\bar{d}\bar{s} \cos k_y + \frac{3}{2} \lambda J \Delta_y \cos k_y \\
D'_-(k_y) &= D(k_y) - \frac{3}{2} \lambda J \Delta_y \cos k_y \\
&= 2\sqrt{2}t\bar{d}\bar{s} \cos k_y - \frac{3}{2} \lambda J \Delta_y \cos k_y
\end{aligned} \tag{B71}$$

Note that all the constants which are not explicitly dependent on  $\bar{s}$ ,  $\mu$ ,  $\bar{d}$ , and  $\xi$  are ignored. As previously, the above Hamiltonian can be diagonalized by using Bogoliubov transformation. That is,

$$\begin{aligned}
H &= N\epsilon_0 + \sum_{k_y} \omega'_{k_y} \gamma_\alpha^\dagger(k_y) \gamma_\alpha(k_y) + \frac{3}{2} \sum_{k_y} (\omega'_{k_y} - A'_{k_y}) \\
&+ \sum_{k_y} \Omega'_+(k_y) \beta_{+a}^\dagger(k_y) \beta_{+a}(k_y) \\
&+ \sum_{k_y} (\epsilon'_+(k_y) - \Omega'_+(k_y)) \\
&+ \sum_{k_y} \Omega'_-(k_y) \beta_{-a}^\dagger(k_y) \beta_{-a}(k_y) \\
&+ \sum_{k_y} (\epsilon'_-(k_y) - \Omega'_-(k_y))
\end{aligned} \tag{B72}$$

Saddle-point equations of the full Hamiltonian with quartic terms are similar to those without quartic terms except the fact that even the  $t$  boson part is not expressed explicitly.

$$\begin{aligned}
\frac{\partial(\epsilon_{gr}/J)}{\partial \bar{s}^2} &= -\frac{3}{4} - \frac{\mu}{J} + \frac{3}{2} \lambda \int_0^\pi \frac{dk_y}{\pi} \cos k_y \frac{A'_{k_y} - 2B'_{k_y}}{\omega'_{k_y}} \\
&- \frac{t/J}{\bar{s}} \int_0^\pi \frac{dk_y}{\pi} \cos k_y \left\{ \frac{\bar{s}\epsilon'_+(k_y) + \sqrt{2}\bar{d}D'_+(k_y)}{\Omega'_+(k_y)} \right. \\
&\left. + \frac{\bar{s}\epsilon'_-(k_y) + \sqrt{2}\bar{d}D'_-(k_y)}{\Omega'_-(k_y)} \right\} = 0
\end{aligned} \tag{B73}$$

$$\frac{\partial(\epsilon_{gr}/J)}{\partial(\mu/J)} = \bar{d}^2 - \bar{s}^2 + \frac{5}{2} - 2x - \frac{3}{2} \int_0^\pi \frac{dk_y}{\pi} \frac{A'_{k_y}}{\omega'_{k_y}} = 0 \tag{B74}$$

$$\begin{aligned}
\frac{\partial(\epsilon_{gr}/J)}{\partial \bar{d}^2} &= \frac{\mu}{J} - 2\frac{t}{J} \frac{\xi}{t} \\
&+ \frac{t/J}{\bar{d}} \int_0^\pi \frac{dk_y}{\pi} \cos k_y \left\{ \frac{2\bar{d}\epsilon'_+(k_y) - \sqrt{2}\bar{s}D'_+(k_y)}{\Omega'_+(k_y)} \right. \\
&\left. + \frac{2\bar{d}\epsilon'_-(k_y) - \sqrt{2}\bar{s}D'_-(k_y)}{\Omega'_-(k_y)} \right\} = 0
\end{aligned} \tag{B75}$$

$$\begin{aligned}
\frac{\partial(\epsilon_{gr}/J)}{\partial(\xi/J)} &= -2 - 2\bar{d}^2 + 2x \\
&+ \int_0^\pi \frac{dk_y}{\pi} \left\{ \frac{\epsilon'_+(k_y)}{\Omega'_+(k_y)} + \frac{\epsilon'_-(k_y)}{\Omega'_-(k_y)} \right\} = 0
\end{aligned} \tag{B76}$$

However, the above saddle-point equations are not meaningful without the knowledge of  $P_y$ ,  $Q_y$ ,  $\Pi_y$ , and  $\Delta_y$  used in  $A'_{k_y}$ ,  $B'_{k_y}$ ,  $\epsilon'_\pm(k_y)$ , and  $D'_\pm(k_y)$ . These are the formulas for them.

$$P_y = \frac{3}{2} \int_0^\pi \frac{dk_y}{\pi} \cos k_y \frac{A'_{k_y}}{\omega'_{k_y}} \tag{B77}$$

$$Q_y = -3 \int_0^\pi \frac{dk_y}{\pi} \cos k_y \frac{B'_{k_y}}{\omega'_{k_y}} \tag{B78}$$

$$\Pi_y = -\frac{1}{2} \int_0^\pi \frac{dk_y}{\pi} \cos k_y \left\{ \frac{\epsilon'_+(k_y)}{\Omega'_+(k_y)} + \frac{\epsilon'_-(k_y)}{\Omega'_-(k_y)} \right\} \tag{B79}$$

$$\Delta_y = \frac{1}{2} \int_0^\pi \frac{dk_y}{\pi} \cos k_y \left\{ \frac{D'_+(k_y)}{\Omega'_+(k_y)} - \frac{D'_-(k_y)}{\Omega'_-(k_y)} \right\} \tag{B80}$$

Upon solving the saddle-point equations, it is convenient to view  $P_y$ ,  $Q_y$ ,  $\Pi_y$ , and  $\Delta_y$  as unknown parameters similar to  $\bar{s}$ ,  $\bar{d}$ ,  $\mu$ , and  $\xi$ . Then, the original saddle-point conditions are equivalent to solving four saddle-point equations and four equations for  $P_y$ ,  $Q_y$ ,  $\Pi_y$ , and  $\Delta_y$  simultaneously.

### APPENDIX C: COMPUTATIONS FOR THE SQUARE LATTICE

This section is devoted to the two-dimensional array of coupled t-J ladders. Hamiltonian for the coupling between two-leg t-J ladders can be written as follows.

$$\begin{aligned}
H_\perp &= -t' \sum_i \sum_{\langle n,m \rangle} \{c_{2ina}^\dagger c_{1ima} + c_{1ima}^\dagger c_{2ina}\} \\
&+ \lambda' J \sum_i \sum_{\langle n,m \rangle} S_{1im}^\alpha S_{2in}^\alpha
\end{aligned} \tag{C1}$$

where the index  $i$  indicates the  $i$ -th dimer within a given ladder and the indices  $n$  ( $m \equiv n+1$ ) indicate the  $n$ -th ( $m$ -th) ladder. Derivation of the mean-field Hamiltonian for the dynamics perpendicular to the ladder direction, is rather similar to that of the parallel direction. But caution should be used in keeping track of signs of various

terms in Hamiltonian. Let us start from the hopping term between ladders.

$$\begin{aligned}
& c_{2ina}^\dagger c_{1ima} \\
&= \left\{ h_{2ina}^\dagger d_{in} + \frac{1}{\sqrt{2}} \varepsilon_{ab} s_{in}^\dagger h_{1inb} + \frac{1}{\sqrt{2}} \varepsilon_{ac} \sigma_{cb}^\alpha t_{in\alpha}^\dagger h_{1inb} \right\} \\
&\times \left\{ d_{im}^\dagger h_{1ima} + \frac{1}{\sqrt{2}} \varepsilon_{ac} h_{2imc}^\dagger s_{im} - \frac{1}{\sqrt{2}} \varepsilon_{ae} \bar{\sigma}_{ed}^\beta h_{2imd}^\dagger t_{im\beta} \right\} \\
&\Rightarrow \bar{d}^2 h_{2ina}^\dagger h_{1ima} - \frac{1}{2} \varepsilon_{ab} \varepsilon_{ac} \bar{s}^2 h_{2imc}^\dagger h_{1inb} \\
&+ \frac{1}{\sqrt{2}} \bar{d} \bar{s} \varepsilon_{ac} h_{2ina}^\dagger h_{2imc}^\dagger + \frac{1}{\sqrt{2}} \bar{d} \bar{s} \varepsilon_{ab} h_{1inb} h_{1ima} \\
&- \frac{1}{2} \varepsilon_{ac} \varepsilon_{ae} \sigma_{cb}^\alpha \bar{\sigma}_{ed}^\beta t_{in\alpha}^\dagger t_{im\beta} h_{1inb} h_{2imd}^\dagger \quad (C2)
\end{aligned}$$

Also, assuming that there is no magnetic ordering, the product of spin operators is given by:

$$\begin{aligned}
& S_{1im\alpha} S_{2in\alpha} \\
&= \tilde{S}_{1im\alpha} \tilde{S}_{2in\alpha} + \frac{1}{4} \sigma_{ab}^\alpha \sigma_{cd}^\alpha h_{1ima}^\dagger h_{1imb} h_{2inc}^\dagger h_{2ind} \\
&= -\frac{1}{4} (s_{im}^\dagger t_{im\alpha} + t_{im\alpha}^\dagger s_{im} - i \epsilon_{\alpha\beta\gamma} t_{im\beta}^\dagger t_{im\gamma}) \\
&\times (s_{in}^\dagger t_{in\alpha} + t_{in\alpha}^\dagger s_{in} + i \epsilon_{\alpha\mu\nu} t_{in\mu}^\dagger t_{in\nu}) \\
&+ \frac{1}{4} \sigma_{ab}^\alpha \sigma_{cd}^\alpha h_{1ima}^\dagger h_{1imb} h_{2inc}^\dagger h_{2ind} \\
&\Rightarrow -\frac{1}{4} \bar{s}^2 (t_{im\alpha}^\dagger t_{in\alpha} + t_{in\alpha}^\dagger t_{im\alpha} + t_{im\alpha}^\dagger t_{in\alpha}^\dagger + t_{im\alpha} t_{in\alpha}) \\
&+ \frac{1}{4} (t_{im\alpha}^\dagger t_{in\alpha} t_{in\beta}^\dagger t_{im\beta} - t_{im\alpha}^\dagger t_{in\alpha}^\dagger t_{im\beta} t_{in\beta}) \\
&+ \frac{1}{4} \sigma_{ab}^\alpha \sigma_{cd}^\alpha h_{1ima}^\dagger h_{1imb} h_{2inc}^\dagger h_{2ind} \quad (C3)
\end{aligned}$$

Performing the quadratic decoupling and ignoring irrelevant constants, the Hamiltonian  $H_\perp$  is written as follows. (Note that  $k_x$  is the momentum associated with the perpendicular direction to ladders, while  $k_y$  is with the parallel direction. Also, in laboratory unit, momentum in the parallel direction is given by  $p_y = k_y/a$ , and that in the perpendicular direction is given by  $p_x = k_x/2a$  where  $a$  is the lattice spacing and  $-\pi < k_x, k_y \leq \pi$ .)

$$H_\perp = H_{\perp,h^2} + H_{\perp,t^2h^2} + H_{\perp,t^2} + H_{\perp,t^4} + H_{\perp,h^4} \quad (C4)$$

$$\begin{aligned}
H_{\perp,h^2} &= \frac{t'}{2} (\bar{s}^2 - 2\bar{d}^2) \sum_{\mathbf{k}} \cos k_x \{ h_{+a}^\dagger(\mathbf{k}) h_{+a}(\mathbf{k}) \\
&\quad - h_{-a}^\dagger(\mathbf{k}) h_{-a}(\mathbf{k}) \} \\
&\quad - \sqrt{2} t' \bar{d} \bar{s} \sum_{\mathbf{k}} \cos k_x \{ h_{+\uparrow}^\dagger(\mathbf{k}) h_{+\downarrow}^\dagger(-\mathbf{k}) \\
&\quad + h_{+\downarrow}(-\mathbf{k}) h_{+\uparrow}(\mathbf{k}) \} \\
&\quad - \sqrt{2} t' \bar{d} \bar{s} \sum_{\mathbf{k}} \cos k_x \{ h_{-\uparrow}^\dagger(\mathbf{k}) h_{-\downarrow}^\dagger(-\mathbf{k}) \\
&\quad + h_{-\downarrow}(-\mathbf{k}) h_{-\uparrow}(\mathbf{k}) \} \quad (C5)
\end{aligned}$$

$$\begin{aligned}
H_{\perp,t^2h^2} &= -\frac{t'}{2} P_x \sum_{\mathbf{k}} \cos k_x \{ h_{+a}^\dagger(\mathbf{k}) h_{+a}(\mathbf{k}) \\
&\quad - h_{-a}^\dagger(\mathbf{k}) h_{-a}(\mathbf{k}) \} \\
&\quad - t' \Pi_x \sum_{\mathbf{k}} \cos k_x t_\alpha^\dagger(\mathbf{k}) t_\alpha(\mathbf{k}) \quad (C6)
\end{aligned}$$

$$\begin{aligned}
H_{\perp,t^2} &= -\frac{\lambda' J}{4} \bar{s}^2 \sum_{\mathbf{k}} \cos k_x \{ 2 t_\alpha^\dagger(\mathbf{k}) t_\alpha(\mathbf{k}) \\
&\quad + t_\alpha^\dagger(\mathbf{k}) t_\alpha^\dagger(-\mathbf{k}) + t_\alpha(\mathbf{k}) t_\alpha(-\mathbf{k}) \} \quad (C7)
\end{aligned}$$

$$\begin{aligned}
H_{\perp,t^4} &= \frac{\lambda' J}{4} \sum_{\mathbf{k}} \cos k_x \{ 2 P_x t_\alpha^\dagger(\mathbf{k}) t_\alpha(\mathbf{k}) \\
&\quad - Q_x (t_\alpha^\dagger(\mathbf{k}) t_\alpha^\dagger(-\mathbf{k}) + t_\alpha(\mathbf{k}) t_\alpha(-\mathbf{k})) \} \quad (C8)
\end{aligned}$$

$$\begin{aligned}
H_{\perp,h^4} &= -\frac{3}{8} \lambda' J \Pi_x \sum_{\mathbf{k}} \cos k_x \{ h_{+a}^\dagger(\mathbf{k}) h_{+a}(\mathbf{k}) \\
&\quad - h_{-a}^\dagger(\mathbf{k}) h_{-a}(\mathbf{k}) \} \\
&\quad - \frac{3}{4} \lambda' J \Delta_x \sum_{\mathbf{k}} \cos k_x \{ h_{+\uparrow}^\dagger(\mathbf{k}) h_{+\downarrow}^\dagger(-\mathbf{k}) \\
&\quad + h_{+\downarrow}(-\mathbf{k}) h_{+\uparrow}(\mathbf{k}) \} \\
&\quad + \frac{3}{4} \lambda' J \Delta_x \sum_{\mathbf{k}} \cos k_x \{ h_{-\uparrow}^\dagger(\mathbf{k}) h_{-\downarrow}^\dagger(-\mathbf{k}) \\
&\quad + h_{-\downarrow}(-\mathbf{k}) h_{-\uparrow}(\mathbf{k}) \} \quad (C9)
\end{aligned}$$

where

$$\begin{aligned}
P_x &= \sum_{\mathbf{k}} \cos k_x \langle t_\alpha^\dagger(\mathbf{k}) t_\alpha(\mathbf{k}) \rangle \\
Q_x &= \sum_{\mathbf{k}} \cos k_x \langle t_\alpha^\dagger(\mathbf{k}) t_\alpha^\dagger(-\mathbf{k}) \rangle. \\
\Pi_x &= \frac{1}{2} \sum_{\mathbf{k}} \cos k_x \{ \langle h_{+a}^\dagger(\mathbf{k}) h_{+a}(\mathbf{k}) \rangle - \langle h_{-a}^\dagger(\mathbf{k}) h_{-a}(\mathbf{k}) \rangle \} \\
\Delta_x &= \frac{1}{2} \sum_{\mathbf{k}} \cos k_x \{ \langle h_{+\uparrow}^\dagger(\mathbf{k}) h_{+\downarrow}^\dagger(-\mathbf{k}) \rangle \\
&\quad - \langle h_{-\uparrow}^\dagger(\mathbf{k}) h_{-\downarrow}^\dagger(-\mathbf{k}) \rangle \} \quad (C10)
\end{aligned}$$

where the bonding and anti-bonding fermions are assumed to be well separated in energy so that the mixing terms between them are ignored.

Combining  $H_\perp$  with the Hamiltonian describing the dynamics inside ladder, the mean-field Hamiltonian for the two-dimensional array of coupled t-J ladders is obtained.

$$\begin{aligned}
H &= N^2 \epsilon_0 / 2 + \sum_{\mathbf{k}} \{ \tilde{A}_{\mathbf{k}} t_\alpha^\dagger(\mathbf{k}) t_\alpha(\mathbf{k}) \\
&\quad + \tilde{B}_{\mathbf{k}} (t_\alpha^\dagger(\mathbf{k}) t_\alpha^\dagger(-\mathbf{k}) + t_\alpha(\mathbf{k}) t_\alpha(-\mathbf{k})) \} \\
&\quad + \sum_{\mathbf{k}} \{ \tilde{\epsilon}_+(\mathbf{k}) h_{+a}^\dagger(\mathbf{k}) h_{+a}(\mathbf{k})
\end{aligned}$$

$$\begin{aligned}
& -\tilde{D}_+(\mathbf{k})(h_{+\uparrow}^\dagger(\mathbf{k})h_{+\downarrow}^\dagger(-\mathbf{k}) + h_{+\downarrow}(-\mathbf{k})h_{+\uparrow}(\mathbf{k}))\} \\
& + \sum_{\mathbf{k}} \{ \tilde{\epsilon}_-(\mathbf{k})h_{-a}^\dagger(\mathbf{k})h_{-a}(\mathbf{k}) \\
& + \tilde{D}_-(\mathbf{k})(h_{-\uparrow}^\dagger(\mathbf{k})h_{-\downarrow}^\dagger(-\mathbf{k}) + h_{-\downarrow}(-\mathbf{k})h_{-\uparrow}(\mathbf{k}))\} \quad (C11)
\end{aligned}$$

where

$$\begin{aligned}
\epsilon_0 &= -\frac{3}{4}J\bar{s}^2 - \mu(\bar{s}^2 - \bar{d}^2 + 2x - 1) \\
& - \xi(2\bar{d}^2 - 2x) \quad (C12)
\end{aligned}$$

$$\begin{aligned}
\tilde{A}_{\mathbf{k}} &= \frac{J}{4} - \mu + \lambda J\bar{s}^2 \left( \cos k_y - \frac{\lambda'}{2\lambda} \cos k_x \right) \\
& + \lambda J \left( P_y \cos k_y + \frac{\lambda'}{2\lambda} P_x \cos k_x \right) \\
& + 2t \left( \Pi_y \cos k_y - \frac{t'}{2t} \Pi_x \cos k_x \right) \quad (C13)
\end{aligned}$$

$$\begin{aligned}
\tilde{B}_{\mathbf{k}} &= \frac{\lambda J}{2}\bar{s}^2 \left( \cos k_y - \frac{\lambda'}{2\lambda} \cos k_x \right) \\
& - \frac{\lambda J}{2} \left( Q_y \cos k_y + \frac{\lambda'}{2\lambda} Q_x \cos k_x \right) \quad (C14)
\end{aligned}$$

$$\begin{aligned}
\tilde{\epsilon}_+(\mathbf{k}) &= t(\bar{s}^2 - 2\bar{d}^2) \left( \cos k_y + \frac{t'}{2t} \cos k_x \right) - t - \xi \\
& - \frac{3}{4}\lambda J \left( \Pi_y \cos k_y + \frac{\lambda'}{2\lambda} \Pi_x \cos k_x \right) \\
& + t \left( P_y \cos k_y - \frac{t'}{2t} P_x \cos k_x \right) \quad (C15)
\end{aligned}$$

$$\begin{aligned}
\tilde{\epsilon}_-(\mathbf{k}) &= t(\bar{s}^2 - 2\bar{d}^2) \left( \cos k_y - \frac{t'}{2t} \cos k_x \right) + t - \xi \\
& - \frac{3}{4}\lambda J \left( \Pi_y \cos k_y - \frac{\lambda'}{2\lambda} \Pi_x \cos k_x \right) \\
& + t \left( P_y \cos k_y + \frac{t'}{2t} P_x \cos k_x \right) \quad (C16)
\end{aligned}$$

$$\begin{aligned}
\tilde{D}_+(\mathbf{k}) &= 2\sqrt{2}t\bar{d}\bar{s} \left( \cos k_y + \frac{t'}{2t} \cos k_x \right) \\
& + \frac{3}{2}\lambda J \left( \Delta_y \cos k_y + \frac{\lambda'}{2\lambda} \Delta_x \cos k_x \right) \quad (C17)
\end{aligned}$$

$$\begin{aligned}
\tilde{D}_-(\mathbf{k}) &= 2\sqrt{2}t\bar{d}\bar{s} \left( \cos k_y - \frac{t'}{2t} \cos k_x \right) \\
& - \frac{3}{2}\lambda J \left( \Delta_y \cos k_y - \frac{\lambda'}{2\lambda} \Delta_x \cos k_x \right) \quad (C18)
\end{aligned}$$

Diagonalization via Bogoliubov transformation and the correspondent saddle-point equations are similar to those of single ladder case. That is to say,

$$\begin{aligned}
\epsilon_{gr} &= \epsilon' + \frac{3}{2} \int \int \frac{d^2\mathbf{k}}{\pi^2} \tilde{\omega}(\mathbf{k}) \\
& - \int \int \frac{d^2\mathbf{k}}{\pi^2} \tilde{\Omega}_+(\mathbf{k}) - \int \int \frac{d^2\mathbf{k}}{\pi^2} \tilde{\Omega}_-(\mathbf{k}) \quad (C19)
\end{aligned}$$

where

$$\begin{aligned}
\epsilon'_0 &= -\frac{3}{4}J\bar{s}^2 - \mu(\bar{s}^2 - \bar{d}^2 + 2x - \frac{5}{2}) \\
& - \xi(2 + 2\bar{d}^2 - 2x) \quad (C20)
\end{aligned}$$

$$\tilde{\omega}(\mathbf{k}) = \sqrt{\tilde{A}_{\mathbf{k}}^2 - 4\tilde{B}_{\mathbf{k}}^2} \quad (C21)$$

$$\tilde{\Omega}_{\pm}(\mathbf{k}) = \sqrt{\tilde{\epsilon}_{\pm}^2(\mathbf{k}) + \tilde{D}_{\pm}^2(\mathbf{k})}. \quad (C22)$$

where the upper and lower limit of integral,  $\pi$  and 0, are not explicitly written. Saddle-point equations are given as follows.

$$\begin{aligned}
\frac{\partial(\epsilon_{gr}/J)}{\partial\bar{s}^2} &= -\frac{3}{4} - \frac{\mu}{J} \\
& + \frac{3}{2}\lambda \int \int \frac{d^2\mathbf{k}}{\pi^2} \left( \cos k_y - \frac{\lambda'}{2\lambda} \cos k_x \right) \\
& \times \frac{\tilde{A}_{\mathbf{k}} - 2\tilde{B}_{\mathbf{k}}}{\tilde{\omega}_{\mathbf{k}}} \\
& - \frac{t/J}{\bar{s}} \int \int \frac{d^2\mathbf{k}}{\pi^2} \left( \cos k_y + \frac{t'}{2t} \cos k_x \right) \\
& \times \frac{\bar{s}\tilde{\epsilon}_+(\mathbf{k}) + \sqrt{2}\bar{d}\tilde{D}_+(\mathbf{k})}{\tilde{\Omega}_+(\mathbf{k})} \\
& - \frac{t/J}{\bar{s}} \int \int \frac{d^2\mathbf{k}}{\pi^2} \left( \cos k_y - \frac{t'}{2t} \cos k_x \right) \\
& \times \frac{\bar{s}\tilde{\epsilon}_-(\mathbf{k}) + \sqrt{2}\bar{d}\tilde{D}_-(\mathbf{k})}{\tilde{\Omega}_-(\mathbf{k})} = 0 \quad (C23)
\end{aligned}$$

$$\begin{aligned}
\frac{\partial(\epsilon_{gr}/J)}{\partial(\mu/J)} &= \bar{d}^2 - \bar{s}^2 + \frac{5}{2} - 2x \\
& - \frac{3}{2} \int \int \frac{d^2\mathbf{k}}{\pi^2} \frac{\tilde{A}_{\mathbf{k}}}{\tilde{\omega}_{\mathbf{k}}} = 0 \quad (C24)
\end{aligned}$$

$$\begin{aligned}
\frac{\partial(\epsilon_{gr}/J)}{\partial\bar{d}^2} &= \frac{\mu}{J} - 2\frac{t}{J}\frac{\xi}{t} \\
& + \frac{t/J}{\bar{d}} \int \int \frac{d^2\mathbf{k}}{\pi^2} \left( \cos k_y + \frac{t'}{2t} \cos k_x \right) \\
& \times \frac{2\bar{d}\tilde{\epsilon}_+(\mathbf{k}) - \sqrt{2}\bar{s}\tilde{D}_+(\mathbf{k})}{\tilde{\Omega}_+(\mathbf{k})} \\
& + \frac{t/J}{\bar{d}} \int \int \frac{d^2\mathbf{k}}{\pi^2} \left( \cos k_y - \frac{t'}{2t} \cos k_x \right) \\
& \times \frac{2\bar{d}\tilde{\epsilon}_-(\mathbf{k}) - \sqrt{2}\bar{s}\tilde{D}_-(\mathbf{k})}{\tilde{\Omega}_-(\mathbf{k})} = 0 \quad (C25)
\end{aligned}$$

$$\frac{\partial(\epsilon_{gr}/J)}{\partial(\xi/J)} = -2 - 2\bar{d}^2 + 2x$$

$$+ \int \int \frac{d^2 \mathbf{k}}{\pi^2} \left\{ \frac{\tilde{\epsilon}_+(\mathbf{k})}{\tilde{\Omega}_+(\mathbf{k})} + \frac{\tilde{\epsilon}_-(\mathbf{k})}{\tilde{\Omega}_-(\mathbf{k})} \right\} = 0 \quad (\text{C26})$$

Also, the parameters due to quartic terms are defined as follows.

$$P_y = \frac{3}{2} \int \int \frac{d^2 \mathbf{k}}{\pi^2} \cos k_y \frac{\tilde{A}_{\mathbf{k}}}{\tilde{\omega}_{\mathbf{k}}} \quad (\text{C27})$$

$$Q_y = -3 \int \int \frac{d^2 \mathbf{k}}{\pi^2} \cos k_y \frac{\tilde{B}_{\mathbf{k}}}{\tilde{\omega}_{\mathbf{k}}} \quad (\text{C28})$$

$$\Pi_y = -\frac{1}{2} \int \int \frac{d^2 \mathbf{k}}{\pi^2} \cos k_y \left\{ \frac{\tilde{\epsilon}_+(\mathbf{k})}{\tilde{\Omega}_+(\mathbf{k})} + \frac{\tilde{\epsilon}_-(\mathbf{k})}{\tilde{\Omega}_-(\mathbf{k})} \right\} \quad (\text{C29})$$

$$\Delta_y = \frac{1}{2} \int \int \frac{d^2 \mathbf{k}}{\pi^2} \cos k_y \left\{ \frac{\tilde{D}_+(\mathbf{k})}{\tilde{\Omega}_+(\mathbf{k})} - \frac{\tilde{D}_-(\mathbf{k})}{\tilde{\Omega}_-(\mathbf{k})} \right\} \quad (\text{C30})$$

$$P_x = \frac{3}{2} \int \int \frac{d^2 \mathbf{k}}{\pi^2} \cos k_x \frac{\tilde{A}_{\mathbf{k}}}{\tilde{\omega}_{\mathbf{k}}} \quad (\text{C31})$$

$$Q_x = -3 \int \int \frac{d^2 \mathbf{k}}{\pi^2} \cos k_x \frac{\tilde{B}_{\mathbf{k}}}{\tilde{\omega}_{\mathbf{k}}} \quad (\text{C32})$$

$$\Pi_x = -\frac{1}{2} \int \int \frac{d^2 \mathbf{k}}{\pi^2} \cos k_x \left\{ \frac{\tilde{\epsilon}_+(\mathbf{k})}{\tilde{\Omega}_+(\mathbf{k})} - \frac{\tilde{\epsilon}_-(\mathbf{k})}{\tilde{\Omega}_-(\mathbf{k})} \right\} \quad (\text{C33})$$

$$\Delta_x = \frac{1}{2} \int \int \frac{d^2 \mathbf{k}}{\pi^2} \cos k_x \left\{ \frac{\tilde{D}_+(\mathbf{k})}{\tilde{\Omega}_+(\mathbf{k})} + \frac{\tilde{D}_-(\mathbf{k})}{\tilde{\Omega}_-(\mathbf{k})} \right\} \quad (\text{C34})$$

As previously, it is convenient to have some limiting case when the explicit solution is available. We will take the case of  $x = 0$ , i.e. no-doping case.

$$\frac{\partial(\epsilon_{gr}/J)}{\partial \bar{s}^2} = -\frac{3}{4} - \frac{\mu}{J} + \frac{3}{2} \lambda \int \int \frac{d^2 \mathbf{k}}{\pi^2} \frac{f_{\mathbf{k}}}{\sqrt{1 + \eta f_{\mathbf{k}}}} = 0 \quad (\text{C35})$$

$$\frac{\partial(\epsilon_{gr}/J)}{\partial(\mu/J)} = \frac{5}{2} - \bar{s}^2 - \frac{3}{2} \int \int \frac{d^2 \mathbf{k}}{\pi^2} \frac{1 + \frac{\eta}{2} f_{\mathbf{k}}}{\sqrt{1 + \eta f_{\mathbf{k}}}} = 0 \quad (\text{C36})$$

where  $\eta = \frac{2\lambda \bar{s}^2}{1/4 - \mu/J}$  and  $f_{\mathbf{k}} = \cos k_y - \frac{\lambda'}{2\lambda} \cos k_x$ . As before, it is possible to combine the above two equations to get a single equation only for  $\eta$ . That is to say,

$$\frac{\eta}{2\lambda} = \frac{5}{2} - \frac{3}{2} \int \int \frac{d^2 \mathbf{k}}{\pi^2} \frac{1}{\sqrt{1 + \eta f_{\mathbf{k}}}} \quad (\text{C37})$$

### 1. Superconducting Order Parameters

This subsection relates the parameters in the above computations to the physical order parameters describing the nature of the superconducting state. In the case of two-dimensional array of coupled ladders, there are three order parameters to be defined:

$$\chi_0 \equiv \varepsilon_{ab} \langle c_{1ia}^\dagger c_{2ib}^\dagger \rangle \quad (\text{C38})$$

$$\chi_{\parallel} \equiv \varepsilon_{ab} \langle c_{1,i+1,na}^\dagger c_{1ib}^\dagger \rangle \quad (\text{C39})$$

$$\chi_{\perp} \equiv \varepsilon_{ab} \langle c_{1i,n+1,a}^\dagger c_{2ib}^\dagger \rangle \quad (\text{C40})$$

The first one,  $\chi_0$ , is the pairing order parameter within dimer. Using constraints, it is written as follows.

$$\begin{aligned} \chi_0 &= \varepsilon_{ab} \langle \{ h_{1ina}^\dagger d_{in} + \frac{1}{\sqrt{2}} \varepsilon_{ac} s_{in}^\dagger h_{2inc} - \frac{1}{\sqrt{2}} \varepsilon_{ac} \sigma_{cd}^\alpha t_{in\alpha}^\dagger h_{2ind} \} \\ &\quad \times \{ h_{2inb}^\dagger d_{in} + \frac{1}{\sqrt{2}} \varepsilon_{bc} s_{in}^\dagger h_{1inc} + \frac{1}{\sqrt{2}} \varepsilon_{bc} \bar{\sigma}_{cd}^\beta t_{in\beta}^\dagger h_{1ind} \} \rangle \\ &= \varepsilon_{ab} \cdot \frac{1}{\sqrt{2}} \langle \varepsilon_{ac} s_{in}^\dagger d_{in} h_{2inc} h_{2inb}^\dagger \rangle = \sqrt{2} \bar{s} \bar{d} \end{aligned} \quad (\text{C41})$$

The pairing order parameter in the parallel direction,  $\chi_{\parallel}$ , is evaluated as follows.

$$\begin{aligned} \chi_{\parallel} &= \varepsilon_{ab} \{ \bar{d}^2 \langle h_{1,i+1,na}^\dagger h_{1inb}^\dagger \rangle + \frac{1}{2} \varepsilon_{ac} \varepsilon_{bd} \bar{s}^2 \langle h_{2,i+1,na} h_{2ind} \rangle \\ &\quad + \frac{1}{\sqrt{2}} \varepsilon_{bc} \bar{d} \bar{s} \langle h_{1,i+1,na}^\dagger h_{2inc} \rangle + \frac{1}{\sqrt{2}} \varepsilon_{ac} \bar{d} \bar{s} \langle h_{2,i+1,nc} h_{1inb}^\dagger \rangle \\ &\quad + \frac{1}{2} \varepsilon_{ac} \varepsilon_{be} \sigma_{cd}^\alpha \sigma_{ef}^\beta \langle t_{i+1,na}^\dagger t_{in\beta}^\dagger h_{2,i+1,nd} h_{2inf} \rangle \} \\ &= (\bar{d}^2 - \frac{1}{2} \bar{s}^2 + Q) \Gamma - \sqrt{2} \bar{d} \bar{s} \tilde{\Pi} \end{aligned} \quad (\text{C42})$$

where  $Q$  and  $\Gamma$  are defined previously, and  $\tilde{\Pi}$  is given by:

$$\tilde{\Pi} = -\frac{1}{2} \int \int \frac{dk dq}{\pi^2} \cos k \left\{ \frac{\tilde{\epsilon}_+(k, q)}{\tilde{\Omega}_+(k, q)} - \frac{\tilde{\epsilon}_-(k, q)}{\tilde{\Omega}_-(k, q)} \right\}. \quad (\text{C43})$$

Similarly, pairing order parameter in the perpendicular direction,  $\chi_{\perp}$ , is computed to give the following formula.

$$\begin{aligned} \chi_{\perp} &= \varepsilon_{ab} \{ \bar{d}^2 \langle h_{2ina}^\dagger h_{1i,n+1,b}^\dagger \rangle + \frac{1}{2} \varepsilon_{ac} \varepsilon_{bd} \bar{s}^2 \langle h_{1inc} h_{2i,n+1,d} \rangle \\ &\quad + \frac{1}{\sqrt{2}} \varepsilon_{bc} \bar{d} \bar{s} \langle h_{2ina}^\dagger h_{2i,n+1,c} \rangle + \frac{1}{\sqrt{2}} \varepsilon_{ac} \bar{d} \bar{s} \langle h_{1inc} h_{1i,n+1,b}^\dagger \rangle \\ &\quad - \frac{1}{2} \varepsilon_{ac} \varepsilon_{be} \sigma_{cd}^\alpha \sigma_{ef}^\beta \langle t_{ina}^\dagger t_{i,n+1,\beta}^\dagger h_{1ind} h_{2i,n+1,f} \rangle \} \\ &= (\bar{d}^2 - \frac{1}{2} \bar{s}^2 - Q_{\perp}) \Gamma_{\perp} - \sqrt{2} \bar{d} \bar{s} \tilde{\Pi}_{\perp} \end{aligned} \quad (\text{C44})$$

where  $Q_{\perp}$  and  $\Gamma_{\perp}$  are defined previously, and  $\tilde{\Pi}_{\perp}$  is given by:

$$\tilde{\Pi}_{\perp} = -\frac{1}{2} \int \int \frac{dk dq}{\pi^2} \cos q \left\{ \frac{\tilde{\epsilon}_+(k, q)}{\tilde{\Omega}_+(k, q)} + \frac{\tilde{\epsilon}_-(k, q)}{\tilde{\Omega}_-(k, q)} \right\}. \quad (\text{C45})$$

### APPENDIX D: EFFECT OF COULOMB INTERACTION

This section is devoted to the effect of Coulomb repulsion. Hamiltonian due to the Coulomb interaction between the nearest neighbors is written in terms of the bond operators as follows.

$$\begin{aligned}
H_{Coulomb} &= V \sum_i \sum_n n_{1in} n_{2in} \\
&+ V \sum_{\langle i,j \rangle} \sum_n \{n_{1in} n_{1jn} + n_{2in} n_{2jn}\} \\
&+ V \sum_i \sum_{\langle n,m \rangle} n_{2in} n_{1im} \quad (D1)
\end{aligned}$$

where

$$\begin{aligned}
n_{1in} &\equiv c_{1ina}^\dagger c_{1ina} \\
&= h_{1ina}^\dagger h_{1ina} + s_{in}^\dagger s_{in} + t_{in\alpha}^\dagger t_{in\alpha} \\
&= 1 - h_{2ina}^\dagger h_{2ina} - d_{in}^\dagger d_{in} \quad (D2)
\end{aligned}$$

and

$$\begin{aligned}
n_{2in} &\equiv c_{2ina}^\dagger c_{2ina} \\
&= h_{2ina}^\dagger h_{2ina} + s_{in}^\dagger s_{in} + t_{in\alpha}^\dagger t_{in\alpha} \\
&= 1 - h_{1ina}^\dagger h_{1ina} - d_{in}^\dagger d_{in}. \quad (D3)
\end{aligned}$$

The first term is evaluated as follows.

$$\begin{aligned}
&\sum_i \sum_n n_{1in} n_{2in} \\
&= \sum_i \sum_n (1 - h_{2ina}^\dagger h_{2ina} - d_{in}^\dagger d_{in}) \\
&\quad \times (1 - h_{1inb}^\dagger h_{1inb} - d_{in}^\dagger d_{in}) \\
&= \sum_i \sum_n \{1 - d_{in}^\dagger d_{in} - (h_{1ina}^\dagger h_{1ina} + h_{2ina}^\dagger h_{2ina})\} \\
&= \sum_i \sum_n \{1 - 2x + d_{in}^\dagger d_{in}\} \\
&\Rightarrow \frac{N^2}{2} (1 - 2x + \bar{d}^2) \quad (D4)
\end{aligned}$$

where  $N^2/2$  is the total number of dimers. Note that the constraint conditions are used.

The second term is due to the Coulomb interaction between the dimers along the ladder direction, which is computed by:

$$\begin{aligned}
&\sum_{\langle i,j \rangle} \sum_n \{n_{1in} n_{1jn} + n_{2in} n_{2jn}\} \\
&\Rightarrow \sum_{\langle i,j \rangle} \sum_n \{(1 - \bar{d}^2 - h_{2ina}^\dagger h_{2ina})(1 - \bar{d}^2 - h_{2jnb}^\dagger h_{2jnb}) \\
&\quad + (1 - \bar{d}^2 - h_{1ina}^\dagger h_{1ina})(1 - \bar{d}^2 - h_{1jnb}^\dagger h_{1jnb})\} \\
&= N^2 (1 - \bar{d}^2) (1 - 2x + \bar{d}^2) \\
&+ \sum_{\langle i,j \rangle} \sum_n \{h_{1ina}^\dagger h_{1ina} h_{1jnb}^\dagger h_{1jnb} + h_{2ina}^\dagger h_{2ina} h_{2jnb}^\dagger h_{2jnb}\}. \quad (D5)
\end{aligned}$$

Similarly, the third term is evaluated as follows.

$$\begin{aligned}
&\sum_i \sum_{\langle n,m \rangle} n_{2in} n_{1im} \\
&= \frac{N^2}{2} (1 - \bar{d}^2) (1 - 2x + \bar{d}^2) \\
&+ \sum_i \sum_{\langle n,m \rangle} h_{1ina}^\dagger h_{1ina} h_{2imb}^\dagger h_{2imb} \quad (D6)
\end{aligned}$$

Therefore,

$$\begin{aligned}
H_{Coulomb} &= \frac{N^2}{2} V (4 - 3\bar{d}^2) (1 - 2x + \bar{d}^2) \\
&+ V \sum_{\langle i,j \rangle} \sum_n \{h_{1ina}^\dagger h_{1ina} h_{1jnb}^\dagger h_{1jnb} + h_{2ina}^\dagger h_{2ina} h_{2jnb}^\dagger h_{2jnb}\} \\
&+ V \sum_i \sum_{\langle n,m \rangle} h_{1ina}^\dagger h_{1ina} h_{2imb}^\dagger h_{2imb} \\
&= \frac{N^2}{2} V (4 - 3\bar{d}^2) (1 - 2x + \bar{d}^2) + H_{Coul, h^4} \quad (D7)
\end{aligned}$$

The full treatment of  $H_{Coul, h^4}$  is beyond the scope of our present paper. However, we will follow the philosophy of BCS theory in that electrons interacting with the Coulomb repulsion under the neutralizing background are described in terms of the Landau-Fermi liquid. Assuming that the hopping parameter,  $t$ , and the spin-coupling parameter,  $J$ , are already renormalized quantities due to the Coulomb repulsion, one has only to consider the Hartree contribution of  $H_{Coul, h^4}$ , which is given by:

$$H_{Coul, h^4}^{Hartree} = \frac{N^2}{2} 3V (x - \bar{d}^2)^2 \quad (D8)$$

which is obtained by using the constraint conditions. Also, note that the mixing between the bonding and anti-bonding fermions is ignored.

Therefore, in our approximation, the Hamiltonian (per site) due to the Coulomb repulsion is given as follows:

$$\begin{aligned}
\frac{H_{Coulomb}}{N^2/2} &\simeq V (4 - 3\bar{d}^2) (1 - 2x + \bar{d}^2) + H_{Coul, h^4}^{Hartree} \\
&= V (4 - 8x + 3x^2) + V \bar{d}^2 \quad (D9)
\end{aligned}$$

Since Eq.(D9) depends only on  $\bar{d}^2$ , the modification of saddle-point equations is straightforward. That is,

$$\frac{\partial(\epsilon_{gr}/J)}{\partial \bar{d}^2} = 0 \rightarrow \frac{\partial(\epsilon_{gr}/J)}{\partial \bar{d}^2} + V = 0 \quad (D10)$$

All the other saddle-point equations are the same as before.

Now it is reasonable to assume the limit of large Coulomb repulsion which not only captures the essential physics that we are interested in, but also will simplify explicit computations. So we will take the limit  $V \rightarrow \infty$ ; consequently  $\bar{d} = 0$ . While this limit is not physical for large doping, our primary interest lies in the case of small doping.

- <sup>1</sup> See *e.g.* S. Sachdev, *Science*, **288**, 475 (2000) and references therein.
- <sup>2</sup> J. Bobroff, H. Alloul, W. A. MacFarlane, P. Mendels, N. Blanchard, G. Collin, and J.-F. Marucco, *Phys. Rev. Lett.* **86**, 4116 (2001).
- <sup>3</sup> H. Alloul *et al.*, *Phys. Rev. Lett.* **67**, 3140 (1991); A. V. Mahajan *et al.*, *Phys. Rev. Lett.* **72**, 3100 (1994); J. Bobroff *et al.*, *Phys. Rev. Lett.* **83**, 4381 (1999); P. Mendels *et al.*, *Europhys. Lett.* **46**, 678 (1999); A. V. Mahajan *et al.* *Eur. Phys. J. B* **13**, 457 (2000); M.-H. Julien *et al.*, *Phys. Rev. Lett.* **84**, 3422 (2000).
- <sup>4</sup> A. V. Balatsky, M. I. Salkola, and A. Rosengren, *Phys. Rev. B* **51**, 15547 (1995); M. I. Salkola, A. V. Balatsky, and D. J. Scalapino, *Phys. Rev. Lett.* **77**, 1841 (1996).
- <sup>5</sup> W. A. Atkinson, P. J. Hirschfeld, A. H. MacDonald, and K. Ziegler, *Phys. Rev. Lett.* **85**, 3926 (2000).
- <sup>6</sup> N. Read and S. Sachdev, *Phys. Rev. Lett.* **62**, 1694 (1989); *Phys. Rev. B* **42**, 4568 (1990).
- <sup>7</sup> S. Sachdev and N. Read, *Int. J. Mod. Phys. B* **5**, 219 (1991).
- <sup>8</sup> S. Sachdev and R. Jalabert, *Mod. Phys. Lett. B* **4**, 1043 (1990).
- <sup>9</sup> M. Vojta and S. Sachdev, *Phys. Rev. Lett.* **83**, 3916 (1999); M. Vojta, Y. Zhang, and S. Sachdev, *Phys. Rev. B* **62**, 6721 (2000).
- <sup>10</sup> S. Sachdev, C. Buragohain, and M. Vojta, *Science* **286**, 2479 (1999); M. Vojta, C. Buragohain, and S. Sachdev, *Phys. Rev. B* **61**, 15152 (2000).
- <sup>11</sup> S. Sachdev and M. Vojta, *Physica B* **280**, 333 (2000).
- <sup>12</sup> S. Sachdev and M. Vojta, *Proceedings of the XIII International Congress on Mathematical Physics*, July 2000, London, cond-mat/0009202.
- <sup>13</sup> A. M. Finkelstein, V. E. Kataev, E. F. Kukovitskii, and G. B. Teitel'baum, *Physica C* **168**, 370 (1990).
- <sup>14</sup> P. W. Anderson, *Science* **235**, 1196 (1987).
- <sup>15</sup> T. Senthil and M. P. A. Fisher, *Phys. Rev. B* **63**, 134521 (2001).
- <sup>16</sup> E. Fradkin and S. Kivelson, *Mod. Phys. Lett. B* **4**, 225 (1990).
- <sup>17</sup> O. P. Sushkov, J. Oitmaa, and Zheng Weihong, *Phys. Rev. B* **63**, 104420 (2001).
- <sup>18</sup> M. S. L. du Croo de Jongh, J. M. J. van Leeuwen, W. van Saarloos, *Phys. Rev. B* **62**, 14844 (2000).
- <sup>19</sup> H. Tsunetsugu, M. Troyer, and T. M. Rice, *Phys. Rev. B* **49**, 16078 (1994); M. Troyer, H. Tsunetsugu, and T. M. Rice, *Phys. Rev. B* **53**, 251 (1996).
- <sup>20</sup> D. Poilblanc, O. Chiappa, J. Riera, S. R. White, and D. J. Scalapino, cond-mat/0005403.
- <sup>21</sup> J. Rossat-Mignod, L. P. Regnault, C. Vettier, P. Bourges, P. Burlet, J. Bossey, J. Y. Henry, and G. Lapertot, *Physica C* **185-189**, 86 (1991).
- <sup>22</sup> H. A. Mook, M. Yethiraj, G. Aeppli, T. E. Mason, and T. Armstrong, *Phys. Rev. Lett.* **70**, 3490 (1993).
- <sup>23</sup> H. F. Fong, B. Keimer, D. Reznik, D. L. Milius, and I. A. Aksay, *Phys. Rev. B* **54**, 6708 (1996); H. F. Fong, B. Keimer, D. L. Milius, and I. A. Aksay, *Phys. Rev. Lett.* **78**, 713 (1997).
- <sup>24</sup> P. Bourges in *The Gap Symmetry and Fluctuations in High Temperature Superconductors* ed. J. Bok, G. Deutscher, D. Pavuna, and S. A. Wolf (Plenum, New York, 1998); cond-mat/9901333.
- <sup>25</sup> H. He, Y. Sidis, P. Bourges, G. D. Gu, A. Ivanov, N. Koshizuka, B. Liang, C. T. Lin, L. P. Regnault, E. Schoenherr, and B. Keimer, *Phys. Rev. Lett.* **86**, 1610 (2001).
- <sup>26</sup> J. M. Tranquada, J. D. Axe, N. Ichikawa, A. R. Moodenbaugh, Y. Nakamura, and S. Uchida, *Phys. Rev. Lett.* **78**, 338 (1997).
- <sup>27</sup> V. J. Emery, S. A. Kivelson, J. M. Tranquada, *Proc. Natl. Acad. Sci* **96**, 8814 (1999) and references therein.
- <sup>28</sup> R. J. McQueeney, Y. Petrov, T. Egami, M. Yethiraj, G. Shirane, and Y. Endoh, *Phys. Rev. Lett.* **82**, 628 (1999); T. Egami, cond-mat/0102449; R. J. McQueeney, J. L. Sarrao, P. G. Pagliuso, P. W. Stephens, and R. Osborn, cond-mat/0104118.
- <sup>29</sup> D. Withoff and E. Fradkin, *Phys. Rev. Lett.* **64**, 1835 (1990); L. S. Borkowski and P. J. Hirschfeld, *Phys. Rev. B* **46**, 9274 (1992); K. Chen and C. Jayaprakash, *J. Phys.: Condens. Matter* **7**, L491 (1995); K. Ingersent, *Phys. Rev. B* **54**, 11936 (1996); C. R. Cassanella and E. Fradkin, *Phys. Rev. B* **53**, 15079 (1996) and **56**, 11246 (1997); R. Bulla, Th. Pruschke, and A. C. Hewson, *J. Phys.: Condens. Matter* **9**, 10463 (1997); K. Ingersent and Q. Si, cond-mat/9810226; C. Gonzalez-Buxton and K. Ingersent, *Phys. Rev. B* **57**, 14254 (1998).
- <sup>30</sup> A. Polkovnikov, S. Sachdev, and M. Vojta, *Phys. Rev. Lett.* **86**, 296 (2001).
- <sup>31</sup> J.-X. Zhu and C. S. Ting, cond-mat/0008156.
- <sup>32</sup> A. V. Chubukov, S. Sachdev, and J. Ye, *Phys. Rev. B* **49**, 11919 (1994).
- <sup>33</sup> N. Nagaosa and P. A. Lee, *Phys. Rev. B* **61**, 9166 (2000).
- <sup>34</sup> O. P. Sushkov, cond-mat/0002421.
- <sup>35</sup> S. Mazumdar, S. Ramasesha, R. T. Clay, and D. K. Campbell, *Phys. Rev. Lett.* **82**, 1522 (1999).
- <sup>36</sup> S. Mazumdar, R. T. Clay, and D. K. Campbell, cond-mat/9910164.
- <sup>37</sup> S. Mazumdar, R. T. Clay, and D. K. Campbell, *Phys. Rev. B* **62**, 13400 (2000).
- <sup>38</sup> S. A. Kivelson, E. Fradkin, and V. J. Emery, *Nature* **393**, 550 (1998).
- <sup>39</sup> V. J. Emery, S. A. Kivelson, and O. Zachar, *Phys. Rev. B* **56**, 6120 (1997).
- <sup>40</sup> S. Sachdev, *Phys. Rev. B* **40**, 5204 (1989).
- <sup>41</sup> E. W. Carlson, D. Orgad, S. A. Kivelson, and V. J. Emery, *Phys. Rev. B* **62**, 3422 (2000).
- <sup>42</sup> J. Zaanen, O. Y. Osman, H. V. Kruis, Z. Nussinov, and J. Tworzydło, cond-mat/0102103.
- <sup>43</sup> M. Vojta, Y. Zhang, and S. Sachdev, *Phys. Rev. Lett.* **85**, 4940 (2000); *Int. J. Mod. Phys. B* **14**, 3719 (2000).
- <sup>44</sup> S. R. White and D. J. Scalapino, *Phys. Rev. Lett.* **80**, 1272 (1998); **81**, 3227 (1998); *Phys. Rev. B* **60**, R753 (1999).
- <sup>45</sup> A. H. Castro Neto, cond-mat/0102281.
- <sup>46</sup> C. Lannert, M. P. A. Fisher, and T. Senthil, *Phys. Rev. B* **63**, 134510 (2001).
- <sup>47</sup> S. Sachdev and R. N. Bhatt, *Phys. Rev. B* **41**, 9323 (1990).
- <sup>48</sup> A. V. Chubukov and Th. Jolicoeur, *Phys. Rev. B* **44**, 12050 (1991).
- <sup>49</sup> T. M. Rice, S. Gopalan, M. Sigrist, *Europhys. Lett.* **23**, 445 (1993).
- <sup>50</sup> S. Gopalan, T. M. Rice, and M. Sigrist, *Phys. Rev. B* **49**, 8901 (1994).



- <sup>51</sup> J. Piekarewicz and J. R. Shepard, Phys. Rev. B **60**, 9456 (1999).
- <sup>52</sup> V. N. Kotov, O. Sushkov, Zheng Weihong, and J. Oitmaa, Phys. Rev. Lett. **80**, 5790 (1998); V. N. Kotov, J. Oitmaa, O. Sushkov, and Zheng Weihong, Phil. Mag. B **80**, 1483 (2000).
- <sup>53</sup> Y. Matsushita, M. P. Gelfand, and C. Ishii, J. Phys. Soc. Jpn., **68** 247 (1999).
- <sup>54</sup> K. Totsuka, S. Miyahara, K. Ueda, Phys. Rev. Lett. **86**, 520 (2001).
- <sup>55</sup> D. Carpentier and L. Balents, cond-mat/0102218.
- <sup>56</sup> R. Eder, A. Dorneich, M. G. Zacher, W. Hanke, and S.-C. Zhang, Phys. Rev. B **59**, 561 (1999); A. Furusaki, S.-C. Zhang, Phys. Rev. B **60**, 1175 (1999).
- <sup>57</sup> E. Demler and S. Das Sarma, Phys. Rev. Lett. **82**, 3895 (1999).
- <sup>58</sup> T. Sommer, M. Vojta, and K. W. Becker, cond-mat/0104356.
- <sup>59</sup> Y. L. Lee, Y. W. Lee, C.-Y. Mou, and Z. Y. Weng, Phys. Rev. B **60**, 13418 (1999).
- <sup>60</sup> R. Eder, Phys. Rev. B **57**, 12832 (1998).
- <sup>61</sup> M. Vojta and K. W. Becker, Phys. Rev. B **60**, 15201 (1999).
- <sup>62</sup> C. Jurecka and W. Brenig, cond-mat/0103511.
- <sup>63</sup> S. Sachdev, *Quantum Phase Transitions*, Cambridge University Press, Cambridge (1999).
- <sup>64</sup> M. G. Zacher, R. Eder, E. Arrigoni, and W. Hanke, cond-mat/0103030.
- <sup>65</sup> M. Granath, V. Oganessian, S. A. Kivelson, E. Fradkin, and V. J. Emery, cond-mat/0010350.
- <sup>66</sup> R. D. Duncan and C. A. R. Sá de Melo, Phys. Rev. B **62**, 9675 (2000).
- <sup>67</sup> C. Nayak, Phys. Rev. B **62**, 4880 (2000).
- <sup>68</sup> L. Pintschovius and M. Braden, Phys. Rev. B **60**, R15039 (1999).
- <sup>69</sup> H. A. Mook and F. Dogan, Nature **401**, 145 (1999); H. A. Mook, P. Dai, F. Dogan, and R. D. Hunt, Nature **404**, 729 (2000).
- <sup>70</sup> Y. Petrov, T. Egami, R. J. McQueeney, M. Yethiraj, H. A. Mook, and F. Dogan, cond-mat/0003414.
- <sup>71</sup> G. Khaliullin and P. Horsch, Physica C **282-287**, 1751 (1997); P. Horsch, G. Khaliullin, and V. Oudovenko, Physica C **341-348**, 117 (2000).
- <sup>72</sup> C. Gros and R. Werner, Phys. Rev. B **58**, R14677 (1998).
- <sup>73</sup> R. Werner, C. Gros, and M. Braden, Phys. Rev. B **59**, 14356 (1999).
- <sup>74</sup> M. J. Massey, R. Merlin, and S. M. Girvin, Phys. Rev. Lett. **69**, 2299 (1992).
- <sup>75</sup> Z.-X. Shen, A. Lanzara, and N. Nagaosa, cond-mat/0102224.
- <sup>76</sup> S. Ono, Yoichi Ando, T. Murayama, F. F. Balakirev, J. B. Betts, and G. S. Boebinger, Phys. Rev. Lett. **85**, 638 (2000).
- <sup>77</sup> E. Demler, S. Sachdev, and Y. Zhang, cond-mat/0103192.
- <sup>78</sup> J. C. Wynn, D. A. Bonn, B. W. Gardner, Yu-Ju Lin, Ruixing Liang, W. N. Hardy, J. R. Kirtley, and K. A. Moler, preprint.
- <sup>79</sup> S. Sachdev, Phys. Rev. B **45**, 389 (1992); N. Nagaosa and P. A. Lee, Phys. Rev. B **45**, 966 (1992); Jung Hoon Han and Dung-Hai Lee, Phys. Rev. Lett. **85**, 1100 (2000); M. Franz and Z. Tesanovic, Phys. Rev. B **63**, 064516 (2001).
- <sup>80</sup> Ch. Renner, B. Revaz, K. Kadowaki, I. Maggio-Aprile, and O. Fischer, Phys. Rev. Lett. **80**, 3606 (1998); S. H. Pan, E. W. Hudson, A. K. Gupta, K.-W. Ng, H. Eisaki, S. Uchida, and J. C. Davis, Phys. Rev. Lett. **85**, 1536 (2000).
- <sup>81</sup> S. H. Pan, J. P. O'Neal, R. L. Badzey, C. Chamon, H. Ding, J. R. Engelbrecht, Z. Wang, H. Eisaki, S. Uchida, A. K. Gupta, K.-W. Ng, E. W. Hudson, K. M. Lang, and J. C. Davis, preprint.
- <sup>82</sup> G. L. Squires, *Introduction to the Theory of Thermal Neutron Scattering*, Dover Publications, New York (1978); see also <http://rrdjazz.nist.gov/resources/n-lengths/>.
- <sup>83</sup> J. V. Jose, L. P. Kadanoff, S. Kirkpatrick, and D. R. Nelson, Phys. Rev. B **16**, 1217 (1977).